THIAZOLE VS. THIOPHENE: HETEROCYCLE EFFECTS ON THE PROPERTIES OF FUSED-RING CONJUGATED MATERIALS

A Dissertation
Submitted to the Graduate Faculty
of the
North Dakota State University
of Agriculture and Applied Science

By

Eric James Uzelac

In Partial Fulfillment of the Requirements
for the Degree of
DOCTOR OF PHILOSOPHY

Major Department:
Chemistry and Biochemistry

October 2017

Fargo, North Dakota

North Dakota State University
Graduate School

Title

Thiazole vs. Thiophene: Heterocycle Effects on the Properties of Fused-Ring Conjugated Materials

By

Eric James Uzelac

The Supervisory Committee certifies that this ***disquisition*** complies with North Dakota State University's regulations and meets the accepted standards for the degree of

DOCTOR OF PHILOSOPHY

SUPERVISORY COMMITTEE:

Dr. Seth C. Rasmussen
Chair

Dr. Kenton Rodgers

Dr. Gregory Cook

Dr. Andrew Croll

Approved:

11-13-17
Date

Dr. Gregory Cook
Department Chair

ABSTRACT

Conjugated polymers and related molecular materials comprise a field of materials chemistry focused on the development of semiconducting organic plastics that find use in applications such as organic solar cells and organic light-emitting diodes. The optical and electronic properties of these molecules, such as absorption and emission of light, can be tuned through engineering at the molecular level. However, many of the current molecules of choice suffer from high-lying frontier orbitals, which results in a mismatch of energy levels to common components of electronic devices along with potential oxidative instability, constraining device performance in real environments.

To rectify these issues, the electron-deficient thiazole heterocycle has been incorporated into fused-ring conjugated motifs of both organic and inorganic nature. The new thiazole materials all exhibited the expected stabilization of their frontier orbitals compared to the thiophene analogues. The absorption profiles of the thiazole materials are similar to the thiophene analogues, but with reduced molar absorptivity as a general trend, potentially limiting the efficiency of thiazole derived materials as components of photovoltaic devices. Through experimentation and development of multiple new classes of organic and inorganic thiazole materials, it was found that a larger proportion of thiazole content correlates to a larger decrease in molar absorptivity, but also a larger relative stabilization of the frontier orbitals. The limitations in molar absorptivity can thus be mitigated to an extent by increasing the molecule's effective conjugation path through functionalization with additional conjugated units, but with the countereffect of less-stabilized frontier orbitals.

ACKNOWLEDGEMENTS

I would foremost like to thank my advisor, Dr. Seth C. Rasmussen, for his continued support and conversations over the last five years. His door was always open to discuss books, movies, games, and, of course, chemistry. I do not take for granted being able to work for such an approachable and relatable boss, and plenty of good times were had during the course of my schooling. I truly have Seth to thank for teaching me how to think like a scientist.

Also, I would like to thank my committee members Dr. Greg Cook, Dr. Andrew Croll, and especially Dr. Kent Rodgers, whose guidance and support was instrumental in my passing of the maxi proposal the second time around. Also, thanks to Amy Kain, for her quick response any time I needed assistance, Greg Oswald for making teaching smooth and enjoyable, and Dr. Angel Ugrinov for obtaining X-ray data.

I would like to thank my fiancée, Sammy, who walked through the door of Ladd 105 on a warm summer day and became the greatest source of happiness I have ever known. I could not have done this without her boundless support, and look forward to our wedding as next step in our long and happy voyage through life.

I would like to thank my family, who was always there to talk during both the good and rough times, who never stopped encouraging me to preserve through my PhD. Hunting, fishing, holidays, and tea with my grandparents provided much-needed intermissions from graduate life. I am glad to have been able to spend many weekends with my family in Grand Rapids over the course of my graduate studies. I would also like to thank my colleagues past and present: Dr. Michael Mulholland, Casey McCausland, M.S., Dr. Ryan Schwiderski, Kristine Konkol, Trent Anderson, and Evan Culver. Thanks also to the members of the D&D/Savage Worlds group, especially the Dungeon Masters Erik Janssen and Jesse Joyce, whose weekly adventures

provided an engaging escape for the majority of my time here. Also, many thanks to Eric Serum, who spent many hours discussing organic chemistry with me when I needed it most.

It must be said that I would not have gone to graduate school if it were not for two wonderful people. The engaging teaching style and great personality of Melissa Ewen at Grand Rapids High School made chemistry courses interesting and drove me towards a chemistry major at St. John's. There, Dr. Thomas Nicholas Jones let me into his research group for two years and showed me that chemistry research was a challenging and highly-satisfying endeavor. Although I infamously brominated his laboratory, he never lost faith in me to work hard and get results.

As evidenced by this lengthy section, I have a lot of people to thank, and I do not take their support for granted. Thank you all.

TABLE OF CONTENTS

LIST OF TABLES

LIST OF FIGURES

LIST OF SCHEMES

CHAPTER 1. INTRODUCTION

1.1. Conjugated and Conducting Polymers

Conjugated polymers (CPs) and related molecular materials are a highly-studied and expanding field of materials chemistry. CP-based materials feature optical and electronic properties traditionally observed in inorganic semiconducting materials coupled with the processability and low production costs of plastics.[1] Consequently, CPs find wide use in organic light-emitting diodes (OLEDs), organic photovoltaics (OPVs), electrochromics, and organic field-effect transistors (OFETs).[1-14] The defining property of these materials is conjugation, a union which manifests as an overlap of *p*-orbitals across the molecule's backbone. This conjugation leads to delocalization of π-electrons over the molecule's backbone, commonly referred to as the π-system. To attain conjugation, the single and double bonds must be alternating and thus each have a bond order of approximately 1.5 through resonance, as exemplified in the simplest conjugated polymer, polyacetylene (Figure 1.1a). In the case of heterocycles, non-bonded electrons occupying *p*-orbitals within the plane of the π-system can participate as well, as seen in polypyrrole and polythiophene.[1] Some common examples of conjugated polymers are shown in Figure 1.1b.

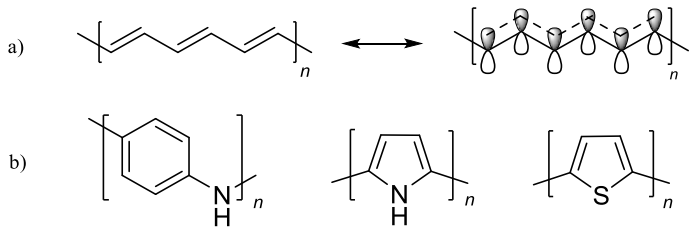

Figure 1.1. (a) polyacetylene with *p*-orbitals shown, b) polyaniline, polypyrrole, and polythiophene

All CPs will exhibit conductivity if electron delocalization is not compromised by factors such as molecular geometry and torsional strain, which limit the overlap of the orbitals comprising the π-system.[l] This conductivity has been shown to reach as high as 120,000-170,000 S cm^{-1} in highly-structured polyacetylene, attained through vigorous oxidation and stretching of the polymer film.[15] For context, conductivity in the range of 10^5 S cm^{-1} is on the same order of magnitude as the highest-conducting metals such as silver, which exhibits a conductivity of 630,500 S cm^{-1}.[16] These materials can be therefore described as "synthetic metals", using a term first coined by Herbert McCoy in 1911 and popularized by Alfred Ubbelohde in 1969 to denote materials that are conductive like metals, but produced from non-metallic components.[17,18] To better understand the explosive growth of the field, it is important to examine the history of these materials, starting from the earliest examples.

The development of conjugated and conducting polymers into the expansive field today resulted from discoveries made by researchers worldwide throughout the 19th and 20th centuries. The most significant discoveries in the field of conducting polymers tend to fall within three paths: the development of polypyrrole, polyaniline, and polyacetylene.[19-21] The first reported conjugated polymer was polyaniline, published by F. Ferdinand Runge who treated aniline nitrate with copper salts and HCl to produce a green-black material in 1834. Other scientists applied similar oxidative conditions to produce "aniline black" residues for printing applications, and by 1862 Roberts, Dale, and Co. was selling aniline dyes to printers. One of the more prominent reports of aniline oxidation was by Henry Letheby in 1862, in which the author used a platinum electrode and battery to generate a blue-green powder from an acidic solution of aniline. This result carries extra significance because it was the first documented electropolymerization of a conjugated unit.[20]

The first detailed characterization of the electronic properties of polyaniline was carried out in the mid-1960s by Rene Buvet and Marcel Jozefowicz. Pressed pellets of oxidized polyaniline materials (emeraldine salts) of controlled compositions were found to be quite conductive and this conductivity was concluded to be electronic. The conductivity of the oxidized polyaniline was also found to be dependent on both the extent of protonation, with the conductivity increased linearly with decreasing pH to give conductivities that ranged from 10^{-9} to 30 S cm^{-1}.[20]

Polypyrrole was first reported by Angelo Angeli, the chair of the Istituto di Studi Superiori in Florence, Italy. He exposed pyrrole to mixtures of hydrogen peroxide and acetic acid to form oxidized polypyrrole, a precipitate he deemed "pyrrole black" when reported in 1915.[19] He expanded this family to functionalized pyrroles, which allowed production of colored species similar to pyrrole black, also discovering that many oxidizing agents could produce these compounds. Although Angeli did not characterize these compounds, he correctly estimated that carbon-carbon bonds were being formed between the alpha positions of the pyrrole rings, and proposed a structure that was very similar to the currently-accepted structure of oxidized polypyrrole (Figure 1.2). A few years later, another Italian scientist named Riccardo Ciusa was investigating the production of a graphite derivate from pyrrole, and heated tetraiodopyrrole in a vacuum to generate a black material similar to graphite. He repeated these experiments with thiophene and furan which produced similar materials, but did not characterize these heterocyclic materials beyond elemental composition and appearance.[19]

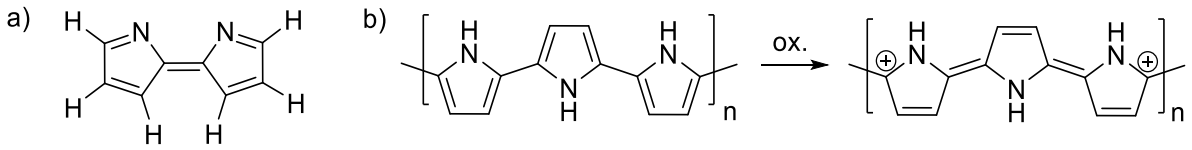

Figure 1.2. Angeli's proposed empirical unit comprising polypyrrole (a), compared to the accepted structure of oxidized polypyrrole (b)[19]

Ciusa's polypyrrole work lay dormant for 40 years, but was revitalized around 1959 by Donald Weiss, an Australian chemist at the Council for Scientific and Industrial Research. He was interested in electrically-activatable adsorbents for electric desalination, and synthesized graphitic powders using a procedure modified from Ciusa's.[19] Instead of performing his reaction on tetraiodopyrrole *in vacuo*, Weiss used a stream of nitrogen. The difference in technique may have allowed the iodine vapors produced from the reaction to interact with the polymer instead of being driven away. Iodine, being an oxidizing agent, oxidized Weiss' polymer and incorporated iodide counterions into the molecule, forming a salt, which increases the number of intrinsic charge-carriers and enhances conductivity.[1,4,6,20] Weiss reported both "adsorbed" and "substituted" iodine, which supports these arguments.[20] Measuring the electronic character, Weiss found the polymer to exhibit a resistivity of 11-200 Ω cm, which corresponds to conductivities of 0.005-0.09 S cm^{-1}, the highest reported for an organic polymer in 1963.[19]

Meanwhile, work on polypyrrole was pushed forward once more in Italy, with collaborations at the University of Parma between Gian Piero Gardini, Luigi Chierici, and Vittorio Bocchi in the late 1960's.[19] In addition to studying the intermediates formed under Angeli's oxidative polymerization conditions, the researchers also investigated the electropolymerization of pyrrole in H_2SO_4 by using a current of 100 mA applied to platinum electrode. The resulting material exhibited a conductivity of 7.54 S cm^{-1}, orders of magnitude higher than Weiss's. This work was noted by Arthur Diaz, a scientist at IBM, who optimized the

electropolymerization conditions in the late 1970's by growing films thinly and slowly in an aprotic solvent, resulting in materials which exhibited conductivities of 10-100 S cm^{-1}.[19]

Around the same time period, Giulio Natta successfully polymerized acetylene using a catalytic mixture of triethylaluminum and titanium oxide, publishing this work in 1958.[21] The polyacetylene samples exhibited resistivities of 10^{10} Ω cm, which were to five to eight orders of magnitude lower than non-conjugated hydrocarbon polymers. Additionally, X-ray analysis showed that the polymer exhibited an all-*trans* configuration. In 1963, a breakthrough occurred due to the actions of Hyung Chick Pyun, a visiting Korean researcher who was working with Hideki Shirakawa. Pyun had attempted to synthesize polyacetylene but added 1000 times the proper catalyst amount to the reaction, possibly due to reading "mmol" as "mol".[20] As a result, a silvery film, metallic in appearance, was produced instead of the intended powder. It was eventually concluded that the gross excess of catalyst had increased the rate of reaction such that polymerization proceeded at the air-solvent interface, rather than solution as was typical. Shirakawa's X-ray analysis confirmed an all-*trans* configuration for the polymer which was identical to Natta's, and electrical measurements showed a conductivity of 10^{-4} to 10^{-5} S cm^{-1}.

The field of conjugated polymers expanded greatly when polyacetylene brought three researchers together. In 1975, Alan MacDiarmid, a visiting professor at Kyoto University, met Shirakawa over tea, where MacDiarmid showed Shirakawa his golden poly(sulfurnitride) films.[21] Shirakawa compared samples of his poylacetylene films with MacDiarmid's, and MacDiarmid's interest led to the appointment of Shirakawa as a visiting researcher to the University of Pennsylvania in 1976. Together, MacDiarmid, Shirakawa, and professor Alan J. Heeger[22] worked to increase the purity of polyacetylene films, but noticed that purer films actually increased resistivity. The scientists found that treating their pure materials with bromine vapor

brought conductivity values up to a record-breaking 500 S cm^{-1}, and similar experiments with sodium also resulted in increased conductivity. Because their starting materials were pure and well-ordered, the collaboration between these researchers at University of Pennsylvania resulted in a family of highly-conductive polymers upon doping with both oxidizing and reducing agents.[1,4,6,22] Overall, Heeger, MacDiarmid, and Shirakawa made a critical impact on the field by producing such highly-conductive conjugated polymers with simple doping techniques. This discovery led to a surge of work on conjugated polymers, and the three men went on to receive the Nobel Prize in Chemistry for their work in 2000. Conjugated polymers and small molecules continue to be an important research area and the subject of around 500-800 publications annually with 766 articles published in 2016 alone.[23]

1.2. Bandgap in Conjugated Materials

The conductivity of CPs derives from the phenomenon of orbital mixing and electron delocalization found in these materials.[1,11,24,25] Provided spatial overlap exists, the atomic orbitals which make up molecular orbitals of similar energy can mix and hybridize, forming new orbital pairs in conjugated systems. The new orbital pairs are non-degenerate, meaning one orbital is slightly stabilized, while the other is slightly destabilized (Figure 1.3a). As a result, the molecule's new highest-occupied molecular orbital (HOMO) is destabilized and the lowest-unoccupied molecular orbital (LUMO) is now stabilized. As conjugation increases, the effects of orbital mixing amplify, resulting in a myriad of energetically similar molecular orbitals within a lengthy polymer. As more conjugated units are added, the growing extent of orbital mixing continues to gradually raise the energy of the HOMO and lower the energy of the LUMO of the molecule or polymer chain.[1,11,24,25] This results in a narrowing of the energetic gap as conjugation increases, shown in Figure 1.3. The effect diminishes, however, as the length of the

polymer approaches the limit of electron delocalization, which was shown in polythiophenes to be approximately 20-30 units.[1]

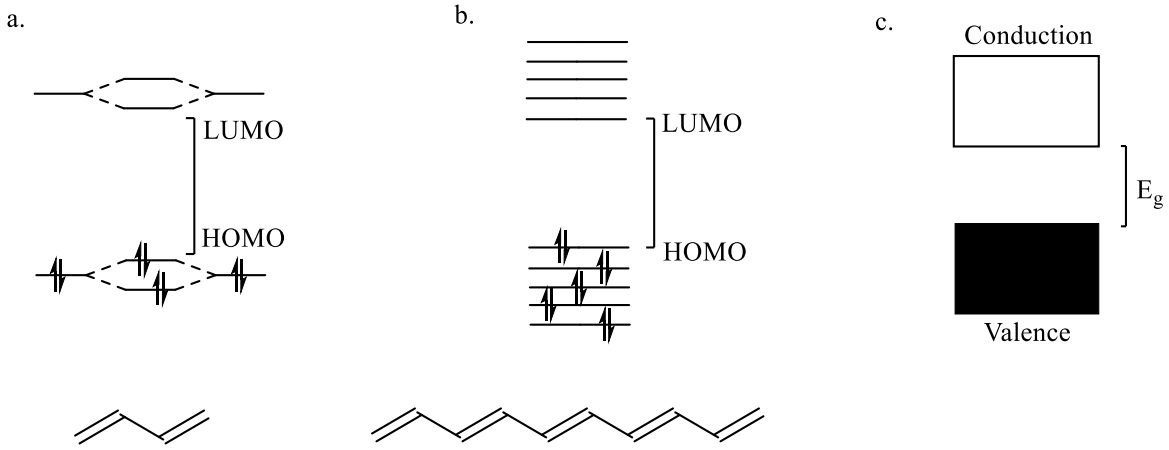

Figure 1.3. Simplified molecular orbital structure of a shorter (a) and longer (b) oligomer in solution, and band structure of material in the solid state (c)

Whereas an individual oligomer or polymer in solution will still feature a HOMO and LUMO due to discrete orbitals (Figure 1.3b), the solid state allows π-electrons to delocalize across molecules as the polymer transitions from its chiral, coil-like configuration in solution to its planar form in the solid state. This enhanced delocalization is a not only a result of increased molecular planarity, but also an intermolecular interaction called π-stacking, which most often manifests through a quadrupolar attraction between the electron-rich π-system and electron-deficient sp^2 carbon-hydrogen plane in the molecular backbone. The π-system "sandwiches" the molecular backbone, shown in Figure 1.4.[26,27] This interaction enhances electron delocalization because the quadrupole distorts the π-system's electric field and provides a stabilizing effect. Additionally, since π-stacked units in these configurations exhibit close molecular contacts, "hopping" of electrons and holes from one localized state to another can occur by way of electron-transfer (ET).[26-28] This hopping is the method by which charge-carriers migrate across molecular boundaries, giving conjugated materials their conductivity.

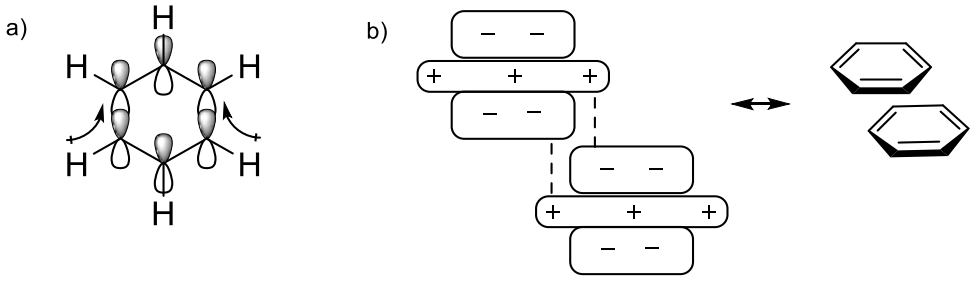

Figure 1.4. (a) electron density drawn to benzene's π-system, (b) resulting in off-centered packing due to π-stacking

Assisted by π-stacking, the solid-state interactions between *p*-orbitals both across and within conjugated units leads to "bands" of indiscrete orbitals, depicted in Figure 1.3.[1,11,24,25] When bands of orbitals are formed, a bandgap (E_g) results, which is a bulk solid-state property defined as the energetic separation between the filled valence band of bonding molecular orbitals, and empty conduction band of antibonding molecular orbitals (Figure 1.3c).[9] The top edge of the valence band can be viewed as analogous to a HOMO, and the bottom edge of the conduction band as analogous to a LUMO. The bandgap is a critical parameter for conjugated materials because it determines both electronic and optical properties of the material such as energy of absorption, conductivity, and luminescence color.[1-5]

Bandgap is described in units of electron volts (eV), and the size of the E_g determines how a polymer is classified. While there is no defined bandgap range for semiconducting materials, they will all behave as insulators at 0 K, but allow a small thermal population of the valence band at any point above this temperature based upon the Fermi-Dirac distribution.[29,30] Materials with a bandgap of 1.5-2.0 eV, such as polythiophene, are deemed *reduced bandgap*, while those below 1.5 eV are referred to as *low bandgap*.[1,31] As pure conductors have no distinct valence band and conduction band but a Fermi level within a singular continuous band of orbitals, they exhibit no bandgap.[29] A bandgap is necessary for control over electron and hole

flow in organic electronic applications, but smaller bandgaps are more ideal. With a smaller bandgap, conductivity is enhanced through higher population of intrinsic charge-carriers at a given temperature. Additionally, the energy needed to thermally or photophysically excite the molecule decreases with a smaller bandgap, and control of this energy can lead to low-energy transitions within the visible range of the electromagnetic spectrum and thus highly-colored materials.[8] Figure 1.5 shows the E_g values of some common classes of conjugated polymers.

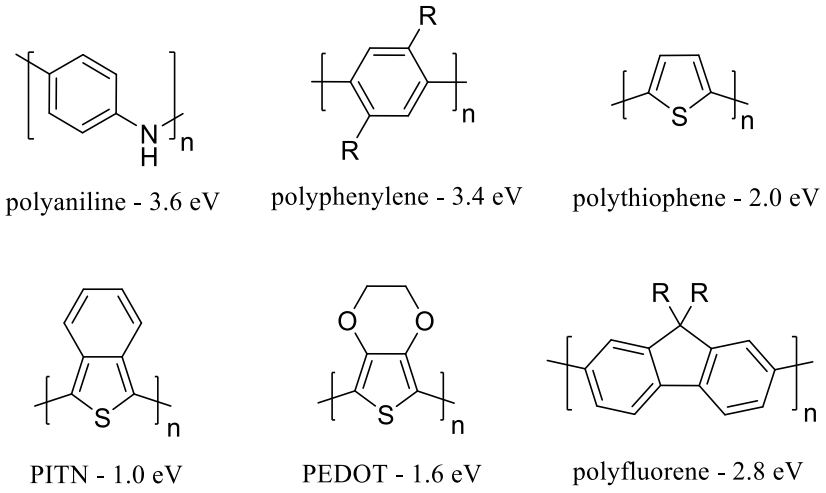

Figure 1.5. Bandgaps of commonly-used conjugated polymers

A material's E_g and HOMO-LUMO gap are commonly determined by two experimental methods: electrochemical or optical measurements.[1] Foremost, electrochemical determination uses techniques such as cyclic voltammetry to find the material's onset of oxidation and reduction. The tangential line to the slope of the peak is used as this onset, and provides a more accurate measure of the potential at which electrons begin to be removed or added to the molecule's frontier orbitals. For example, the onset of oxidation signifies the energy at which an electron can be removed from the molecule's HOMO, and the onset of reduction is the energy at which an electron can be added to the molecule's LUMO. These potentials are referenced to the Fc/Fc^+ oxidation couple of ferrocene (-5.1 eV from E_{vac}) which is necessary to convert an

electrical potential value referenced to a standard, to a linear energy value in eV vs. vacuum.[29] The molecule's onset of oxidation or onset of reduction are then subtracted from -5.1 eV to estimate the HOMO or LUMO energy level, respectively. It must be stated that electrochemical measurements reveal accurate oxidation and reduction potentials of the material, but are not direct measurements of the HOMO and LUMO. If both oxidation and reduction potentials are visible in the solvent's redox window, the HOMO-LUMO gap can be estimated quite readily from this single technique.

Optical determination of E_g or HOMO-LUMO gap may be necessary for many conjugated materials, as the electrochemical processes involving the frontier orbitals may lie outside the potential window of a suitable solvent-electrolyte combination. For example, the LUMO of many small molecules is quite destabilized. Reduction of the LUMO could occur at more negative potentials than the solvent, and the solvent would therefore reduce before the conjugated molecule. For very stable systems, the reverse could be true: the solvent could oxidize at less positive potentials than the conjugated molecules's HOMO. To *roughly* estimate bandgap using an absorption spectrum (Figure 1.6a), the onset of the low-energy side of the absorption band is extrapolated to baseline. Then, the wavelength's energy is converted to eV via the relationship that 1 eV is equal to 1240 nm. However, the more accurate method is to prepare a Tauc plot (Figure 1.6b),[32] in which the energy of light ($h\nu$) is plotted against $(A \times h\nu)^2$ and the linear portion extrapolated to baseline, revealing a more accurate estimate of the energy gap. A limitation in optical measurement, though, is that only the E_g or HOMO-LUMO gap can be determined. However, the combination of electrochemical and optical data allows estimation of the individual energies. [1]

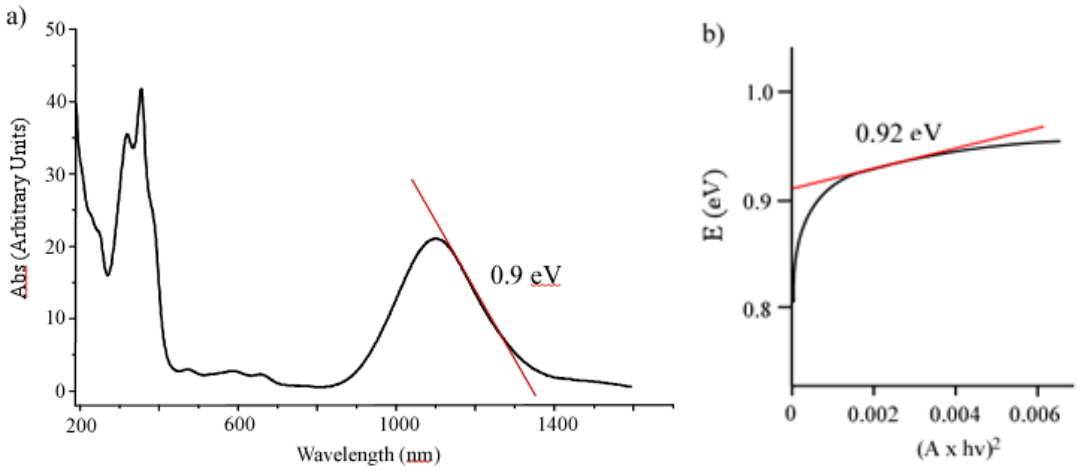

Figure 1.6. Estimating optical bandgap via extrapolation of absorption onset (a) and Tauc plot method (b)

1.3. Bandgap Control and Tuning

The origin and measurement of bandgap and HOMO-LUMO gap in organic semiconductors has been rightly discussed, but materials chemists are primarily concerned with control and tuning of these energy gaps. The magnitude of the E_g largely derives from bond-length alternation across the π-system.[1] Lower degrees of bond-length alternation lead to better electron delocalization across a molecule's π-system and less localization of charge. Yet, before describing ways in which a material's E_g be tuned towards certain applications, it is important to discuss the physical factors that affect E_g and HOMO-LUMO gap: molecular planarity, aromaticity, and intermolecular interactions.

Concerning the first factor, increased backbone planarity equates to a lower E_g, because the conjugation length along the backbone can be altered by torsional strain. Any twisting from baseline of 40° or above will disturb *p*-orbital overlap significantly, resulting in decreased electron delocalization and thus a higher bandgap.[1,3-6] With the second factor, cyclic units with high degrees of aromaticity encourage electron density to reside within their monomeric units,

discouraging delocalization across the polymer backbone and raising E_g. Thus, extent of aromaticity is directly related to E_g. Heterocyclic monomers tend to be less aromatic than benzene, which can be exploited in monomer design to decrease E_g. For the third factor, molecular structures that encourage higher degrees of intermolecular interactions will lower E_g, due to the increased interchain delocalization of π-electrons. Despite increasing solubility of the conjugated material, long or bulky sidechains can prevent molecules from π-stacking effectively due to steric hindrance and increase the resulting E_g. These three factors are interrelated and targeting one factor for optimization can greatly affect the others.

To reduce bandgap via molecular engineering, two main methods have emerged: enhancing the polymer's quinoidal form and utilizing the donor-acceptor approach.[1,10,11] Foremost, the quinoidal form is a non-degenerate resonance structure of a conjugated material with aromatic monomers, shown in Figure 1.8a. The quinoidal form occurs at a higher energy level than the aromatic form and has a greater electron affinity. Since the two states are non-degenerate, they can both contribute to the observed ground state of the conjugated material. Increasing the quinoidal contribution was shown by Brédas to simultaneously destabilize the conduction band and stabilize the valence band, resulting in a smaller bandgap. A synthetic method to encourage quinoidal form in small molecules is shown in Figure 1.7b.[33] Incorporation of functional groups such as dicyanomethylene force quinoidal geometry across the entire length of conjugation to maintain full octets for each carbon atom.

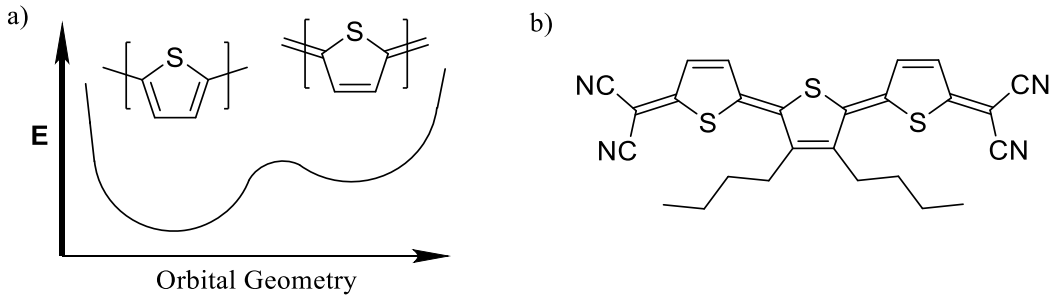

Figure 1.7. Energy states of polythiophene (a) and end-capping to favor the quinoid in an oligomer (b)[33]

The second method of molecular engineering is called the donor-acceptor (DA) approach. First reported by Havinga and coworkers,[34] DA polymers feature alternating monomer units of electron-rich donors and electron-poor acceptors. The electronics of aromatic monomers can be widely altered by modifying the solubilizing sidechains, functional groups, or heteroatoms. A simple dimer of 3,4-diamino- and 3,4-dinitro-thiophene units is depicted in Figure 1.8 as a representative model to demonstrate the DA approach. The corresponding MO diagram models how the monomer's orbitals mix to push the donor's HOMO higher in energy while the acceptor's LUMO is slightly lowered. The new HOMO-LUMO gap for the DA unit is narrower than if the acceptors or donors formed homodimers, and the polymer derived from this dimer exhibited a bandgap of 1.1 eV.[35] Contrary to what this simple model shows, many units previously categorized as either donors or acceptors can act as both types, and thus the DA model is more complicated than what was described above. Current studies from the Rasmussen group show that for fused-ring DA polymers, the HOMO does not lie solely on the donor monomer as previously thought, but tends to be delocalized across the polymer backbone, whereas the LUMO is largely confined to the acceptor monomers.[36] This can explain why the LUMO of the DA system does not change much in energy. As one of the most popular methods to tune a material's bandgap, DA polymers have become quite prolific in the literature.[1,35]

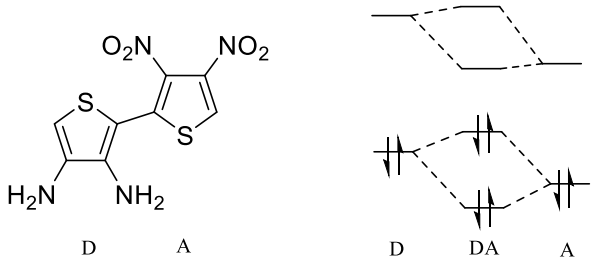

Figure 1.8. A simple DA dimer, with orbital diagram showing decreased HOMO-LUMO gap

A common method to both enhance a polymer's quinoidal form and provide the electronics needed for DA polymers is the use of fused-ring systems in conjugated materials. Highly-aromatic units such as benzene can be fused to heterocyclic monomer's structure, which can limit aromaticity in its fused partner ring to preserve its own aromaticity. This principle was first shown in poly(isothianapthene),[37] which exhibited a bandgap of 1.0 eV, a full electron volt lower than polythiophene.[6] In addition to benzene, heterocycles can be incorporated into monomers via ring fusion, which allows for production of electron-rich or electron poor units for DA polymers. Some examples of fused-ring acceptors and donors are shown in Figure 1.9. Finally, some additional advantages of fused-ring polymers are enhanced planarity, which encourages orbital overlap, and greater π-electron surface area, which enhances π-stacking and encourages interchain interactions as discussed earlier.[26-28]

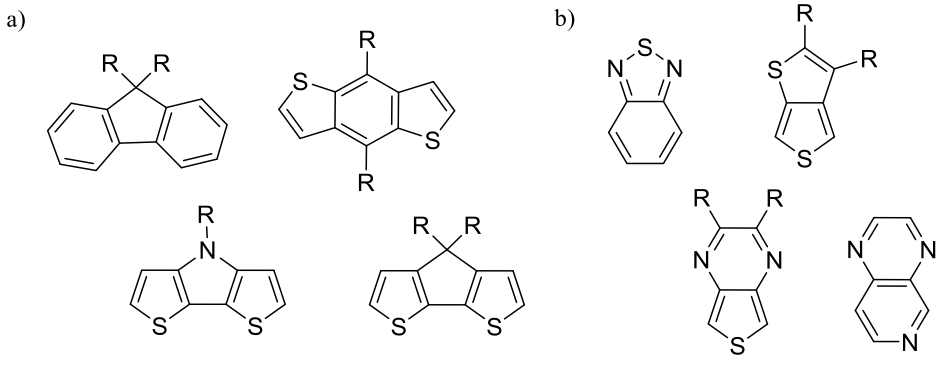

Figure 1.9. Examples of common fused-ring donors (a) and acceptors (b) incorporated into DA polymers

1.4. Thiophene-Based Conjugated Materials

To further the goal of bandgap control and tunability in the field of conjugated materials, the thiophene unit has become an attractive monomer and one of the most widely-used building blocks. Thiophene possesses many advantages over other aromatic systems.[2,6,7,9,36-38] To summarize these traits, the thiophene ring is less aromatic than benzene, more oxidatively stable than furan, and more resistant to basic attack than pyrrole. The polarizable sulfur atom improves charge carrier transport properties and stabilizes polymer chains, which couples with thiophene's unique stacking and self-assembly in the solid state to provide properties that are crucial for applications in electronics. Thiophene exhibits chemical stability in various oxidation states, thermal stability at high temperatures, and great tolerance to synthetic modification, with decades of well-established chemistry.[38] Finally, thiophene is easily produced as a byproduct of petroleum refining[39] or via high-temperature reactions of sulfur dioxide and butanes,[40] making it an inexpensive building block with cost around 0.08 USD per gram.[41] Examples of thiophene-based materials from simple structures to complex fused-ring and inorganic compounds will be presented in the following sections.

The simplest forms of thiophene used in materials chemistry are poly- and oligothiophenes. Examples of each will be presented. Native polythiophene has a bandgap of 2.0 eV,[41] but is limited in material use due to insolubility in organic solvents,[42] This hindrance has been rectified via functionalization of the monomers with solubilizing alkyl chains. For instance, one of the most basic yet ubiquitous thiophene polymers is poly(3-hexylthiophene) (P3HT), depicted in Figure 1.10. Although synthesized with irregular configurations in the 1980's, McCullough reported the first synthesis of regioregular P3HT in 1992.[43,44] Its HOMO and LUMO resided at -5.2 and -3.2 eV respectively, which reflects its powerful electron-donating

and hole-accepting ability. Pairing P3HT with the electron-accepting unit phenyl-C61-buytric acid methyl ester (PCBM) has resulted in organic solar cells with power conversion efficiencies (PCE) beyond 5%.[43] For electronic applications, an additional polythiophene of significance is poly(3,4-ethylenedioxythiophene) (PEDOT). This material is extremely electron-rich, but stable in the oxidized state. PEDOT films are typically doped with poly(styrene sulfonic acid) (PSS) to balance ionic charges, which results in a transparent conducting material.[45] PEDOT:PSS and P3HT are actively applied as hole-transport components for OLEDs and flexible OPVs,[13] serving as primary examples of mass-produced conjugated polymer systems.

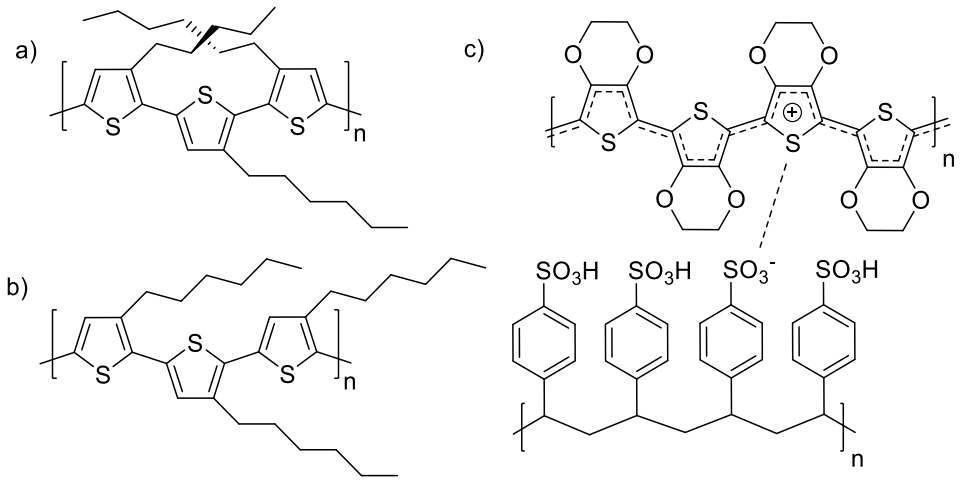

Figure 1.10. P3HT showing irregular (a) and regioregular (b) variants, and the PEDOT:PSS system (c)

Oligothiophenes have been developed in the literature for nearly as long as polythiophenes, and offer certain advantages over their polymeric counterparts.[46] They have a controllable conjugation length, which allows precise tuning of optoelectronic properties in addition to their use as model compounds for the behavior of corresponding polymers, insofar as chain length's effect on such properties.[7]As a result of their small size, they have highly-ordered packing structures which enhance hole-transport properties, an advantage for organic electronic

devices.[48] Additionally, their peripheral units can be easily functionalized, allowing a conjugated core to be applied to many different types of chemistry. For example, thiol-capped oligothiophenes anchor to metal surfaces and are used in nanoparticles.[7,49] Biologically active groups such as carboxylic acids, isocyanates, and amino acids can be attached to oligothiophenes as well (Figure 1.11), allowing the fluorescent thiophene core to be used as a sensor in aqueous solutions where most polythiophenes would be insoluble.[7,50]

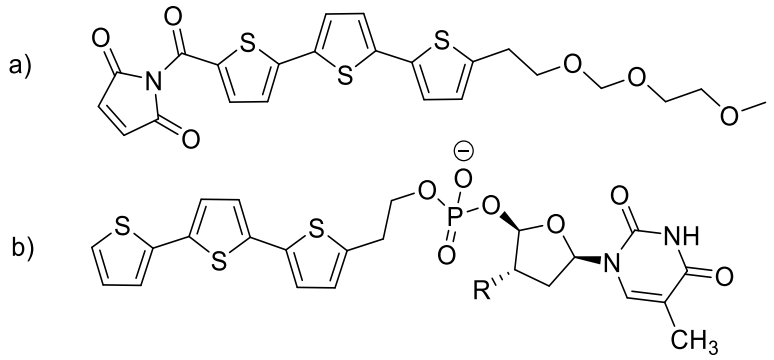

Figure 1.11. Fluorescent oligothiophenes used for antibody labeling (a) and nucleotide labeling (b)

1.5. Fused-Ring Thiophene Materials

While oligothiophenes can be functionalized on their peripheral units for many applications, the thiophene backbone itself can also be functionalized to produce fused-ring units. Two broad categories of fused ring oligothiophenes emerge: moieties fused to the *c*-face of a thiophene (Figure 1.13a), and moieties fused to the *b* or *d* faces. The first category is exemplified by the Rasmussen group's terthienyls, which allow donor-acceptor methods to be applied for small molecules. The featured thieno[3,4-*b*]pyrazine (TP) oligomers (Figure 1.12b) allow the HOMO to be tuned independently of the LUMO based upon proximity of the TP units.[31,36]

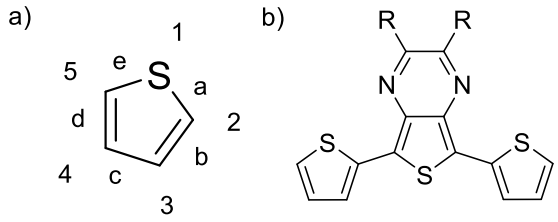

Figure 1.12. Thiophene heterocycle and thieno[3,4-*b*]pyrazine terthienyl

Oligothiophenes fused at the ring's *b* or *d* faces constitute the second category. These oligothiophenes exhibit limited torsional deviations as a result of the fusion bridges, versus simple bithiophenes. In addition to enhancing planarity, this rigidity suppresses non-radiative emission pathways from the excited state, encouraging fluorescence.[51] The rigidity also lowers the energy required for geometrical reorganization that occurs when molecules transition from the ground to excited states.[51,52] Thus, these materials provide higher fluorescent quantum yields and improved charge-carrier mobilities compared to similar thiophene systems.[52] A progression toward optimized fused-ring thiophene materials will be discussed, starting with the simplest example of the two-ring unit theino[3,2-*b*]thiophene (Figure 1.13a).

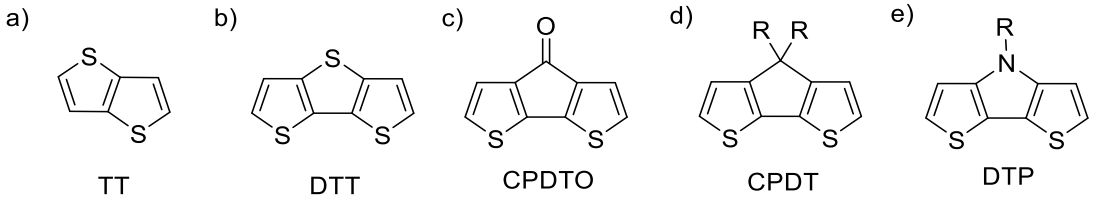

Figure 1.13. (a), thieno[3,2-*b*]thiophene (b), dithieno[3,2-*b*;2',3'-*d*]thiophene (c), cyclopenta[2,1-*b*;3,4-*b*′]dithiophen-4-one (d), cyclopenta[2,1-*b*:3,4-*b*']dithiophen-4-one (e) and ditheino[3,2-*b*;2',3'-*d*]pyrrole

The simplest fused-ring thiophene is thieno[3,2-*b*]thiophene (TT). Homopolymers of TT exhibit a bandgap similar to polythiophene, but with a much lower conductivity.[53] Bridging the 3- and 4'-positions of 2,2'-bithiophene with a sulfur results in a third five-membered ring and

dithieno[3,2-*b*;2',3'-*d*]thiophene (DTT). The DTT molecule (Figure 1.13c) exhibits better charge-carrying ability than the corresponding terthiophene due to better solid-state packing, courtesy of enhanced fused-ring planarity. However, DTT exhibits poor solubility in organic solvents and necessitates functionalization or copolymerization with soluble comonomers to be solution-processible.[61,54] Replacing the backbone-bridging sulfur with a carbon results in cyclopenta[2,1-*b*;3,4-*b'*]dithiophene (CPDT), which allows functional groups to be tethered to the cyclopentane ring. Homopolymers of the ketone-functionalized CPDT (Figure 1.13c) show bandgaps of 1.2 eV,[43] but are akin to DTT in terms of poor solubility. Nevertheless, CPDT units both mono- and di-substituted with solubilizing chains (Figure 1.13d) suffer from poor self-assembly and intermolecular interactions, evidenced by many analogues exhibiting identical absorbances in the solution and solid state.[55]

A fused-ring oligothiophene that acts as one of the strongest electron donors, yet is synthetically robust, is dithieno[3,2-*b*;2',3'-*d*]pyrrole (DTP) (Figure 1.13e).[56-58] The advantages of DTP over CPDT begin with the synthesis, as the number of synthetic steps required to make alkyl CPDTs is often five to seven, compared to two for DTP. This provides a cost and yield advantage for DTPs.[56] Additionally, DTPs do not exhibit ring-opening upon photoexcitation, and provide greater self-assembly in the solid state due to the sp^3 geometric planarity at the pyrrole nitrogen.[55] These factors have allowed the DTP unit to be widely used in such applications as OLEDs. DTP-based polymers even approach commercial viability for OPVs, the designation of which was defined by Dastoor for conjugated materials as requiring three or fewer steps to synthesize from start to finish.[59]

1.6. Hybrid Thiophene Materials

Aside from purely organic polymers and oligomers, thiophenes have also found use as components of inorganic hybrid materials. Thiophene can be incorporated into bulk composite materials in the manner of perovskites, nanocomposites, and coatings for metal clusters.[60-62] These materials often incorporate fluorescent or conductive properties of oligothiophenes into systems designed for drug delivery or redox applications. Additionally, the reverse can occur and metals can be incorporated into polythiophenes. The arrangement of the metal and organic backbone in these hybrid compounds fall into three basic categories: the metal can be linked to the organic backbone through a non-conjugated alkyl spacing chain, electronically connected to the backbone via coordination or conjugation, or directly incorporated into the polymer's conjugated spine.[63,64] Figure 1.15 shows examples of each classification.

Category I polymers use saturated chains to separate the redox activity of the metallic system and thiophene backbone. The redox activity of the coordination complex is considered outer-sphere in nature and largely undisturbed, as the coordination sphere does not overlap with the orbitals that make up the polymer spine. Yet, close proximity between the components can allow electron transfer to occur between the metal complex and the thiophene backbone. Polymers in Category II exhibit greater electronic effects between metallated and non-metallated variants. While still outer-sphere in nature, the coordination and conjugation can enhance both electron delocalization and electron transfer, significantly altering electronics of both the metal and the conjugated system. Additionally, if the metal and polymer's redox potential are matched, an amplifying effect results that greatly increased conductivity. This phenomenon is deemed redox conductivity. Example b in Figure 1.15 exhibited maximum conductivity at the ferrocene

redox potential,[63,65] showing good electron transfer between the CPDT backbone and ferrocenyl groups.

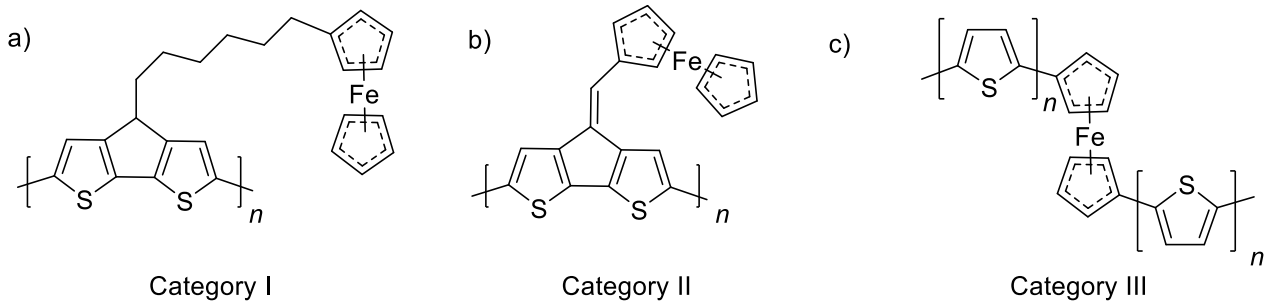

Figure 1.14. Ferrocene units connected to thiophene-based polymers using an alkyl spacer (a), conjugated spacer (b), and direct insertion (c)

The third category of hybrid materials involves direct insertion of the metal into the conjugated material's backbone, as exhibited by example c in Figure 1.15.[63] The orbitals of the metal and backbone can mix to the greatest extent in these polymers due to maximum overlap, causing the nature of electron transfer in these systems to be classified as inner-sphere. Depending on the energetic match between the HOMO of the polymer and the frontier orbitals of the metal, the electronic properties of the both the conjugated backbone and the metal center will be greatly affected,[64] Large bathochromic shifts in the $\pi \rightarrow \pi^*$ bands and charge-transfer bands are often observed. Tuning of the thiophene backbone can push optical absorbances into the NIR, as exemplified by a class of square-planar inorganic complexes known as thiophenedithiolenes (Figure 1.14a).[66-71] These complexes are characterized by their bidentate dithiolate ligands surrounding a core that can consist of a variety of transition metals. The ligands exist in mixed-valence states with different charges present on each ligand, and can exhibit an intervalence charge transfer (IVCT) or ligand-ligand charge transfer band due to promotion of an unpaired electron between dithiolate ligands. Thiophenedithiolenes have found use as superconductors, magnetic materials, and recently as NIR photodetectors.[71,72]

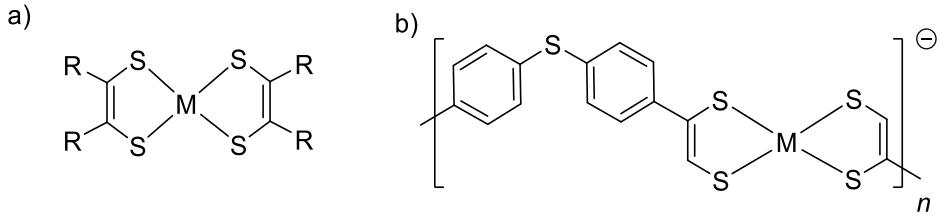

Figure 1.15. General configuration of a square-planar metal dithiolene (a), and polymer exemplifying the Category III polymer configuration with dithiolene core directly inserted into the conjugated backbone[64]

1.7. Thiazole Modifications to Thiophene Materials

The goal of this introduction so far was to describe how the E_g and its analogous HOMO-LUMO gap in conjugated materials affects electronic properties of the material, and how it can be tuned through molecular engineering. The progression from simple polymers towards the fused-ring approach to conjugated units can allow precise control over the properties that determine E_g, and is currently popular with thiophene materials. As a significant example, the most efficient organic solar cell reported as of 2016 utilized fused-ring thiophene oligomers as an active layer, achieving 12.7% efficiency.[73]

A popular approach to precisely tuning the properties of conjugated materials involves incorporation of different heterocycles into the existing motifs. For example, the thiazole ring is gaining notoriety as an electron-deficient alternative to thiophene.[74-77] Thiazole is considered more electron-deficient than thiophene because the electron density from its double bonds are pulled toward the electronegative nitrogen atom, limiting the contribution to the molecule's π-system. Since the thiazole's nitrogen does not contribute its non-bonded electrons to the π-system, its electronegativity impacts the ring's electronics more than in the case of furan, which is still considered electron-rich like thiophene. The three carbons in the thiazole ring all experience lowered electron density compared to thiophene, with C2 having the largest

reduction.[78] Additionally, the pK_a of thiazole is 29.4 compared to 33.0 for thiophene,[79] showing the electron-deficient ring can greater stabilize a negative charge formed by deprotonation.

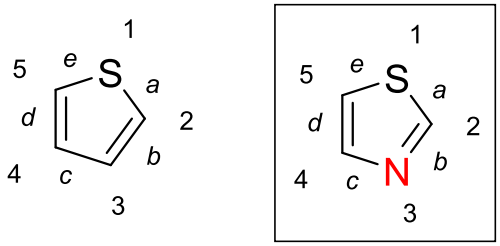

Figure 1.16. Comparison of thiophene and thiazole heterocycles, showing atom and face labels

Although not as prolific as thiophene-based materials in the literature, dozens of polymers and small molecules containing thiazole have been reported thus far as electron-deficient units in OPVs, OFETs, and OLEDs.[74-77] Thiazole-containing polymers for these applications exhibit trends in their optical and electronic properties, including good intermolecular contacts in the solid state,[70] promising performance when blended with common fullerene acceptors,[78-80] and high degrees of interchain interactions.[81-86] These trends lead to high charge-carrier mobility, but also diminished electroluminescent ability and lower external quantum efficiencies compared to current OLED materials.[74]

The existing thiazole materials were also found to exhibit stabilized HOMO and LUMO levels, which is attractive for organic materials. The HOMOs of many thiophene-based polymers such as poly(DTP) lie above the -5.2 eV LUMO of O_2,[87] which means that air can readily oxidize these molecules. Consequently, devices that incorporate such materials are prone to environmental instability. Additionally, the optimal polymer HOMO for OPV devices should lie between -5.27 and -5.9 eV and optimal donor LUMO between -3.7 and -4 eV, to better match the LUMO of common acceptor components such as PCBM, which appears at -4.2 eV.[87,88] The

reason for the slight mismatch in energy levels is to drive the process of exciton dissociation in these devices, which leads to charge separation. For OLEDs, the conducting anode usually has a workfunction of 4.7 to 4.9 eV, and the cathode 2.9 to 4.0 eV,[87,88] so even a slight modulation of the frontier orbitals of polythiophene species such as DTP could allow them to act as both hole- and electron-transport materials. The thiazole heterocycle can potentially offer this stabilization for more classes of materials than thiophene copolymers, but without satisfactory comparisons in the literature, research must be done to compare more families of thiazole oligomers and small molecules to thiophene counterparts.

1.8. Research Goals

Conjugated organic polymers and small molecules have been used as semiconducting materials for applications ranging from light-emitting diodes and conductive plastics to organic solar cells. However, many of the commonly-used fused-ring thiophene materials suffer from consistently high-lying frontier orbital levels, which limit compatibility with common device components and environmental stability of the resulting materials. Substitution of the electron-deficient thiazole ring into thiophene-based materials will provide a method to stabilize the frontier orbitals of these units without altering their structures to a large degree, while simultaneously deriving the structure-function relationships that result. Much work has been published on thiazole containing polymers, but oligomeric systems are not as well known. Considering the advantages of oligomeric units over their polymeric relatives, new families of oligothiazoles must be synthesized to explore how the simple incorporation of thiazole affects the optoelectronic properties of thiophene-based materials. Additionally, the published body of thiazole work does not adequately compare thiazole materials to direct thiophene counterparts, the knowledge of which is critical for precisely optimizing material properties. Thus, thiazole

analogues of the oligothiophene families previously developed by the Rasmussen group will be synthesized and characterized, with focus on the DTP and metal dithiolene systems. Producing new thiazole-containing families of these units will allow direct comparison of the two classes of materials and reveal thiazole's full impact on optical, electronic, and intermolecular properties.

1.9. References

1. Rasmussen, S. C. In *Encyclopedia of Polymeric Nanomaterials*; Müllen, K. Ed.; Springer-Verlag: Berlin, 2013; pp 1-13.
2. Barbella, G.; Melucci, M. In *Handbook of Thiophene-Based Materials: Applications in Organic Electronics and Photonics*; Perepichka, I. F., Perepichka, D. F., Eds.; Wiley: West Sussex, U. K., 2009; Vol. 1, pp 255-292.
3. Rasmussen, S. C.; Ogawa, K.; Rothstein, S. D. In *Handbook of Organic Electronics and Photonics*; Nalwa, H. S., Ed.; American Scientific Publishers: Stevenson Ranch, CA, 2008; Vol. 1, Ch. 1.
4. Christian-Pandya, H.; Vaidyanathan, S.; Galvin, M. In *Handbook of Conducting Polymers*, 3rd ed.; Skotheim, T. A., Reynolds, J. R., Eds.; CRC Press: Boca Raton, FL, 2007; Ch. 5.
5. *Semiconducting Polymers: Chemistry, Physics and Engineering*, Hadziioannou, G.; van Hutten, P. Eds.; Wiley-VCH, Weinheim, 2000.
6. Blanchard, P.; Leriche, P.; Frere, P.; Roncali, J. In *Handbook of Conducting Polymers*, 3rd ed.; Skotheim, T. A., Reynolds, J. R., Eds.; CRC Press: Boca Raton, FL, 2007; Ch. 13.

7. Mishra, A.; Ma, C-Q.; Segura, J.; Bauerle, P. In *Handbook of Thiophene-Based Materials: Applications in Organic Electronics and Photonics*; Perepichka, I., Perepichka, D., Eds.; Wiley: West Sussex, U. K., 2009; Vol. 1, pp 1-157.
8. Friend, R.; Greenham, N. In *Handbook of Conducting Polymers*, 2nd Ed.; Skotheim, T. A., Elsenbaumer, R., Reynolds, J., Eds.; Marcel Dekker, Inc: New York, 1998; pp 823-880.
9. Rasmussen, S. C.; Pomerantz, M. In *Handbook of Conducting Polymers*, 3rd ed.; Skotheim, T. A., Reynolds, J. R., Eds.; CRC Press: Boca Raton, FL, 2007; Ch. 12.
10. Roncali, J. *Chem. Rev*. **1992**, *92*, 711-738.
11. Roncali, J. *Chem. Rev.* **1997**, *97*, 173-205.
12. Thomas, S. W.; Joly, G. D.; Swager, T. M. *Chem. Rev*. **2007**, *107*, 1339−1386.
13. Vosgueritchian, M.; Lipomi, D. J.; Bao, Z. *Adv. Funct. Mater.* **2012**, *22*, 421–428.
14. Gunes, S.; Neugebauer, H. Sariciftci, N. S. *Chem. Rev.* **2007**, *107*, 1324−1338.
15. Naarmann, H.; Theophilou, N. *Synth. Met.* **1987**, *22*, 1-8.
16. CRC Handbook of Chemistry and Physics, 68th ed.; Weast, R. C., Ed.; CRC Press: Boca Raton, FL, 1987, pg F-122.
17. Rasmussen, S. C. *Bull. Hist. Chem.* **2016**, *41*, 64-73.
18. Rasmussen, S. C. *Materials Today* **2016**, *19*, 244-245.
19. Rasmussen, S. C. *Bull Hist. Chem.* **2015**, *40*, 45-55.
20. Rasmussen, S. C. In *Conductive Polymers: Electrical Interactions in Cell Biology and Medicine.* Zhang Z., Rouabhia, M., and Moulton, S. E., Eds; CRC Press: Boca Raton, FL, 2017, pp 1-14.
21. Rasmussen, S. C. *Bull Hist. Chem.* **2014**, *39*, 64-72.

22. Chiang, C. K.; Fincher, C. R.; Park, Y.; Heeger, A. J.; Shirakawa, H.; Louis, E. J.; Gau, S. C.; MacDiarmid, A C.. *Phys. Rev. Lett.* **1977**, *39*, 1098-1101.

23. Scifinder search, https://scifinder.cas.org/scifinder/view/scifinder/scifinderExplore.jsf Accessed 1/9/2017

24. Li, Y. In *Organic Optoelectronic Materials.* Li, Y., Ed; Springer-Verlag: Berlin, 2013; Ch. 2.

25. Van Mullekom, H. A. M.; Vekemans, J. A. J. M.; Havinga, E. E.; Meijer, E. W. *Mat. Sci. Eng.* **2001**, *32*, 1-40.

26. Nakano, T. *Polymer Journal* **2010**, *42*, 103–123.

27. Martinez, C. M.; Iverson, B. L. *Chem. Sci*., **2012**, *3*, 2191-2201.

28. Bredas, J-L.; Beljonne, D.; Coropceneau, V.; Cornil, J. *Chem. Rev.* **2004**, 4971-5003.

29. Khan, A. *Mater. Horiz.*, **2016**, *3*, 7-10.

30. Vissenberg, M. C. J. M.; Matters, M. *Phys. Rev. B.* **1998**, 57, 12964.

31. Mulholland, M. E.; Schwiderski, R. L.; Rasmussen, S. C.*; Chem. Commun*., **2011**, *47*, 11394-11410.

32. Kinbara, E.; Kunugi, Y.; Harima, Y.; Yamashita, K. *Synth. Met.* **2000**, *114*, 295.

33. Zsoldos, Z.; Szabo, I.; Szabo, Z.; Johnson, A. *J. Mol. Structure* **2003**, 665–673.

34. Havinga, E. E.; ten Hoeve, W.; Wynberg, H. *Poly. Bull.* **1992**, *19*, 119-126.

35. Ajayaghosh, A. *Chem. Soc. Rev.*, **2003**, *32*, 181–191.

36. Mulhollhand, M. E.; Schwiderski, R. L.; Rasmussen, S. C.; *Poly. Bull.* **2012**, *69*, 291-301.

37. Wudl, F.; Kobayashi, J.; Heeger, A. J. *J. Org. Chem.* **1984**, *49*, 3382-3384.

38. Guo, X.; Baumgarten, M.; Mullen, K. *Prog. Poly. Sci.* **2013**, *38*, 1832-1908.

39. Mishra, R.; Zha, K.; Kumar, S.; Tomer, I. *Der Pharma Chemica* **2013**, *3*, 38-54.

40. Conary, R. E.; Kreuz, K. A. *Ind. Eng. Chem.* **1950**, *43*, 467-471.

41. Grimsdale, A. C.; Chan, K. L.; Martin, R. E.; Jokisz, P. G.; Holmes, A. B. *Chem. Rev.* **2009**, *109*, 897-1091.

42. Frommer, J. E. *Acc. Chem. Res.*, **1986**, *19*, 2–9.

43. Cheng, Y.; Yang, S.; Hsu, C. *Chem. Rev.* **2009,** *109*, 5868–5923.

44. Chang, J.-F.; Sun, B.; Breiby, D. W.; Nielsen, M. M.; Solling, T. I.; Giles, M.; McCulloch, I.; Sirringhaus, H. *Chem Mater* **2004**, *16*, 4772–4776.

45. Groenendaal, L.; Jonas, F.; Freitag, D.; Pielartzik, H. Reynolds, J. R. *Adv. Mater.* **2000**, *12*, 481-494.

46. Zhang, L.; Colella, N. S.; Cherniawski, B. P.; Mannsfeld, S. C. B.; Briseno, A. L. *ACS Appl. Mater. Interfaces*, **2014**, *6*, 5327–5343.

47. Mishra, A.; Ma, C-Q.; Bauerlie, P. *Chem. Rev.* **2009,** *109*, 1141–1276.

48. Fichou, D. *J. Mater. Chem.* **2000**, *10*, 571-588.

49. Tamura, M.; Fujihara, H.; *J. Am. Chem. Soc.* **2003**, *125*, 15742-15743.

50. Ammann, M.; Bauerle, P.; *Org. Biomol. Chem.* **2005**, *3*, 4143-4152.

51. Turro, N. J.; Ramamurthy, V. Scaiano, J. C. In *Modern Molecular Photochemistry of Organic Molecules.* Viva Books: Delhi, India, 2017; Ch. 4.

52. Rasmussen, S. C.; Evenson, S. J.; McCausland, C. B. *Chem. Commun.* **2015**, *51*, 4528-4543.

53. Skabara, P. J. In *Handbook of Thiophene-Based Materials: Applications in Organic Electronics and Photonics*; Perepichka, I. F., Perepichka, D. F., Eds.; Wiley: West Sussex, U. K., 2009; Vol. 1, pp 220-254.

54. Biserni, M.; Marinangeli, A.; Mastragostino, M.; Cerroni, M. *J. Electrochem. Soc.* **1985**, 132, 1597-1601.

55. Coppo, P.; Turner, M. L. *J. Mater. Chem.*, **2005**, *15*, 1123–1133.

56. Ogawa, K.; Radke, K. R.; Rothstein, S. D.; Rasmussen, S.C. *J. Org. Chem.* **2001**, *66*, 9067-9070.

57. Ogawa, K.; Rasmussen, S. C. *J. Org. Chem.* **2003**, *68*, 2921-2928.

58. Evenson, S. J; Pappenfus, T. M.; Ruiz Delgado, M. C.; Radke-Wohlers, K. R.; Lopez Navarrete, J. T.; Rasmussen, S.C. *Phys. Chem. Chem. Phys*., **2012**, *14*, 6101–6111.

59. Dastoor, P. Oral Presentation, "Organic solar cells and solar paint: from benchtop to rooftop and beyond". 42nd Annual Great Lakes Regional Meeting of the American Chemical Society, June 27th, 2017, Fargo ND.

60. Chondroudis, K.; Mitzi, D. B. *Chem. Mater*. **1999**, *11*, 3028-3030.

61. Lupu, S. ; Lete, C.; Marin, M. Totir, N.; Balaure, P. C. *Electrochimica Acta* **2009**, *54*, 1932–1938.

62. Quarta, A.; Di Corato, R.; Manna, L.; Argentiere, S.; Cingolani, R.; Barbarella, G.; Pellegrino, T. *J. Am. Chem. Soc***. 2008**, *130*, 10545–10555.

63. Wolf, M. O. *Adv. Mater*. **2001**, *13*, 545-553.

64. Stott, T. L.; Wolf, M. O. *Coord. Chem. Rev.* **2003**, *246*, 89-101.

65. G. Zotti, S. Zecchin, G. Schiavon, A. Berlin, G. Pagani, A. Canavesi, *Chem. Mater.* **1995**, *7*, 2309.

66. Stiefel, E. J., Ed. *Dithiolene Chemistry: Synthesis, Properties, and Applications.* Progress in Inorganic Chemistry, Vol. 52, John Wiley and Sons: Hoboken, NJ, 2004.

67. Cassoux, P. *Coord. Chem. Rev.* **1999**, *185-186,* 213-232.

68. Robertson, N.; Cronin, L. *Coord. Chem. Rev.* **2002**, *227*, 93–127.

69. Kato, R. *Chem. Rev*. **2004**, *104*, 5319-5346.

70. Eisenberg, R.; Gray, H. B. *Inorg. Chem.* **2011**, *50*, 9741-9751.

71. Amb, C. M.; Rasmussen, S. C. *Synth. Met.* **2009**, *159*, 2390-2393.

72. Uzelac, E.; Rasmussen, S. C.; *Eur. J. Inorg. Chem.* **2017**, *33*, 3878-3883.

73. Li, M.; Gao, K.; Wan, X.; Zhang, Q.; Kan, B.; Xia, R.; Liu, F.; Yang, X.; Feng, H.; Ni, W.; Wang, Y.; Peng, J.; Zhang, H.; Liang, Z.; Yip, H.; Peng, X.; Cao, Y.; Chen, Y. *Nature Photonics* **2017**, *11*, 85-90.

74. Lin, Y.; Fan, H.; Li, Y.; Zhan, X. *Adv. Mater*. **2012**, *24*, 3087-3106.

75. Jung, I.; Jung, Y.; Lee, J.; Park, J.; Woo, H.; Lee, J.; Che, H.; Shim, H. *J. Poly. Sci. Part A. Poly. Chem.* **2008**, 7148-7161.

76. Wu, Y.; Zhu, W. *Chem. Soc. Rev.*, **2013**, *42*, 2039-2058.

77. Getmaneko, Y. A.; Risko, C.; Tongwa, P.; Kim, E.-J.; Li, H.; Sandhu, B.; Timofeeva, T.; Bredas, J.-L.; Marder, S. R. *J. Org. Chem.* **2011**, *76*, 2660-2671.

78. Katritzky, A. R.; Pozharskii, A. F. *Handbook of Heterocyclic Chemistry*, 2nd ed.; Pergamon: Oxford, 2000; pp 126.

79. Shen, K.; Fu, Y.; Li, J. N.; Liu, L.; Guo, Q. *Tetrahedron* **2007**, *63*, 1568-1576.

80. McCulloch, I.; Heeney, M.; Bailey, C.; Genevicius, K.; MacDonald, I.; Shkunov, M.; Sparrowe, D.; Tierney, S.; Wagner, R.; Zhang, W.; Chabinyc, M. L.; Kline, R.; Mcgehee, M. D.; Toney, M. F. *Nat. Mater*. **2006**, *5*, 328-333.

81. Zhang, M.; Fan, H.; Guo, X.; He Y.; Zhang Z.; Min, J.; Zhang J.; Zhao G.; Zhan X.; Li, Y. *Macromolecules* **2010**, *43*, 8714-8717.

82. Li, Z.; He, G.; Wan, X.; Liu, Y.; Zhou J.; Long, G.; Zuo, Y.; Zhang, M.; Chen, Y. *Adv. Energy Mater.* **2012**, *2,* 74-79.

83. Sun, Y.; Welch, G.; Leong, L.; Takacs, C.; Bazan, G.; Heeger, A. *Nat. Mater.* **2012**, *11*, 44-48.

84. Shi, Q.; Cheng, P.; Li, Y.; Zhan, X. *Adv. Energy Mater*. **2012**, *2*, 63-67.

85. Yamamoto, T.; Suganuma, H.; Maruyama, T.; Inoue, T.; Muramatsu, Y.; Arai, M.; Komarudin, D.; Ooba, N.; Tomaru, S.; Sasaki, S.; Kubota, K. *Chem. Mater.* **1997**, *9*, 1217-1225.

86. Nanos, J. L.; Kampf, J. W.; Curtis, M. D.; Gonzalez, L.; Martin, D. C. *Chem. Mater.* **1995**, *7*, 2232-2234.

87. Blouin, N.; Michaud, A.; Gendron, D.; Wakim, S.; Blair, E.; Neagu-Plesu R.; Belletete, M.; Durocher, G.; Tao, Y. Leclerc, M. *J. Am. Chem. Soc.* **2008**, *130*, 732-742.

88. Lu, L.; Zheng, T.; Wu, Q.; Schneider, A.; Zhao, D.; Yu, L. *Chem. Rev.* **2015**, *115*, 12666−12731.

CHAPTER II. SYNTHESIS OF BROMINATED THAIZOLES AS PRECURSORS TO THIAZOLE-BASED MATERIALS

2.1. Introduction

Brominated aromatic systems are a cornerstone in the synthesis of conjugated chemical materials, providing a functional group that allows cross-couplings, oxidative couplings, and many other synthetic transformations. Most of the conjugated materials reported to date involve carbon-carbon bond formation via brominated precursors. A subset of these systems, bromothiophenes, provide a bridge to the production of functionalized thiophenes,[1] which are used as building blocks for not just materials such as conjugated polymers, but pharmaceuticals and natural products as well.[2-4] To synthetically tune the optical and electronic properties of thiophene-based species, the closely-related thiazole heterocycle has seen an increase in popularity as an electron-deficient unit to replace thiophene.[5–9] Thus, a need to produce various bromothiazoles has emerged.

Although thiazole only differs from thiophene by replacing one C-H group with a nitrogen atom, methods that are commonly used to produce bromothiophenes, such as regioselective brominations with *N*-bromosuccinimide (NBS) or Br_2, cannot be directly applied to thiazole. Thiazole is both less aromatic and less electron rich than thiophene, which disfavors electrophilic aromatic substitution on the thiazole ring compared to thiophene and necessitates harsher reaction conditions to achieve bromination.[10,11] Additionally, the nitrogen atom renders the thiazole ring asymmetric, and each carbon of the ring thus has a different electron density. Consequently, each position on the thiazole ring is energetically inequivalent, leading to different reactivity and different methods needed to functionalize them.[12,13]

There are seven members of the bromothiazole family (Figure 2.1), all of which have been previously reported in the literature: 2-bromothiazole,[14–16] 4-bromothiazole,[17–19] 5-bromothiazole,[15,17,20] 2,4-dibromothiazole,[16,17,19,21,22] 2,5-dibromothiazole,[15–17,20,23] 4,5-dibromothiazole,[19,21] and 2,4,5-tribromothiazole,[19,24,25]. However, the studies reporting most of these molecules are dated, having taken place in the mid 20th-century. Thus, the characterization for these compounds has been incomplete, possibly due to limits of available instrumentation at the time. Additionally, some of the molecules were not fully characterized because of the reaction conditions, with 4,5-dibromothiazole serving as the best example. It has only been synthesized as a component of an inseparable mixture or in trace amounts.[19,21]

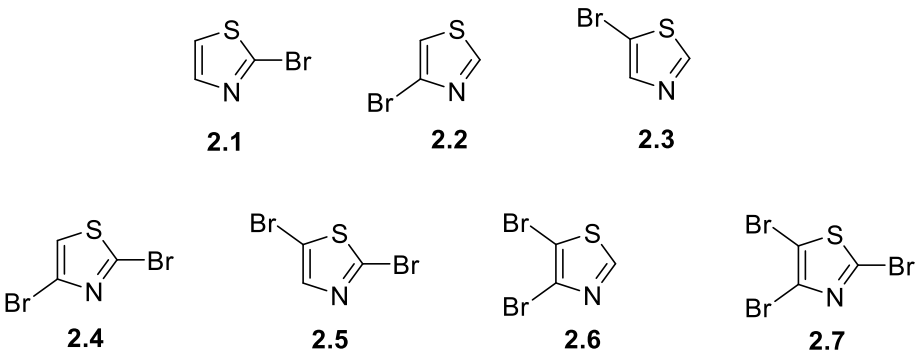

Figure 2.1. Seven members of the brominated thiazole family: 2-bromothiazole (**2.1**), 4-bromothiazole (**2.2**), 5-bromothiazole (**2.3**), 2,4-dibromothiazole (**2.4**), 2,5-dibromothiazole (**2.5**), 4,5-dibromothiazole (**2.6**), and 2,4,5-tribromothiazole (**2.7**)

The Rasmussen lab had been using 2-bromothiazole (**2.1**) and 2,4-dibromothiazole (**2.4**) for various projects in the past, and followed the existing literature procedures without issue. However, the new ideas to incorporate thiazole into the fused-ring cores of materials studied by the group required other brominated thiazoles to be synthesized. Because of the existing limitations in the synthetic methods and characterization of the bromothiazole family, it was decided to revisit the syntheses of each member to seek optimized reaction conditions and full

characterization. The journey towards optimization of each of the seven molecules will be discussed in the following subsections. This work was recently published in *The Journal of Organic Chemistry.*[26]

2.2. Synthesis of 2-bromothiazole

As opposed to thiophene, the parent thiazole ring is electron-deficient and therefore experiences reduced reactivity to direct bromination. The starting material 2-aminothiazole is used instead, which is comparatively electron-rich and inexpensive. The Rasmussen group originally used this starting material in a custom Sandmeyer-type reaction in which 2-aminothiazole was protonated with HBr and cooled in an ice bath, followed by diazonium formation with $NaNO_2$ and substitution with bromide to yield 2-bromothiazole **2.1** (Scheme 2.1, Route A). This method provided both the necessary acidic conditions and bromine atom in one reagent, but suffered from low product yield at 25-33%.

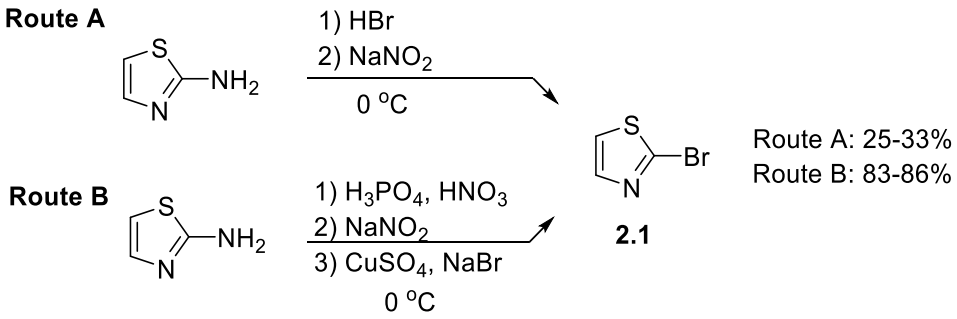

Scheme 2.1. Synthesis of 2-bromothiazole

The optimized method, however, has been reported in multiple variants. Ganapathi and Venkataraman reported a Sandmeyer-type reaction in 1945,[14] which involves the amino group's conversion to a diazonium compound with $NaNO_2$ and subsequent attack by bromide originating from NaBr/$CuSO_4$ mixture (Scheme 2.1, Route B). The authors reported 75% yield, which is substantially higher than the HBr conditions we employed. Since the mechanism of the

Sandmeyer reaction is traditionally thought to occur via a copper(I)-catalyzed radical mechanism,[27] the lack of this copper species in our conditions may have caused the reduction in yield, with a less-facile substitution mechanism predominating. However, the copper used in Ganapathi's conditions is copper(II), and so the role of Cu atom may simply be to coordinate to the π-bond of the diazonium species, encouraging substitution.

A modified procedure with careful temperature control and longer reaction times was reported by Roussel and Metzger in 1962,[15] which involved an increase in yield to 80%, although others have reported 90% yield with their methods.[28] Utilizing these conditions, it was noted that keeping the reaction temperature as close to 0 °C as possible was crucial, as any deviation towards 5 °C would result in product decomposition and black film formation in the reaction vessel. Sampson and coworkers reported the synthesis again in 2001,[16] although their methods were largely similar to the previous authors with no additional yield increase noted. The procedure from Roussel and Metzger was found to be the most optimized synthesis of 2-bromothiazole, and provided consistent 83-86% yields when employed herein.

2.3. Synthesis of 4-bromothiazole

Featuring a bromine in the least reactive position on the thiazole ring, 4-bromothiazole has typically been produced from 2,4-dibromothiazole via metal-halogen exchange with Grignard reagents or butyllithium.[17-19] Since the Rasmussen group had ample experience synthesizing 2,4-dibromothiazole, its debromination was explored early in this study. The typical yields for the production of 4-bromothiazole are around 70%, but cryogenic temperatures and pyrophoric reagents are necessary using the literature procedures. We sought to avoid these costs and conditions, and employed hydride attack via $NaBH_4$ in acetonitrile at reflux (Scheme 2.2).

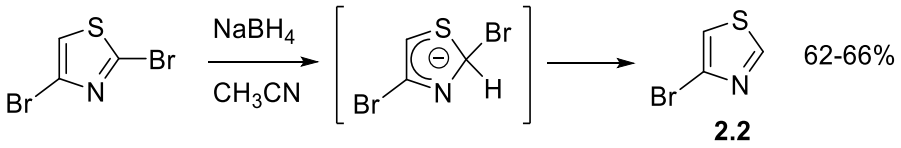

Scheme 2.2. Synthesis of 4-bromothiazole via hydride attack with $NaBH_4$

Examining the solvent, temperature, and stoichiometry through repeated trials led to the ideal reaction conditions. $NaBH_4$ was found to be insoluble in solvents with lower polarity such as chloroform and THF. Reflux temperatures were also necessary for this reaction, as the hydride attack did not proceed at room temperature. Finally, two equivalents of hydride were needed to convert all of the starting material to products, as 1.0-1.5 equivalents produced a mixture of starting material and product that required careful column chromatography to separate. The highest yields were 62-66% for this synthesis, which is a small decrease from the previous reports. Yet, the new method is advantageous nonetheless due to avoidance of both cryogenic conditions and pyrophoric reagents.

2.4. Synthesis of 2,4-dibromothiazole

Similar to 2-bromothiazole, 2,4-dibromothiazole (**2.4)** has not been produced via reaction from the parent thiazole ring or a brominated precursor, as the 4-position of thiazole is much less reactive to electrophilic bromination than the 2- or 5-positions. A deoxygenation and bromination of 2,4-hydroxythiazole via phosphoryl bromide ($POBr_3$) was first reported by Reynaud and coworkers in 1962,[21] which gave the desired product in 60% yield. Stattney substituted 2,4-thiazolidinedione for the dihydroxythiazole in 2006,[17] providing a more cost-effective starting material. In 2012, Sampson and coworkers replaced $POBr_3$ with phosphorous pentoxide (P_4O_{10}), commonly known by the empirical formula P_2O_5.[29] They added tetrabutylammonium bromide as a bromide source, and attained 95% yield.[16] This yield may be

scale-dependent, as our reactions with Sampson's methods were at approximately one-tenth the scale and produced **2.4** in 85-91% (Scheme 2.3).

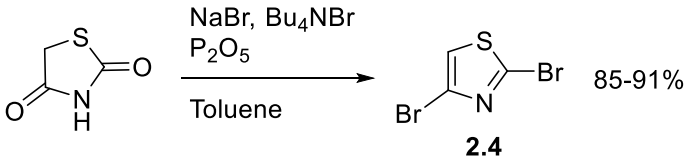

2.4

Scheme 2.3. Sampson's methods to produce **2.4**

When seeking further optimization of Sampson's conditions, attempts to change the bromide source was the main focus. Although tetrabutylammonium bromide is readily available, using an even less expensive source of bromide would allow for more cost-effective production on a larger scale. Thus, we attempted to produce **2.4** with NaBr. No product was observed using Sampson's conditions, and solubility of the bromide salt appeared to be the hinderance. To increase solubility of NaBr[30] and thus prompt nucleophilic attack by a bromide, a catalytic amount of either 1,4,7,10,13,16-hexaoxacyclooctadecane (18-crown-6) or tetramethylethylenediamine (TMEDA) was added to further trials. Still, no product was observed during any screening of these reaction conditions.

An interesting phenomenon observed during the workup of **2.4** was the growth of large, clear, needle-like crystals on the edge of the glassware. Attempts were made to grow crystals via slow evaporation, recrystallization in hexanes, and recrystallization in methanol. While these methods did produce the same type of crystals observed during workups, the crystals were very malleable and difficult to lacerate for x-ray diffraction preparation. Although we were not able to obtain x-ray data, the crystal structure of **2.4** was recently published.[31] When crystals of the other bromothiazoles **2.6** and **2.7** were attempted to be analyzed, the same malleability and rubbery properties were observed, and no crystallography data was obtained. Nevertheless, with such

high yield and simple conditions, Sampson's method represents the most optimized synthesis of **2.4**. However, our experiments with crystal growing led to the modification of the purification of **2.4**, as running the product through a short silica plug provided an easier and quicker alternative to purification than sublimation.

2.5. Synthesis of 2,5-dibromothiazole

The synthesis of 2,5-dibromothiazole **2.5** has been accomplished in the literature by two main routes: the Sandmeyer reaction of brominated aminothiazole, and the direct bromination of 2-bromothiazole **2.1**. Each method and its optimization will be discussed. The first reported synthesis of **2.5** utilized the Sandmeyer reaction, and was published in 1945 by Erlenmeyer and Kiefer.[23] It involved the bromination of 2-aminothiazole with liquid bromine to yield the intermediate 2-amino-5-bromothiazole, which underwent a Sandmeyer reaction to convert the amine to a bromide (Scheme 2.4). The authors used a copper/HBr mixture, which gave the product in 40% yield, but the authors did not specify the yield of 2-amino-5-bromothiazole. In 1954, Beyerman and coworkers replaced the copper/HBr mixture with the familiar NaBr/$CuSO_4$ to produce the desired material,[20] and Roussel further modified the reaction in 1962 to give an overall yield of 38% from the 2-aminothiazole starting material.[15]

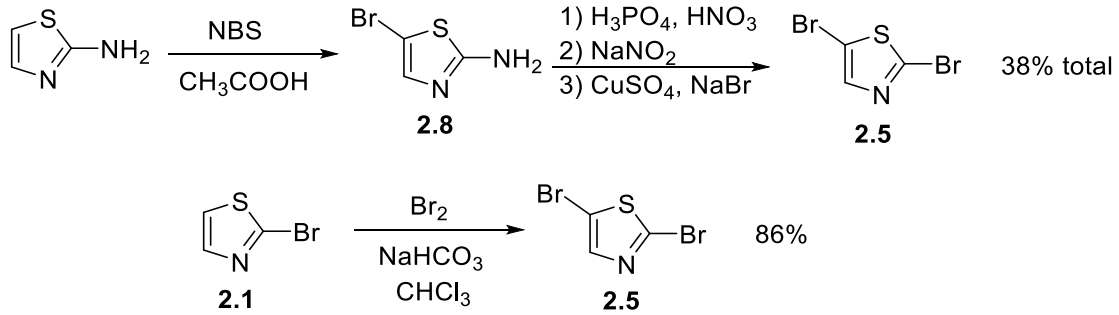

Scheme 2.4. Synthesis of **2.5** via Sandmeyer conditions or direct bromination of **2.1**

The second route to 2,5-dibromothiazole was first reported by Stanetty in 2006,[17] and used an aqueous mixture of HBr and Br_2 to generate **2.5** in 55% yield. The subdued reactivity of **2.1** to electrophilic aromatic substitution necessitated 4.8 equivalents of Br_2 to produce **2.5**. The large excess of bromine is necessary to increase the reaction rate to the point where **2.5** can be produced. Sampson and coworkers modified the reaction conditions to use $CHCl_3$ and $NaHCO_3$ with Br_2 at room temperature (Scheme 2.5), which along with an increase in reaction time from 3 h to 96 hs, produced **2.5** in 79% yield. Still, approximately four equivalents of Br_2 were being discarded with this procedure, prompting us to examine methods to optimize this reaction. Attempts were first made to produce **2.5** by substituting NBS as the brominating agent, but synthesis was unsuccessful, returning starting material no matter the excess involved. The reaction was then attempted with acetic acid as the solvent, both at room temperature and reflux. It was thought that the acid would protonate NBS, providing a more electrophilic bromine atom for substitution, but this approach also returned starting material.

Attempts were then made to synthesize **2.5** using the reaction of LDA with **2.1,** under the idea that lithiation of the 5-position of the ring would provide increased reactivity towards the electrophilic NBS bromine atom (Scheme 2.5). Once lithiation had occurred, the NBS was added at cryogenic temperatures and the reaction was allowed to warm to room temperature overnight. However, while lithiation was successful as evidenced by the return of **2.1** as starting material, an insufficient amount of product was formed. These conditions were repeated with Br_2 as the brominating agent, but no significant differences in yield were noted.

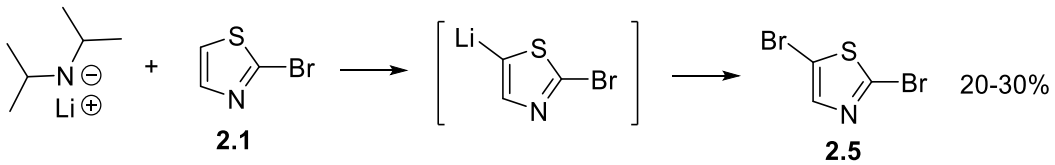

Scheme 2.5. Attempted lithiation and bromination of **2.1** to synthesize **2.5**

Finally, efforts shifted to limiting the amount of bromine used in the reaction. To obtain the best balance between atom efficiency and yield, we found that 2.5 equivalents of Br_2 and 24 h reaction time produced exclusively **2.5** in 65-70% yield. Lower stoichiometric equivalents of Br_2 led to a greater portion of starting material in the reaction no matter the excess stirring time, while greater equivalents did not increase the yield of **2.5**. Although this yield is circa 10% lower than what Sampson reported, the reaction time is cut by 75% and the amount of Br_2, the most expensive and toxic reagent, is cut in half.

Since bromine is a highly-toxic reagent that can cause pulmonary edema or asphyxiation from as little as 546 ppm for 10 min exposure,[32-34] completely removing Br_2 from the synthesis of **2.5** was attractive. Since both routes to **2.5** involve Br_2 use at some point, we reexamined the route through 2-aminothiazole. Since adding electron-rich functional groups to thiazole should increase its favorability to electrophilic aromatic substitution, we attempted bromination with NBS. Despite NBS being a weaker brominating agent, the reaction was successful with yields around 56-57%. This intermediate was found to be quite unstable and polymerize quickly, even under N_2 atmosphere in the dark, so the Sandmeyer reaction to convert the amino group to a bromine was performed as soon as **2.8** was generated. The reaction of **2.8** to **2.5** was performed in 60-65% yield leading to an overall yield of 37% for the Sandmeyer route. Although this is about 20% lower in yield than direct bromination, it allows for the production of **2.5** without the use of Br_2.

2.6. Synthesis of 2,4,5-tribromothiazole

2,4,5-tribromothiazole **2.7** was first reported in 1964 by Robba and Moreeau,[24] who reacted 2,4-hydroxythiazole with excess bromine, attaining 85% yield. Another method utilizing the harsh reaction conditions of bromine and acetic acid was reported in 1967 by Herkes and

Blazer,[25] which uses 2,4-dibromothaizole **2.4** as a starting material. Since these methods both utilized Br_2, we sought to produce **2.7** with the less harsh and less toxic NBS (Scheme 2.6).

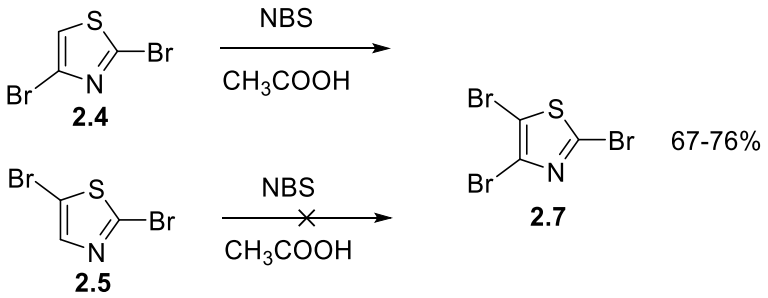

Scheme 2.6. Successful bromination of **2.4** to produce **2.7,** whereas duplication with **2.5** was unsuccessful

Although the monobromination of **2.5** with NBS was not successful, the extra electron density provided by the bromine at the 4-position should allow electrophilic aromatic substitution to proceed. The reaction of **2.4** with 1.5 eq. NBS in acetic acid produced **2.7** in 68-76% yield (Scheme 2.6). Larger excess of NBS did not increase this yield. Additional attempts to produce **2.7** from **2.5** were undertaken as well, but the sharp decrease in reactivity between thiazole's 5- and 4-positions was significant enough to prevent bromination, despite the added electron density of an α-bromine at the 4-positon.[35] Overall, although our method suffers from a 10% reduction in yield compared to Herkes and Blazer, the avoidance of Br_2 as a reagent is worthwhile for safety reasons.

2.7. Synthesis of 4,5-dibromothiazole

The molecule 4,5-dibromothiazole (**2.6**) is the only member of the brominated thiazole family that has never been fully reported in isolation. Between Moreau's work in 1962 and Iddon's work in 1992, both publications report **2.6** in either trace amounts or as part of a complex mixture involving **2.4** and **2.5**. The desired compound was not able to be purified. Considering the electronic similarity between thiazole's 2- and 5-positions,[35] bromination of 4-

bromothiazole **2.2** was theorized to produce a complex mixture of products with bromines on various positions. Thus, our efforts to selectively access **2.6** and obtain a pure sample began with attempts to debrominate **2.7**.

Initial conditions used were simple, beginning with butyllithium in ethereal solvents such as THF and diethyl ether. However, the reactions almost exclusively produced **2.4**. This was attributed to the halogen dance, a gradual exchange of substituents on a lithaited thiazole due to thermodynamics vs. kinetics.[36,37] A proposed mechanism of the halogen dance to yield **2.6** from **2.7** is shown in Scheme 2.7. As stated before, the 2- and 5-positions of thiazole are very similar in energy,[35] but we found via GC/MS that the initial metal halogen exchange predominates on the 5-position. Over time, unreacted **2.7** undergoes metal-halogen exchange with 2,4-dibromo-5-thiazolyllithium to lithiate the 2-position, placing the lithium on the thermodynamic position. We found that halogen dance favors the kinetic product over the thermodynamic product in ethereal solvent, potentially due to the fast rate of reaction. If the rate of lithiation of **2.7** is greatly increased, transfer to the thermodynamic position decreases.

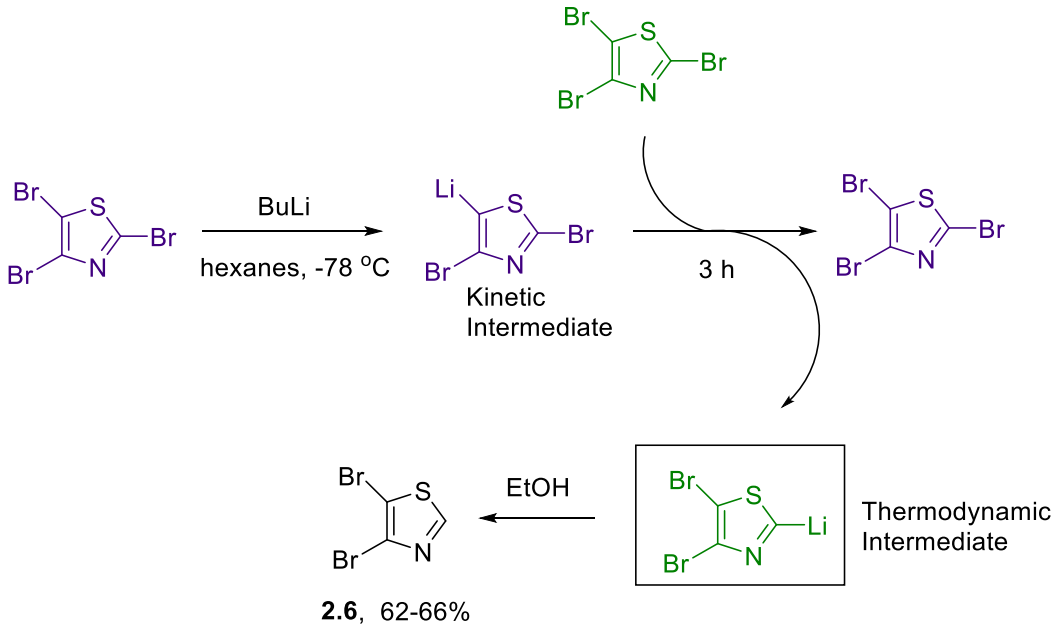

Scheme 2.7. Synthesis of **2.6** via exploitation of the halogen dance to gradually lithiate the 2-position

The next attempts at synthesizing **2.6** involved Grignard reagents, including the sterically-bulky isopropyl magnesium chloride. The steric bulk was thought to prohibit attack at the 5-position due to the large adjacent bromine. However, **2.4** was produced almost exclusively from these reactions as well. Borrowing our ideas from the synthesis of 4-bromothiazole **2.2**, we used $NaBH_4$ for a hydride source, with the idea that at high temperatures, the reactivity difference between the 2- and 5- positions would become negligible. Once again, only **2.4** was produced.

Considering the thermodynamic vs. kinetic products for this reaction and that the speed of the lithiation was preventing the halogen dance from occurring, we decided to examine the butyllithium conditions once more with a new idea. Considering that butyllithium forms aggregates in solution,[37] a solvent that disfavors the breakup of these aggregates was postulated to slow the initial metal-halogen exchange of **2.7** and allow time for the halogen dance to lithiate the desired position. Hexanes was chosen, and monitoring the reaction with GC/MS showed that

the product shifted from **2.4** to the desired **2.6** over the course of 3 h. The yield of this reaction ranged from 60-66%, and simple purification via column chromatography provided analytically-pure samples without contamination from other analogues.

2.8. Synthesis of 5-bromothiazole

The final member of the bromothiazole family (**2.3**) proved the most arduous to synthesize. First reported by Beyerman and coworkers in 1954, the most practical literature preparation of this species came from Stattney and coworkers in 2006, who debrominated 2,5 dibromothiazole with isopropylmagnesium chloride to generate **2.3** in 20% yield. Our efforts to produce this species began with the reexamination of Stattney's conditions to elucidate why the yield was so low. However, no matter the type of alkyllithium species or Grignard employed, attempts at performing this method never produced isolatable product, only a mix of starting material and 2-bromothiazole (Scheme 2.8). Next, the sodium borohydride conditions used to produce **2.3** were applied, but only 2-bromothiazole was produced yet again. The absence of the bromine on the 4-position should have made the 5-position less reactive towards metal-halogen exchange due to resonance effects. Yet, even if the thermodynamic product should have been **2.3**, the kinetic product **2.2** was still favored. The energies of the 5- and 2-positons must be relatively close in energy during the transition state, because although 2-bromothiazole undergoes selective photolysis more rapidly than 5-bromothiazole, 5-bromothiazole reacts with sodium methoxide faster than 2-bromothiazole. Nevertheless, these routes were set aside.

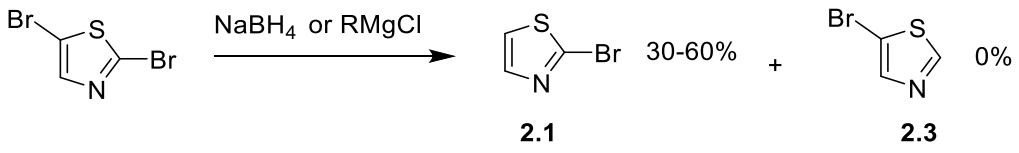

Scheme 2.8. Attempted synthesis of **2.3** via previously reported conditions and hydride attack

The next attempts at synthesizing this molecule involved protection of the 2-position with silyl groups, depicted in Scheme 2.9. It was postulated that protecting the 2-position and subsequently brominating would selectively brominate the 5 position, after which deprotection would yield 5-bromothiazole. Since trimethylsilyl will migrate positions around lithiated thiazoles akin to the halogen dance,[36,37] the bulky triisopropylsilyl (TIPS) group was chosen. 2-triisopropylsilyl-5-bromothiazole was synthesized according to literature procedures, but upon deprotection with tetrabutylammonium fluoride (TBAF) in THF, a black decomposition product coated the reaction vessel. Lithiated thiazoles are known to be unstable at temperatures greater than -40 °C,[38] so deprotection was attempted at -78 °C. Unfortunately, the cryogenic temperatures halted the reaction of fluoride anion with the TIPS group. With the conditions of anion stability and reactivity unable to be fulfilled simultaneously, the TIPS route was not pursued further.

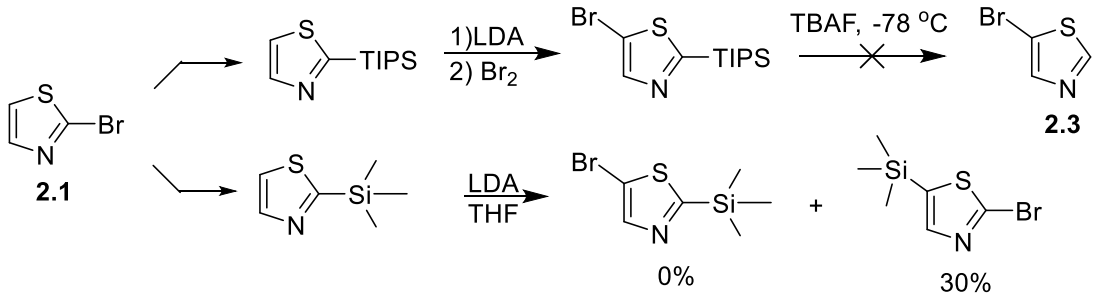

Scheme 2.9. Attempted synthesis of **2.3** via silyl protection of the 2-position

Since TMS groups are able to be removed with both fluoride anion and acidic conditions with HCl, the reaction was attempted again with TMS. Theoretically, deprotection of 2-trimethylsilyl-5-bromothiazole under acidic conditions should limit decomposition and ring opening, because protonation would occur at a much faster rate. However, the synthesis of the precursor was unable to be performed in adequate yield. The halogen dance resulted in synthesis

of 2-bromo-5-trimethylsilylthiazole, but no desired product. Thus, both attempted routes to **2.3** through silyl protection were discarded.

The next idea to produce **2.3** was a re-visitation of the conditions used to synthesize **2.6** (Scheme 2.10). Since the thermodynamic product was produced over time by using hexanes as a solvent with butyllithium, attempts were made to duplicate this reaction with **2.5** instead of **2.7**. It has been documented that the 5-bromo-2-lithiothiazole species can be produced in hexanes,[39] However, the solubility of the two species was significantly different due to polarity, and **2.5** was practically insoluble in hexanes, especially at cryogenic temperatures. This fact caused us to initially avoid attempting this reaction, but lack of success with other routes led to an attempt. Upon addition of n-butyllithium, the solid chunks on the reaction vessel floor eventually were incorporated into solution, and **2.3** was afforded in approximately 28% yield, albeit in a complex mixture that did not separate well using column chromatography.

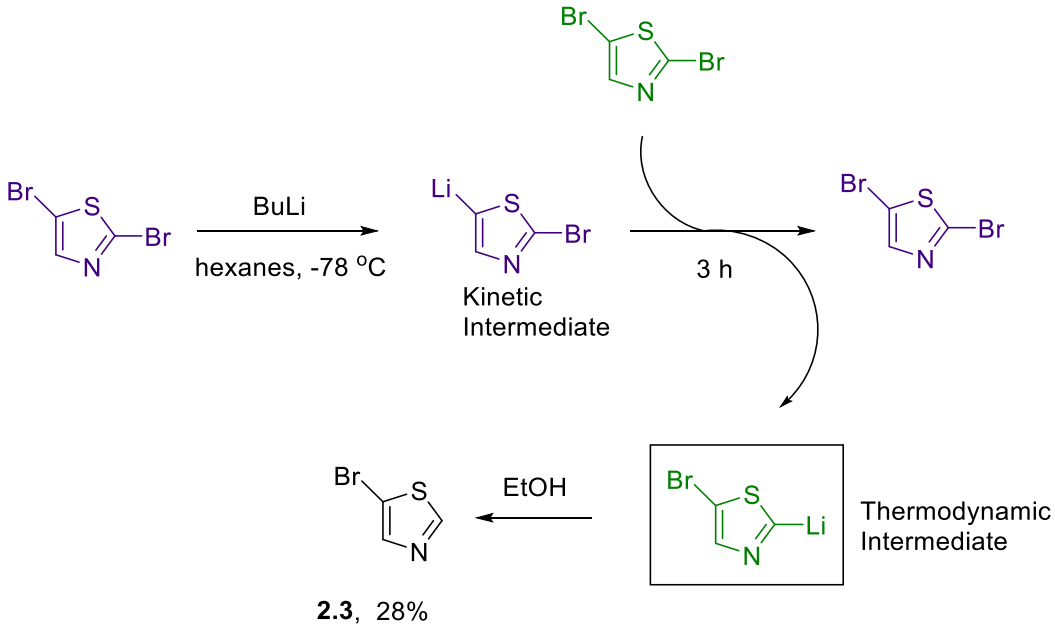

Scheme 2.10. Exploitation of the halogen dance in hexanes to produce **2.3**

Despite producing **2.3** in higher yield than the literature reported, the difficulties in purifying the molecule from the complex mixture prompted us to reexamine other conditions. In Beyerman's 1954 report, the authors were able to produce 5-bromothiazole from 2-amino-5-bromothiazole via Sandmeyer conditions, with the substitution of a reducing acid for a bromide source. Since the production of **2.8** was already optimized for this study, Beyerman's methods were utilized to produce **2.3** in 54%, approximately 10% higher than the original report. Strict temperature control and quenching of the reaction early as opposed to overnight stirring could account for this difference. This method was declared to be the most optimal, as it prevented a complex mixture of products and the **2.3** produced was mostly pure, requiring only a short silica plug to remove trace impurities.

2.9. Conclusions

For the first time, the synthesis and full characterization of the entire brominated thiazole family has been accomplished. Exploitation of the halogen dance was critical to production of some of the members, and new knowledge of how the solvent and positions affect the halogen dance was obtained. With our new methods, every one of the brominated thiazole analogues can be produced in acceptable yield, isolated, and purified. The production of brominated thiazoles still requires more effort than the analogous bromothiophenes, but synthesis of the full family is now available without having to use the highly-toxic reagent Br_2. Additionally, the only reaction that requires cryogenic conditions and pyrophoric reagents is 4,5-dibromothiazole.

With these advances in mind, this work represents the most practical and "green" approach to synthesis of these increasingly important compounds, and will help the field of thiazole chemistry move forward by providing researchers with optimized methods to produce

these functionalized building blocks. Both materials chemists and natural product chemists should benefit from this work.

2.10. Experimental

General Information. 2-Aminothiazole and 2,4-thiazolidinedione were purchased from Alfa Aesar. NBS was recrystallized from water as previously described.[40] Dry CH_3CN was treated with CaH_2 and distilled prior to use. Dry toluene was obtained via distillation over sodium benzophenone. The solvents $CHCl_3$ and hexanes used as reaction media were dried over $MgSO_4$ prior to use. All other materials were reagent grade and used without further purification. With the exception of the Sandmeyer reactions, all reactions were carried out under a nitrogen atmosphere. All glassware was oven-dried, assembled hot, and cooled under a dry nitrogen stream before use. Chromatographic separations were performed using standard column chromatography methods with silica gel (230−400 mesh) in 1 in. diameter columns. Melting points were determined using a digital thermocouple with a 0.1 °C resolution. All NMR data were obtained in $CDCl_3$ on a 400 MHz spectrometer at 25 °C, and referenced to the $CHCl_3$ signal. Peak multiplicity is reported as follows: s = singlet, d = doublet, and br = broad. HRMS (ESI-TOF) was performed in house.

2-Bromothiazole (**2.1**). 2-Aminothiazole (5.01 g, 50.0 mmol) was added to 85% H_3PO_4 (20 mL) and sonicated to dissolve the amine. The red solution was added to a 500 mL, round-bottom flask submerged in an ice−NaCl bath, and the temperature lowered to 0 °C. Concentrated HNO_3 (10 mL) was then added, and the stirred mixture was again cooled to a constant 0 °C. $NaNO_2$ (4.48 g, 65.0 mmol) was dissolved in 10 mL of deionized H_2O and added dropwise to the acid over 1 h, keeping the temperature below 5 °C. The reaction was stirred for an additional 1 h at 0 °C. Meanwhile, a solution of NaBr (13.2 g, 130 mmol) and $CuSO_4{\cdot}5H_2O$ (10.37 g, 41.0

mmol) in 100 mL of H_2O was prepared in a 1 L beaker and cooled to 0 °C in a second ice−NaCl bath. The red diazonium solution was pipetted dropwise into the beaker, keeping the temperature below 5 °C. The blue solution gradually turned green, with vigorous effervescence and a gradual buildup of film on the sides of the beaker. After complete addition of the acid solution, the dark-green mixture was stirred for an additional 30 min, during which bubbling ceased. The solution was adjusted to pH 8 with solid Na_2CO_3 and extracted with diethyl ether to yield an orange-red oil. This crude product was run through a short silica plug (ca. 3 cm) (5% Et_2O in hexanes) to yield a colorless to faint yellow oil in 83−86% yield (6.81−7.05 g). ^{1}H NMR: δ 7.61 (d, 1H, J = 3.56 Hz), 7.30 (d, 1H, J = 3.56 Hz). ^{13}C NMR: δ 143.1, 136.1, 123.0. NMR data agree well with previously reported values.[16]

4-Bromothiazole (**2.2**). To a 50 mL, round-bottom flask equipped with reflux condenser were added **2.4** (0.243 g, 1.0 mmol) and $NaBH_4$ (0.076 g, 2.0 mmol). The solids were dissolved in acetonitrile, and the solution was refluxed overnight. Water (50 mL) was added to the yellow, opaque mixture, extracted with diethyl ether, and dried over $MgSO_4$. The residue was purified via column chromatography (1:1 $CHCl_3$/hexanes) to give a faint yellow oil in 62−66% yield (0.10−0.11 g). ^{1}H NMR: δ 8.75 (d, 1H, J = 2.26 Hz), 7.30 (d, 1H, J = 2.26 Hz). ^{13}C NMR: δ 153.9, 126.6, 116.9. NMR data agree well with previously reported values.[17]

2,4-Dibromothiazole (**2.4**). To a 500 mL, round-bottom flask equipped with a reflux condenser were added 2,4-thiazolidinedione (3.51 g, 30 mmol), phosphorus pentoxide, (21.29 g, 150 mmol), and tetrabutylammonium bromide (20.56 g, 70 mmol). The solids were dissolved in 60 mL of toluene and heated to a gentle reflux for 20 h. The solution was cooled to room temperature, and 100 mL of saturated Na_2CO_3 was added. The solution was adjusted to pH 8 with solid Na_2CO_3 and extracted with diethyl ether, and the organic layer dried over $MgSO_4$. The

resulting residue was purified via a short silica plug (ca. 3 cm) in pure hexanes to afford a white solid in 85−91% yield (6.20−6.53 g). mp: 81.4−82.1 °C. ^{1}H NMR: δ7.21 (s, 1H). ^{13}C NMR: δ 136.3, 124.3, 120.8. NMR data agree well with previously reported values.[16,17]

2,5-Dibromothiazole (**2.5**). *Via bromination of* ***2.1***: Na_2CO_3 (3.18 g, 30.0 mmol) was added to N_2-sparged $CHCl_3$ (15 mL) in a 125 mL three-neck flask. **2.1** (2.46 g, 15 mmol) was added to the solution, followed by the dropwise addition of Br_2 (1.92 mL, 37.5 mmol). The reaction was stirred until 1 could no longer be detected by thin-layer chromatography, which took ca. 24 h. Saturated $Na_2S_2O_3$ (15 mL) was then added, and the solution was stirred for 30 min. The solution was made basic with solid Na_2CO_3 and the organic layer extracted with CH_2Cl_2, washed with brine, concentrated in vacuo, and dried over $MgSO_4$. The yellow oil was purified via column chromatography (10% Et_2O in hexanes) to give the product in 65% yield (4.73 g).

Via Sandmeyer reaction of **2.8**: Compound **2.8** (0.984 g, 5.50 mmol) was added to 10 mL of 85% H_3PO_4 and added to a 250 mL three-neck flask equipped with a thermometer. Concentrated HNO_3 (5 mL) was added to give a clear solution, which was then cooled to 0 °C with an ice−NaCl bath. A solution of $NaNO_2$ (0.493 g, 7.15 mmol) in 3 mL of deionized H_2O was then added dropwise over 30 min, keeping the temperature below 5 °C. The mixture was stirred for an additional 30min. NaBr (1.45 g, 14.3 mmol) and $CuSO_4{\cdot}5H_2O$ (1.78 g, 7.15 mmol) were added to 30 mL of deionized water in a 400 mL beaker submerged in a second ice−NaCl bath and cooled to 0 °C. The diazonium solution was added dropwise into the beaker over 30 min, keeping the temperature below 5 °C. The blue solution gradually turned green, with vigorous effervescence. The solution was stirred for an additional 30 min, after which diethyl ether was added. The mixture was neutralized with solid Na_2CO_3, extracted with diethyl ether,

and evaporated in vacuo to give the product in 60−65% yield (0.80−0.86 g). mp: 46.5−47.1 °C ^{1}H NMR: δ. 7.52 (s, 1H).^{13}C NMR: δ 144.0, 135.8, 110.7. NMR data agree well with previously reported values.[16,17]

2-Amino-5-bromothiazole (**2.8**). 2-Aminothiazole (1.02 g, 10.0 mmol) was dissolved in 10 mL of glacial acetic acid and heated to 40−50 °C. After the mixture was stirred for 10 min, NBS (2.31 g, 13.0 mmol) was added, and the clear, tan solution turned dark red, with a corresponding increase in temperature to 60−65 °C. The reaction was stirred for 1 h at 50 °C after which 50 mL of water was added and the solution transferred to a 400 mL beaker. Diethyl ether (100 mL) was added, and solid Na_2CO_3 was used to adjust the solution to pH 8. The mixture was extracted with ethyl acetate, and the combined organic layers were washed three times with water to remove residual succinimide. The orange-red organic layer was evaporated *in vacuo* to give a red solid in 56−57% yield (1.00−1.02 g). The solid was not further purified but used immediately due to limited stability. mp: 77.4 °C (dec) ^{1}H NMR: δ6.98 (s, 1H), 5.06 (br s, 2H). ^{13}C NMR: δ 168.3, 139.5, 95.8. HRMS: m/z 178.9279 calcd for $C_3H_4{}^{79}BrN_2S$ $[M + H]^+$, 178.9272 found.

2,4,5-Tribromothiazole (**2.7**). To an oven-dried, round-bottom flask were added 2,4-dibromothiazole (4.8 g, 20 mmol) and NBS (4.3 g, 24 mmol). Glacial acetic acid (20 mL) was added via syringe and the reaction mixture heated at reflux. The reaction progress was monitored via thin-layer chromatography and allowed to proceed until product formation was complete (ca. 1−2 h). The reaction mixture was then cooled, made basic with solid Na_2CO_3, and extracted with diethyl ether. Purification of the crude product via silica gel chromatography in hexanes gave the product as a white solid in 68−76% yield (4.4−4.9 g). mp: 33.2−33.5 °C. ^{13}C NMR: δ 136.0, 127.8, 109.5. HRMS: m/z 321.7359 calcd for $C_3H{}^{79}Br_2{}^{81}BrNS$ $[M + H]^+$, 321.7357 found.

4,5-Dibromothiazole (**2.6**). 2,4,5-tribromothiazole (0.646 g, 2 mmol) was dissolved in N_2-sparged hexane (100 mL) in a 250 mL round-bottom flask. The solution was cooled to −78 °C, and butyllithium (2.5 M in hexane, 0.88 mL, 2.2 mmol) was added dropwise. The solution was stirred at −78 °C for 3 h, quenched with methanol, and then warmed to room temperature. Brine was added, the mixture was extracted with diethyl ether, and the combined organic layers were dried over $MgSO_4$. The dried organic fraction was then concentrated in vacuo and purified via column chromatography in hexanes to give the product as a white solid in 60−67% yield (0.29−0.36 g). mp: 74.1−74.8 °C. ^{1}H NMR: δ 8.75 (s, 1H). ^{13}C NMR: δ 154.3, 130.0, 108.2. HRMS: m/z 241.8275 calcd for $C_3H_2{}^{79}Br_2NS$ $[M + H]^+$, 241.8251 found.

5-Bromothiazole (**2.3**). Compound **2.8** (1.25 g, 7.0 mmol) was dissolved in 10 mL of 85% H_3PO_4. Concentrated HNO_3 (5 mL) was added, and the solution was cooled to 0 °C in an ice−NaCl bath. $NaNO_2$ (0.77 g, 11.2 mmol) was dissolved in 3 mL of deionized H_2O and pipetted into the acid solution over the course of 30 min, keeping the temperature below 5 °C. The reaction was stirred for an additional 30 min, during which time the red-orange gas no longer evolved. H_3PO_2 (50% by mass, 3.8 mL, 35 mmol) was added dropwise, keeping the temperature below 5 °C. After the addition was complete, the reaction was stirred for 3 h at 0 °C and then brought to room temperature. Solid Na_2CO_3 was used to adjust the pH to 8, and the organic layer was extracted with diethyl ether. The organic layer was dried with $MgSO_4$ and the resulting oil purified via column chromatography (5% diethyl ether in hexanes) to give the product in 54% yield (0.62 g). ^{1}H NMR: δ 8.76 (s, 1H), 7.81 (s, 1H). ^{13}C NMR: δ 154.5, 144.8, 109.5. NMR data agree well with previously reported values.[17]

2.11. References

1. Gronowitz, S.; Hornfeldt, A. *Thiophenes*; Elsevier: Amsterdam, 2004.

2. Skotheim, T. A., Reynolds, J. R., Eds. *Handbook of Conducting Polymers*, 3rd ed.; CRC Press: Boca Raton, FL, 2007. (b) Perepichka, I.F.; Perepichka, D. F. *Handbook of Thiophene-Based Materials*; John Wiley & Sons: Hoboken, 2009.
3. Bohlmann, F.; Zdero, C. In *Thiophene and Its Derivatives*; Gronowitz, S., Ed.; The Chemistry of Heterocyclic Compounds, Vol. 44 (part 1); Wiley & Sons: New York, 1985; pp 261−323.
4. Press, J. In *Thiophene and Its Derivatives*; Gronowitz, S., Ed.; The Chemistry of Heterocyclic Compounds, Vol. 44 (part 4); Wiley & Sons: New York, 1991; pp 397−502.
5. Hiraoka, S.; Shiro, M.; Shionoya, M. *J. Am. Chem. Soc*. **2004**, *126*, 1214−1218.
6. Al-Hashimi, M.; Labram, G. J.; Watkins, S.; Motevalli, M.; Anthopoulos, T. D.; Heeney, M. *Org. Lett*. **2010**, *12*, 5478−5481.
7. Yamamoto, T.; Otsuka, S.-I.; Fukumoto, H.; Sakai, Y.; Aramaki, S.; Fukuda, T.; Emoto, A.; Ushijima, H. *J. Polym. Sci., Part A: Polym. Chem*. **2011**, *49*, 1508−1512.
8. Pammer, F.; Passlack, U. *ACS Macro Lett*. **2014**, *3*, 170−174.
9. Getmanenko, Y. A.; Singh, S.; Sandhu, B.; Wang, C.-Y.; Timofeeva, T.; Kippelen, B.; Marder, S. *J. Mater. Chem. C* **2014**, *2*, 124−131.
10. Konkol, K. L.; Rasmussen, S. C. *Organometallics* **2016**, 35, 3234−3239.
11. Katritzky, A.; Pozharskii, A. *Handbook of Heterocyclic Chemistry*, 2nd ed.; Pergamon: Oxford, 2000; pp 126.
12. Bosco, M.; Forlani, L.; Todesco, P. E.; Troisi, L. *J. Chem. Soc., Perkin Trans*. **1976**, *2*, 398−402.
13. Parkanyi, C.; Vernin, G.; Zamkostian, R. M.; Metzger, J. *Heterocycles*, **1984**, *22*, 1077−1089.

14. Ganapathi, K.; Venkataraman, A. *Proc. Indian Acad. Sci.* **1945**, *22A*, 362−378.

15. Roussel, P.; Metzger, J. *Bull. Soc. Chim. Fr*. **1962**, 2075−2078.

16. Grubb, M.; Schmidt, M. J.; Seed, A. J.; Sampson, P. *Synthesis* **2012**, *44*, 1026−1029.

17. Stanetty, P.; Schnürch, M.; Mihovilovic, M. D. *J. Org. Chem.* **2006**, *71*, 3754−3761.

18. Kelly, T. R.; Lang, F. *Tetrahedron Lett*. **1995**, *36*, 9293−9296.

19. Athmani, S.; Bruce, A.; Iddon, B. *J. Chem. Soc., Perkin Trans. 1* **1992**, 215−219.

20. Beyerman, H. C.; Berben, P. H.; Bontekoe, J. S. *Recl. Trav. Chim. Pays-Bas* **1954**, *73*, 325−332.

21. Reynaud, P.; Robba, M.; Moreau, R. C. *Bull. Soc. Chim. Fr.* **1962**, 1735−1738.

22. Le Flohic, A.; Meyer, C.; Cossy, J. *Tetrahedron* **2006**, *62*, 9017− 9037.

23. Erlenmeyer, H.; Kiefer, H. *Helv. Chim. Acta* **1945**, *28*, 985−991.

24. Robba, M.; Moreau, R. *Ann. Pharm. Fr*. **1964**, *22*, 201.

25. Herkes, F. E.; Blazer, T. A. *J. Heterocycl. Chem*. **1976**, *13*, 1297−1304.

26. Uzelac, E.; Rasmussen, S. C. *J. Org. Chem.* **2017**, *82*, 5947-5951.

27. Kochi, J. K. *J. Am. Chem. Soc.* **1957**, *79*, 2942–2948.

28. Handley, R.; Herington, E. F. G.; Azzaro, M.; Metzger, *J. Bull. Soc. Chim. Fr*. **1963**, 1904−1905.

29. Greenwood, N. N.; Earnshaw, A. *Chemistry of the Elements*; Pergamon Press: Oxford, **1984**; pp 577−581.

30. Marcus, Y. Asher, L. E. *J. Phys. Chem.*, **1978**, *82*, 1246–1254.

31. Aitken, K. M.; Aitken, R. A.; MacGregor, C. I.; Traore, M. D. M.; Slawin, A. M. Z. *J. Chem. Crystallogr*. **2015**, 45, 461−465.

32. Lossos, I. S.; Abolnik, I.; Breuer, R. *Br. J. Ind. Med*. **1990**, *47*, 784.

33. Withers, R. M. J.; Lees, F. P. *J. Hazard. Mater.* **1986**, *13*, 279−299.

34. Davies, P. C.; Purdy, G.; Withers, R. M. J.; Lees, F. P. J. *Hazard. Mater*. **1987**, 14, 273−275.

35. Zambon, A.; Borsato, G.; Brussolo, S.; Frascella, P.; Lucchini, V. *Tetrahedron Lett*. **2008**, *49*, 66−69.

36. Stangeland, E. L.; Sammakia, T. *J. Org. Chem.* **2004**, *69*, 2381-2385.

37. Schnürch, M.; Spina, M.; Khan, A. F.; Mihovilovic, M. D.; Stanetty, P. *Chem. Soc. Rev.* **2007**, *36*, 1046−1057.

38. Collum, D. B. *Acc. Chem. Res*. **1992**, *25*, 448−454.

39. Kaye, P. T.; Meakins, G. D.; Willbe, C.; Williams, P. R. *J. Chem. Soc., Perkin Trans. 1* **1981**, 2335−2339.

40. Armarego, W. L. F.; Perrin, D. D. *Purification of Laboratory Chemicals*, 4th ed.; Butterworth-Heinemann: Oxford, 1997; p 121.

CHAPTER III. INVESTIGATION OF OPTICAL AND ELECTRONIC TRENDS IN PYRROLO[2,3-*d*:5,4-*d*']BISTHIAZOLE MONOMERS

3.1. Introduction

Thiophene-based conjugated materials are widely used in such applications as organic photovoltaics (OPVs), organic light-emitting diodes (OLEDs), and organic field-effect transistors (OFETs),[1-6] due to their excellent optical and electronic properties and ease of synthetic functionality. A subset of these materials, oligothiophenes, offer certain advantages over their polymer counterparts, such as tunable conjugation length, highly-ordered packing structures, and easily-functionalized peripheral units.[7,8] Oligothiophenes can thus act as model compounds for polymeric systems with these advantages coupled with increased solubility, or be incorporated into polymers themselves as repeating units. Fused-ring oligothiophenes offer additional advantageous material properties such as enhanced fluorescence and hole-transport properties, limited torsional deviations, and increased planarity.[7-9]

Of these oligothiophenes, the fused-ring dithieno[3,2-*b*:2',3'-*d*]pyrrole (DTP) has emerged as one of the strongest monomeric electron-donors (Chart 3.1).[10] As such, DTPs have found promise as hole-transport components in donor-acceptor polymer applications and as fluorescent molecules.[11] A brief evolution of the synthesis of DTP will be presented, starting from the first report in 1983 to the Rasmussen group's expansion into acyl derivatives. This discussion is necessary to understand the scope and impact of the current study: the potential "next generation" of fused-ring oligothiophenes, pyrrolo[2,3-*d*:5,4-*d*']bisthiazole (PBTz) (Figure 3.1).

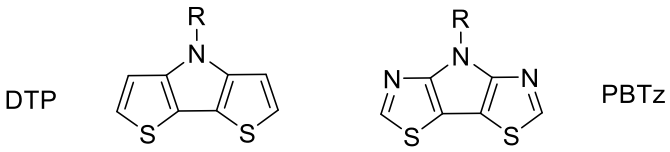

Figure 3.1. Dithieno[3,2-*b*:2',3'-*d*]pyrrole (DTP) and pyrrolo[2,3-*d*:5,4-*d*']bisthiazole (PBTz)

The unfunctionalized DTP unit **3.1** was first reported by Zanirato and coworkers in 1983,[12] with a route derived from 2,3-dibromothiophene.[13] Copper-mediated oxidative coupling of this material afforded 2,2'-dibromo-3,3'-bithiophene **3.1**, which was debrominated, azidized, and annulated via liberation of N_2 and addition to the adjacent thiophene ring (Scheme 3.1).[12] Although Zanirato's cyclization proceeded in 88% yield from the azidized bithiophene, the resulting unfunctionalized DTP **3.2** experienced limited solubility in most organic solvents and thus was limited in applicability to organic materials. Schaivon and coworkers later developed substitution chemistry which introduced alkyl N-functionalization onto the DTP unit in 76% yield (Scheme 3.1), allowing solubility in a variety of organic solvents.[14] However, the overall yield for the synthesis of **3.3** was 13%, which was still in need of optimization if the DTP unit was to become viable in organic electronics applications.

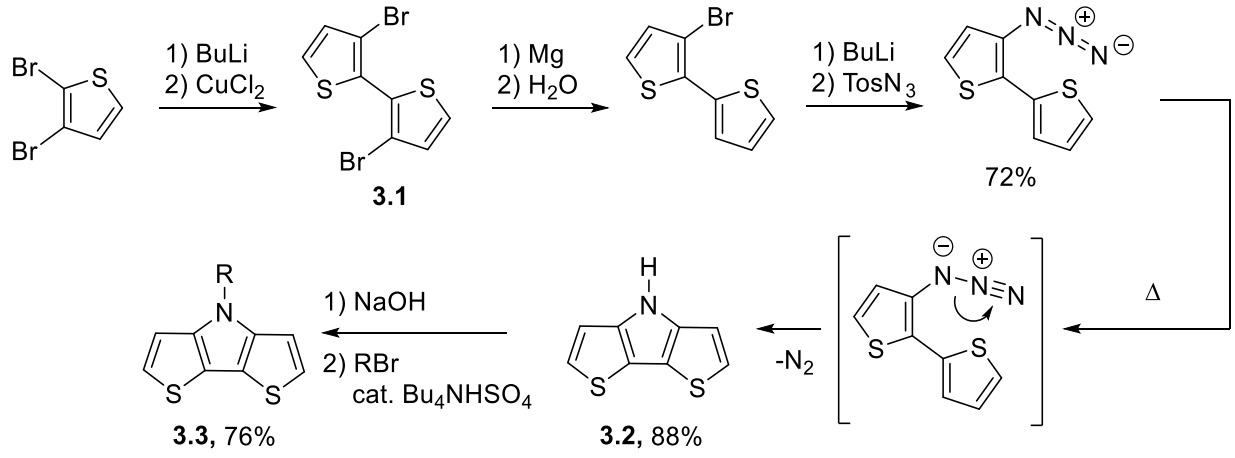

Scheme 3.1. Synthesis of unfunctionalized DTP (**3.2**)[12] and N-functionalized DTP (**3.3**)[14]

In 2003, Rasmussen and Ogawa developed a new route to N-functionalized DTPs by first aminating 3-bromothiophene,[15,16] which was followed by bromination and Ullman coupling at the 2-positions of each thiophene (Scheme 3.2 Route A).[17] This route allowed production of **3.3** in two steps, representing the most optimized synthesis at the time. The same year, Nozaki and coworkers significantly shortened the DTP synthesis from **3.1** by applying a palladium-catalyzed double amination to **3.1**. which afforded a phenyl N-functionalized DTP from **3.1** in one step.[18] This advancement was significant because it removed approximately three steps from the synthetic route displayed in Scheme 3.1, placing the new route equal in length to the Rasmussen group's established pathway. However, the most optimized yields for **3.3** were still obtained via the route from 3-bromothiophene.

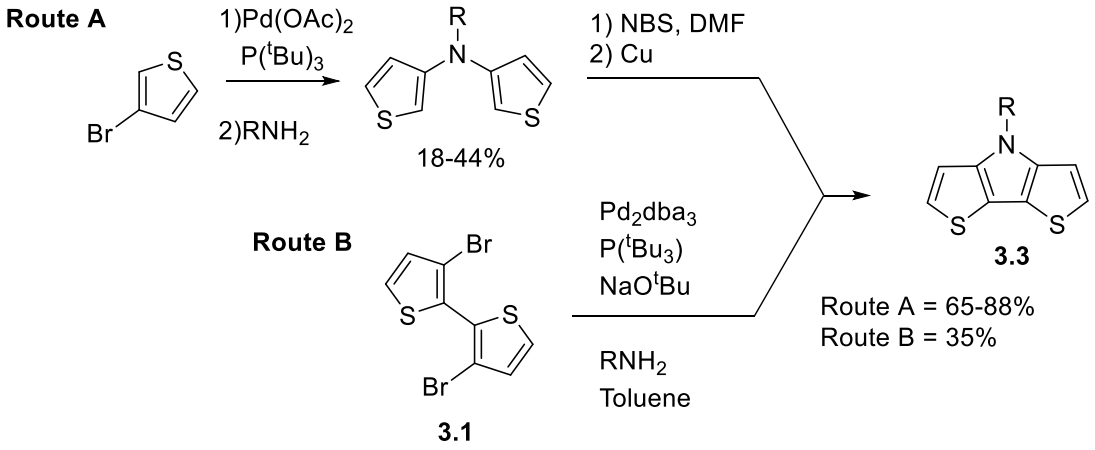

Scheme 3.2. Rasmussen and Ogawa's 2003 route to **3.2** using copper-mediated oxidative coupling (Route A), compared to Nozaki's conditions (Route B)

In 2010, Rasmussen and Evenson developed a new method to synthesize **3.1** (Scheme 3.3).[19] Employing the same starting material, 3-bromothiophene was selectively deprotonated with lithium diisopropylamide (LDA) and then metallated with zinc chloride, producing a stable thienylzinc chloride. This intermediate was oxidatively homocoupled via transmetallation with

copper(II) chloride and O_2 to produce **3.1** in 85-90% yield and DTP **3.3b** in 68% overall. In the meantime, Koeckelbergs et. al. optimized the Buchwald-Hartwig amination conditions originally reported by Nozaki, attaining **3.3** in 80% yield for simple N-functionalized alkyl derivatives.[20,21] Combining the new bithiophene synthesis with Koeckelbergs' conditions produced the most optimized route to the N-functionalized DTP unit to date, with an 83% overall yield for two steps. Overall, the research performed on the DTP unit during the 2000's led to cost-effective and simple access to both alkyl and acyl N-functionalized DTP materials. The popularity of the unit greatly expanded, showcased by the number of DTP-based publications and patents on devices including OLEDs, electrochromics, OPVs, and OFETs,[22-26]

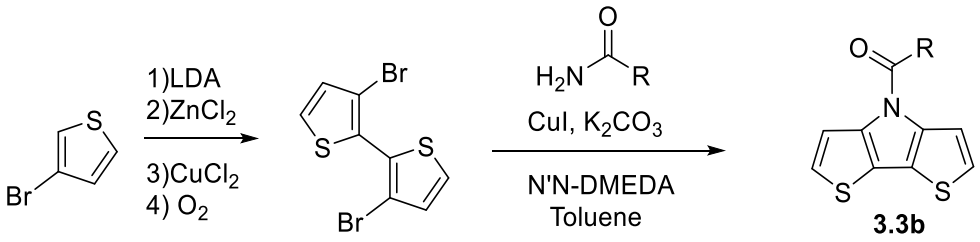

Scheme 3.3. Synthesis of second-generation acyl DTP unit **3.3b**

As a consequence of their electron rich character, the DTP unit suffers from high-lying frontier orbitals which limit its oxidative stability and energy level matching to common optoelectronic device components.[27] Efforts to stabilize the HOMO of the DTP unit were the focus of the Rasmussen group's 2010 study,[19] with the synthesis of acyl DTP units (**3.3b**) featuring an electron-withdrawing carbonyl adjacent to the pyrrole nitrogen. These "second-generation" DTPs were produced by a double Ullman condensation in one step from **3.1**. The materials showed stabilization of the HOMO by approximately 200 mV as well as an asymmetric stabilization of the LUMO by 400 mV.[19] This stabilization allowed the DTP monomer to be

oxidatively stable in its brominated form, easing the synthesis of polymeric and oligomeric DTP-based systems that were developed from this chemistry.[28]

Tuning of the DTP system through not only the side chain, but the fused-ring system itself, is now being explored. An alternative to DTP has recently emerged as an electron-deficient fused-ring unit for donor-acceptor polymers and small molecules. The PBTz system (Figure 3.1) is identical to DTP in structure except for the nitrogen atom in the 3-position of each thiazole ring. Although a simple two-atom change, the incorporation of thiazole has been shown to stabilize the frontier orbitals of the molecules it has been incorporated into thus far.[29,30] However, there are very few accounts in the literature of the PBTz unit. Heeney and coworkers were the first to report PBTz in 2010, producing reduced-bandgap copolymers and finding that the valence and conduction bands were stabilized at the cost of reduced charge-carrier mobilities.[31] Marder and coworkers used PBTz as a tricyclic bridging unit for naphthalene diimide semiconductors in 2014, finding that the PBTz unit suppressed hole transport and behaved as a both a weak donor and weak acceptor.[32] Finally, Al-Hashimi and coworkers published a 2017 study examining properties of PBTz as organic field-effect transistors (OFETs).[33] In all three cases, though, the authors did not attempt to compare the properties of the PBTz monomers to DTP analogues, nor characterize the optoelectronic properties of these PBTz building blocks. Thus, a sufficient frame of reference for the effects of thiazole substitution into these materials was not created.

As mentioned before, data on the PBTz unit itself had been somewhat sparse. Marder and coworkers calculated the HOMO to lie at -5.6 eV,[31] but experimental electrochemical measurements on the naked PBTz ring had not been published. Optical properties of the naked unit itself had not been reported, and the effect of TIPS protection had not been quantified.

Additionally, only alkyl N-functionalization had been reported.[31-33] Thus, the PBTz unit could not be accurately compared to DTP. To solve this issue, a new family of PBTz monomers were synthesized and fully characterized via UV-vis spectroscopy and electrochemical means in order to more directly compare their properties to DTPs. At the time of this dissertation's writing, the results of this study have been recently submitted to *The Journal of Organic Chemistry*.

3.2. Synthesis of PBTz Monomers

The goal of this study was not merely to fully discern the properties of the PBTz unit, but also to reexamine its synthetic pathway. Our studies in Chapter II showed that synthesis of brominated thiazoles tend to be more complicated than their thiophene analogues, and this trend is similarly evident with the thiazole-containing PBTz unit compared to DTP **3.3**. Although based on a bisthiazole precursor akin to **3.1**, the reported syntheses of the PBTz monomer **3.5** (Scheme 3.4) involve more steps than the synthesis of the comparable DTPs, an issue which our group sought to improve via synthetic optimization of the bisthiazole precursors.

The two known synthetic pathways for the synthesis of PBTz were published by Marder and Heeney.[31,32] Both routes converge at the synthesis of 4,4'-dibromo-2,2'-bis(triisopropylsilyl)-5,5'-bisthiazole (**3.4**). To produce **3.4**, each research group utilized syntheses that exploit the halogen dance.[29,34,35] The halogen dance in this case is an interchanging of halogen substituents between thiazole molecules, in which a thiazole lithiated on a kinetically-favored position undergoes metal-halogen exchange with a halogenated thiazole molecule, transferring the lithium to the more thermodynamically-favored position on the second thiazole molecule. Marder and coworkers utilized triisopropylsilyl protection of the thiazole rings first, followed by coupling at their 5-positions, while Heeney and coworkers performed an oxidative coupling of two thiazole species (Scheme 3.4). Each route involves the lithiation of the

4-position and subsequent exchange to the 2- or 5-positon. The sterically-bulky triisopropylsilyl group is necessary for these synthetic routes to prevent rearrangement and provide the correct lithiated intermediate for coupling: although less expensive, the trimethylsilyl group can undergo the halogen dance when attacked by a lithiated thiazole and will exchange positions in a similar manner to eventually place the lithium on the thiazole's most thermodynamically favorable position.[34,36]

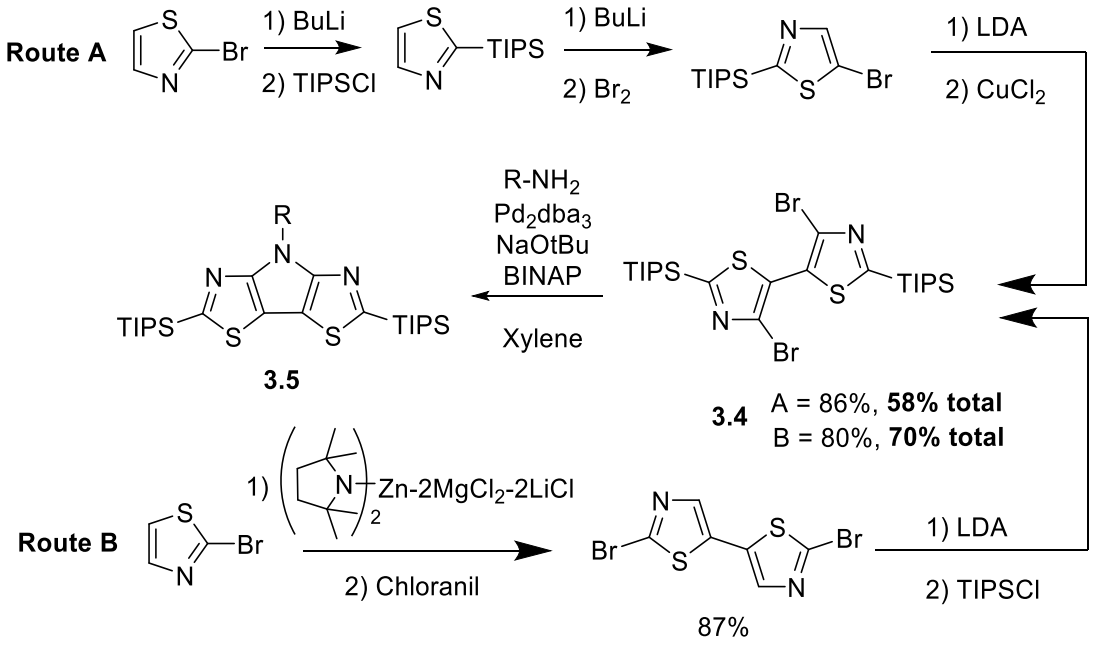

Scheme 3.4. Synthetic routes from Marder (Route A) and Heeney (Route B) toward PBTz, including total yields up to **3.4**

Our new route to **3.4** applied the conditions developed by Rasmussen and Evenson for the bithiophene **3.1**, resulting in the 2,2',4,4'-tetrabromo-5,5'-bisthiazole precursor (**3.6**) as shown in Scheme 3.5. Synthesis of **3.6** was accomplished using oxidative coupling via transmetallation of the thiazolozinc chloride with $CuCl_2$, prompting carbon-carbon bond formation at thaizole's 5- position.[19] The yields obtained for the bisthiazole in the Rasmussen group were originally in the mid 60% range, which prompted a reexamination of the reaction

conditions. It was found that adding 2,4-dibromothiazole simultaneously with zinc chloride into the LDA solution produced the desired thiazolozinc chloride with no evidence of other isomers. Since it had been previously found that the halogen dance will reliably result in lithiation of the 5-position in THF no matter which other positions are brominated,[29] there was no need to wait for the lithiation to be complete before adding zinc chloride. Through additional experimentation, it was also found that bringing the thiazolozinc chloride to room temperature after 1 h and 45 min of stirring did not destabilize the intermediate and cause ring opening as expected, but helped encourage the reaction to proceed to completion via elevated temperature. As reported in Chapter II, lithiated thiazoles are often unstable above -40 °C, but zinc is a larger and more polarizable atom than lithium with a 2^+ charge, which could stabilize the increased electron density about the thiazole's 2-position. Immersing the solution back into the cryogenic bath and completing the oxidative coupling was performed as before, but these new experimental changes brought the yields of **3.6** into the 82-88% range. Intermediate **3.6** is insoluble in most organic solvents, and while this factor is a drawback by requiring a large volume of THF to dissolve the molecule for the next reaction step (0.012 M solution), the limited solubility provided a simple method to purify the compound. Washing **3.6** with methanol sufficiently removed the organic impurities and provided pure material without the use of column chromatography or other purification techniques.

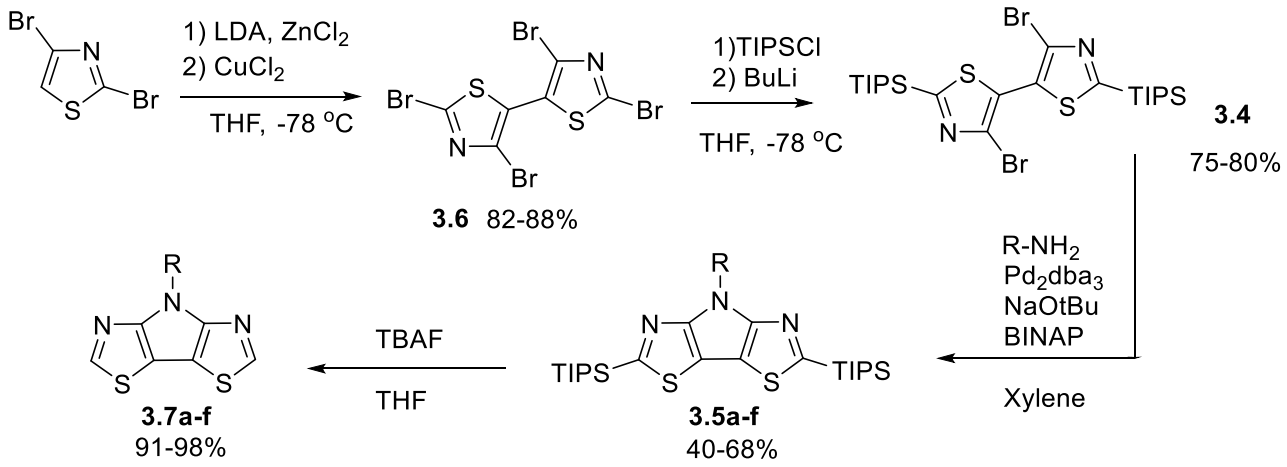

Scheme 3.5. New synthetic pathway to the PBTz unit.

To synthesize **3.4,** the new molecule **3.6** was dissolved in THF, lithiated with butyllithium, and quenched with TIPSCl. Although the halogen dance was not a factor for this reaction, the TIPS group was still employed herein due to consistency with the previous methods, as well as greater stability against the basic conditions of the Buchwald-Hartwig amination. It is documented that TMS groups have less resistance to basic attack compared to TIPS, a factor of five orders of magnitude to be precise.[37] Tangentially, attempts were made to synthesize the PBTz monomers using 2,2'-trimethylsilyl-4,4'-tetrabromo-5,5'-bisthiazole but no product was observed. Nucleophilic attack on the silyl center by *tert*-butoxide or an amine may be more favored at the harsh reflux temperatures of xylene, leading to an anionic thiazole unit which can undergo additional chemistry or decompose. To support this claim, Heeney and coworkers found that no PBTz product was observed when the deprotected **3.4** was used.[32]

The initial reaction conditions used to synthesize **3.6** involved addition of BuLi to **3.4** in THF, followed by 30 min of stirring and then addition of TIPSCl. However, a significant amount of black precipitate formed in the solution during the initial stirring time, which indicated some decomposition of **3.6**. The yields using this method were consistently 60-64%, and thus various

strategies were employed to improve this yield. The decomposition of 2-lithiated thiazoles are documented to occur in THF even at cryogenic temperatures,[38] and diethyl ether was found to stabilize this intermediate. We attempted to address this by performing the experiment in a mixed diethyl ether/THF solvent system with ratios of 10-50% diethyl ether in THF. Unfortunately, the yields decreased with increasing ether content. Starting material was observed on the bottom of the reaction vessel the next day, which can be attributed to the insolubility of **3.6** in diethyl ether. Since the starting material is already only slightly soluble in THF, this addition of diethyl ether to the solvent system was discontinued. The change to the procedure that resulted in higher yields was the addition of TIPSCl to the reaction mixture before BuLi. The reaction between TIPSCl and BuLi is disfavored at cryogenic temperatures,[35,39] and the rate of lithium-halogen exchange should result in the TIPSCl being consumed by the lithiated thiazole long before reaction with BuLi. With this simple change, we were able to attain yields for **3.6** in the 75-80% range.

Overall, the new procedure for generating **3.4** attains a 64% overall yield for two steps from the inexpensive 2,4-thiazolidinedione starting material. To compare, Marder's previous synthesis exhibited approximately 56% yield for three steps from 2-bromothiazole, while Heeney's features two steps from 2-bromothiazole and 64% yield. However, the previous groups did not specify the origin of their 2-bromothiazole, which will either add a step to the synthesis, or avoidable material cost to the procedure. 2-Bromothiazole can be commercially obtained for 4-8 USD per gram,[40,41] whereas 2,4-dibromothiazole provides an alternate starting material with the cost of approximately 1.18 USD per gram.[29] Comparing our synthesis to the literature preparations from 2,4-dibromothiazole as the starting point gives an overall yield of 70% for two steps. Taking Heeney's route one step backwards and applying the optimized synthesis of 2-

bromothiazole from 2-aminothiazole at 85%, one still calculates the overall yield of this synthesis to be 59%. Additionally, the most expensive component of the reaction, the TIPSCl, is not used until the final precursor step, preventing waste of this unit through further synthetic steps. Although Heeney's procedure results in a higher overall yield, our methods to produce **3.6** provide an advantage in terms of material cost and simplicity of reagents used.

Synthesis of the protected monomers **3.5a-f** was accomplished via a modification of the methods of Heeney and Marder's work. Instead of using mesitylene at reflux, or xylenes in a sealed flask, xylenes heated at reflux under N_2 atmosphere provided sufficient thermal energy to form the diaminated product. The overnight reaction time of approximately 16-20 h was necessary to complete the reaction and produce the best yields. Monitoring the reaction progress via TLC showed that the reaction was still incomplete even after 12 h of reflux. It was also noted that a 40% excess of amine was necessary to attain the best yields. Any equivalency above 1.4 did not appear to increase the reaction yield. The yields for monomers **3.5a-f** are in the range of the highest reported species from Heeney's group, and consistently near 50-60%. As a partial explanation our lower yields, all of the PBTz products **3.5a-f** were able to be purified to a yellow-orange solid, whereas the existing reports of **3.5b** and **3.5c** reported a thick yellow oil. The aromatic monomers **3.5d** and **3.5e** exhibited the lowest yields, potentially with steric bulk being a prohibitive factor for carbon-nitrogen bond formation. To support this claim, synthesis of a naphthyl-functionalized PBTz monomer was attempted using 1-naphthylamine, but no product was observed. Finally, deprotection of **3.5a-f** to produce **3.7a-f** was carried out in the same manner as reported by Marder and Heeney.[31,32]

3.3. Electrochemical Characterization of PBTz Monomers

Figure 3.2 depicts representative voltammograms of the TIPS-protected and deprotected alkyl PBTz. Although the figure depicts the data from **3.5e** and **3.7e**, all of the species displayed the same oxidation pattern. A quasireversible oxidation is present for the TIPS-protected monomers, in contrast with a single, irreversible oxidation for the deprotected PBTz. Since the PBTz oxidation generates a radical cation, the resulting unpaired electron can move to the 2-position of each thiazole via resonance and can undergo polymerization or radical coupling between adjacent units if the silyl group is not present. The sterically-hindering TIPS group prevents this additional chemistry and thus the oxidation is quasireversible for the protected monomers.

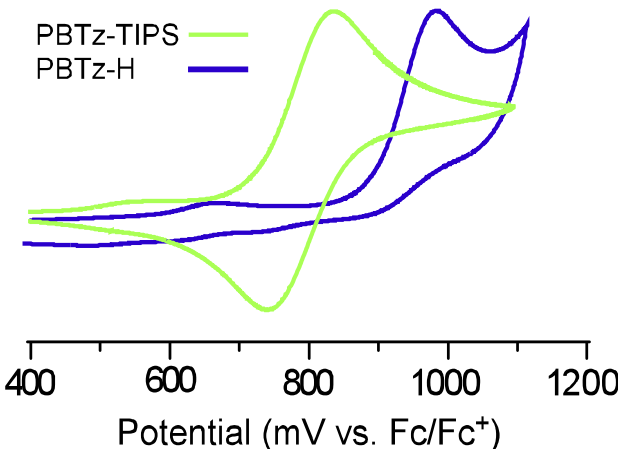

Figure 3.2. Electrochemical comparison of TIPS-protected and deprotected PBTz oxidations

As a point of interest, the TIPS-protected PBTz oxidizes approximately 150-200 mV in the cathodic potential direction compared to the deprotected unit. Traditionally, trialkylsilyl groups tethered to aryl rings have been thought of as electron-withdrawing.[23] Yet, it was shown TIPS does indeed act as an electron-donating group, as measured by a decreased IR frequency of the C-O bond in an organometallic complex substituted with TIPS.[42] This explains the difference

in electrochemical behavior for the TIPS-protected PBTz. Additionally, the data obtained on both alkyl and aromatic PBTz show that the destabilization is consistent across the side chain functionality.

Table 3.1. Electrochemical data for protected and deprotected PBTz species

PBTz Analogue	**$E_{1/2}$, ΔE (mV)**	**E_{pa} (mV)**	**Onset (mV)**	**E_{HOMO} (eV)**
Octyl (**3.6a**)	-	980	870	-6.0
Hexyl (**3.6b**)	-	980	870	-6.0
Dodecyl (**3.6c**)	-	980	870	-6.0
t-Butyl (**3.6d**)	-	960	850	-6.0
Phenyl (**3.6e**)	-	1050	970	-6.1
Hexylphenyl (**3.6f**)	-	1040	950	-6.1
Octyl TIPS (**3.6a**)	780, 140	-	720	-5.8
Hexyl TIPS (**3.6b**)	780, 120	-	720	-5.8
Dodecyl TIPS (**3.6c**)	780, 100	-	720	-5.8
t-Butyl TIPS (**3.4d**)	760, 120	-	710	-5.8
Phenyl TIPS (**3.6e**)	890, 100	-	830	-5.9
Hexylphenyl TIPS (**3.4f**)	880, 100	-	820	-5.9
Octyl DTP[19]	-	510	450	-5.6
Aryl DTP[19]	-	650	-	-5.7
Octanoyl DTP[19]	-	730	670	-5.8
Benzoyl DTP	-	820	-	-5.9

*Potentials referenced to (Fc/Fc^+)

Figure 3.4 shows voltammograms of the PBTz and compares them to the alkyl and acyl DTP units **3.3** and **3.3b**. The electrochemistry shows that the deprotected alkyl monomers exhibit HOMO levels around -6.0 eV in comparison to the ferrocene/ferrocenium redox couple,[43] while the aromatic analogues exhibit a further stabilization near -6.1 eV, in accordance with the electron-withdrawing effect of the aromatic sidechain. With the alkyl and aromatic first-generation DTPs exhibiting HOMO levels near -5.6 and -5.7 eV,[19,28] the PBTz units are stabilized on average 350 mV compared to both the alkyl and aromatic DTPs, and the PBTz stabilization is consistent between aromatic and alkyl DTPs. Interestingly, the PBTz monomers

are even stabilized beyond the level of the second-generation acyl DTPs.[19] Although DFT calculations are a rough estimate of energy levels, the HOMO of the PBTz unit is stabilized beyond what Marder's calculations predicted.[31] Since the acyl DTPs exhibit HOMO levels near -5.8 eV, the PBTz core can be seen to provide the greatest HOMO stabilization while simultaneously allowing the N-functionalization options present in first-generation DTPs. Overall, a significant realization is apparent as a result of this electrochemical study: tuning the HOMO of these fused-ring materials from -5.6 to -6.1 eV can be accomplished in *customizable increments* of approximately 0.1 eV, with progressive stability trending from alkyl DTP < aryl DTP < acyl DTP < acylaryl DTP < alkyl PBTz < aryl PBTz.

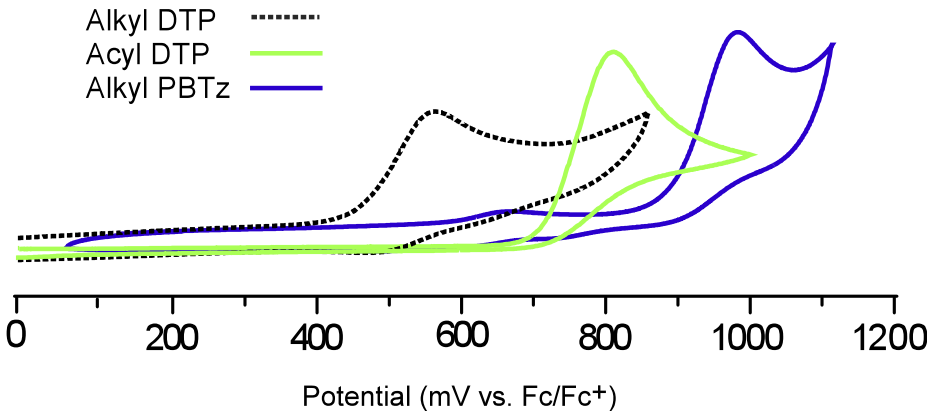

Figure 3.3. Comparison of the DTP and PBTz oxidation potentials

3.4. Optical Properties of PBTz monomers

The optical properties of the PBTz monomers are mostly comparable to DTPs, shown in Figure 3.5. The π→π* transition's absorbance peaks around 305 nm, which is slightly blueshifted from the first-generation DTP **3.3** and strikingly comparable to the second generation **3.3b**. The high-energy transition for **3.3b** is the π→π* transition, while the lower-energy transition is characteristic of an intramolecular charge transfer (CT).[19] Interestingly, the shape of **3.3b**'s absorption is very similar to the broad, featureless absorption for the less-aromatic

thiazole. As with the DTP analogues, the aromatic N-functionalized PBTz showed a higher-energy transition at approximately 245 nm in addition to the normal band. This could be an $S_0 \rightarrow S_2$ transition versus the normal $S_0 \rightarrow S_1$ transition seen in the alkyl analogues.

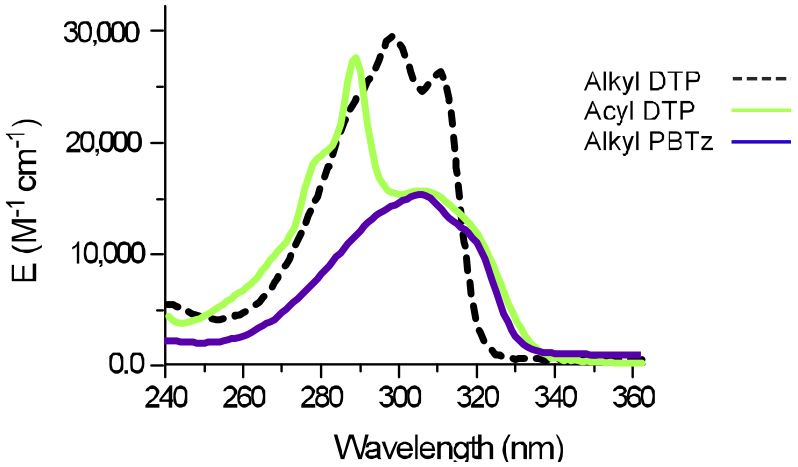

Figure 3.4. UV-vis spectrum comparing absorbances of DTP, PBTz, and acyl DTP

A calculation of the HOMO-LUMO gap was performed based upon the electrochemical and optical measurements via the methods described in Chapter I. The resulting HOMO-LUMO gap was found to be 3.71 eV, which is roughly the same as **3.3b** and approximately 0.2 eV smaller than **3.3**.[19] While the PBTz absorption still arises from the $\pi \rightarrow \pi^*$ transition, there are two probable causes for the reduction in HOMO-LUMO gap akin to **3.3b.** The less-aromatic thiazole could be increasing electron delocalization about the fused-ring system through the inductive effect, in the same way that the electron-withdrawing acyl does. However, increased conjugation would destabilize the HOMO, which was not observed for PBTz. The other possibility is through intramolecular charge transfer, which originally was not expected for the PBTz system. However, DFT calculations performed showed that the thiazole rings did not greatly contribute to the PBTz HOMO, but *significantly* contributed to the LUMO. These data support an intramolecular charge transfer from the electron-rich pyrrole to the electron-poor thiazole,

resulting in the bathochromic shift seen in the onset of absorption and stabilized LUMO calculated for PBTz.

The PBTz molar absorptivity (ε) is reduced compared to the first and second-generation DTPs **3.3** and **3.3b**. The average ε of alkyl and aryl DTP are near 29,000 and 47,000 M^{-1} cm^{-1} respectively, while the alkyl and aromatic PBTz are around 12,000-18,000 M^{-1} cm^{-1}. Interestingly, the ε of the CT contribution for **3.3b** is very similar to the ε of the PBTz unit. Incorporation of the thiazole rings causes the reduction in ε, evidenced in the fact that unfunctionalized thiophene has a molar absorptivity of 6700 and 7300 M^{-1} $cm^{-1}$for its $\pi \rightarrow \pi^*$ transitions while thiazole diminishes to 2300 and 3700 M^{-1} cm^{-1}.[45] Multiple factors can cause this decrease. Thiazole is a smaller heterocycle than thiophene, as can be seen in crystal data, and thus the photoactive surface area is diminished.[29] However, since an extinction coefficient depends on both size of the photoactive site as well as allowedness of the transition,[44] the latter parameter plays a large part in thiazole's ε reduction. The reduced oscillator strength can be also attributed to the charge-transfer character seen in the DFT calculations, as the charge-transfer character would interrupt the π-system from its normal resonance. It was also experimentally shown that that the oscillator strength of thiazole is reduced.[29]

Table 3.2. Optical properties of PBTz monomers

PBTz Analogue	**λ_{max} (nm)**	**ε (M^{-1} cm^{-1})**
Octyl (**3.6a**)	305	14700
t-Butyl (**3.6d**)	306	16600
Phenyl (**3.6e**)	300, 245	18000, 15700
Hexylphenyl (**3.6f**)	305, 246	12700, 10300
Dodecyl (**3.6c**)	304	14200
Hexyl (**3.6b**)	306	15100

An interesting trend is the relation of the molar mass to the molar absorptivity. As stated before, the photoactive surface area of these systems is the PBTz core, with the alkyl sidechain not contributing to the molar absorptivity. The aromatic sidechains should be in conjugation with the PBTz core, and the data show that the phenyl PBTz has the highest extinction coefficient of the series. Interestingly, the hexylphenyl analogue **3.6f** has the lowest extinction coefficient regardless of sidechain type and molecular weight. However, if one disregards the hexyl sidechain's contribution to molar mass, the extinction coefficients raise to 17,000 and 13,700 M^{-1} cm^{-1}, nearing the phenyl analogue.

3.5. X-ray Crystallography

The previous papers published for the PBTz units did not report single crystals for the deprotected units. Marder and co-workers obtained single crystals of the TIPS-protected and brominated units,[31] but did not publish the structure for the deprotected monomer. Thus, single-crystal growth of our PBTz monomers was attempted via the solvent layering, slow evaporation, and solvent diffusion techniques outlined by Bernhard.[46] Attempts with the aromatic PBTz units did not end in success, and the *tert*-butyl PBTz monomer was synthesized with the idea that the small group would lead to better crystals. Unfortunately, the solid obtained for **3.7d** always took the form of a precipitate. The TIPS-protected *tert*-butyl PBTz **3.5d** was able to be analyzed via X-ray crystallography and the resulting structure is shown in Figure 3.6. The PBTz cores are alternate in an edge-to-face packing arrangement, with TIPS groups over each core. This arrangement is different than the face-to-face packing of the crystal structure obtained by Marder and coworkers for **3.5b**. Steric interactions between the bulky *tert*-butyl side chains could be disfavoring face-to-face packing. The N-C bonds of each thiazole in the **3.5d** core are 1.362 and 1.319 Å respectively, and the C-S bonds are 1.773 and 1.712 Å. These bond lengths are

representative of delocalized systems and consistent with the structure of **3.5b** with the maximum difference being 0.005 Å.

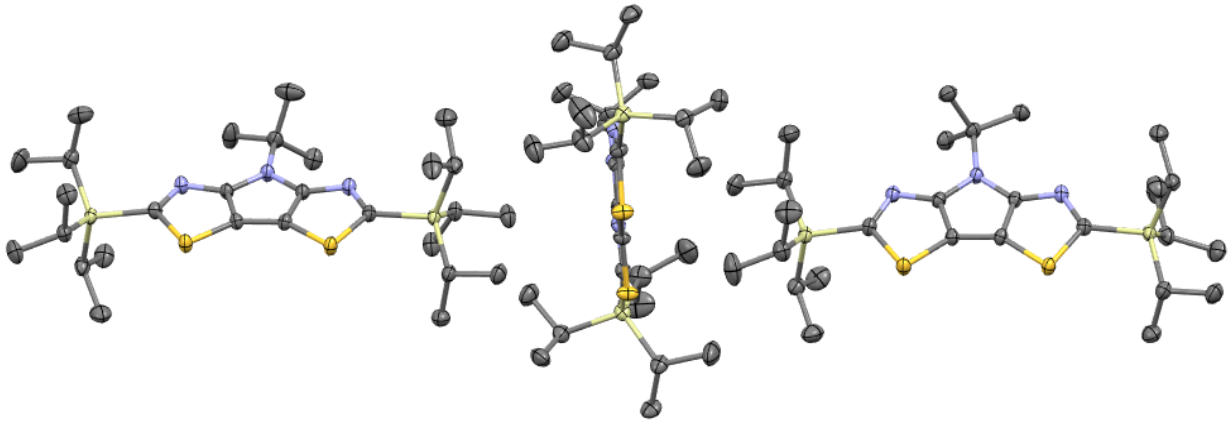

Figure 3.5. Crystal structure of **3.4d** showing edge-to face packing with ellipsoids set at 50% probability and hydrogen atoms omitted for clarity

Upon attempting to isolate single crystals of **3.6e**, a small number of dark-brown crystals were obtained. These produced a somewhat surprising structure of a dimerized PBTz unit with TIPS groups on each periphery. This result carries extra significance because only one report of a dimerized DTP unit exists in the literature,[47] thus this molecule is one of a handful of molecules of its type and the first dimerized PBTz. The structure must have resulted from an unforeseen synthetic error during synthesis of **3.4e**, perhaps a radical coupling between two molecules that lost one TIPS group each due to photolysis. The dimer displays a shortened interannular bond length of 1.43 Å showing good conjugation between the two PBTz units.

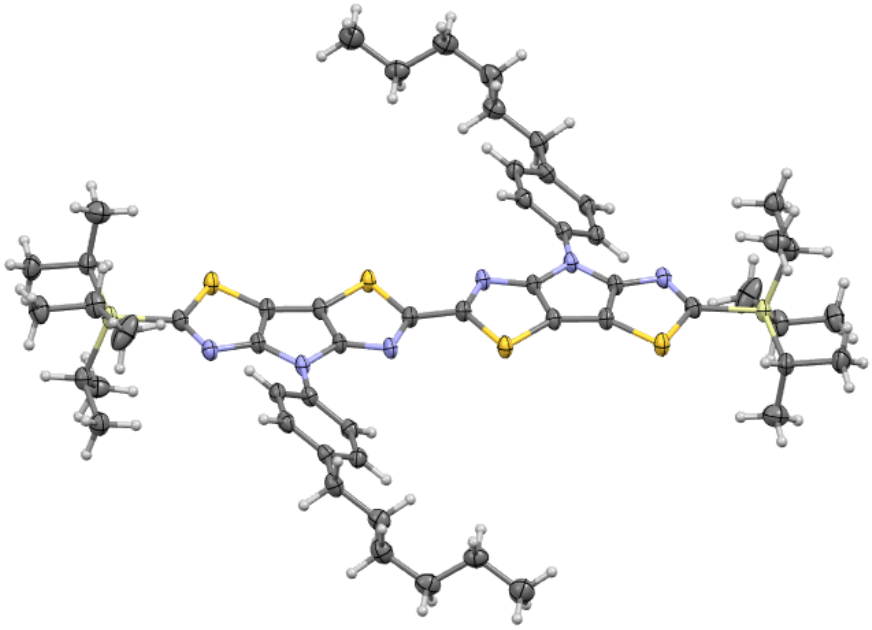

Figure 3.6 Crystal structure of PBTz dimer showing ellipsoid probability of 50%

At long last, crystals of **3.6b** were obtained, somewhat serendipitously. As a last ditch attempt, a vial of pure **3.6b** was heated in a hot bath until the solids melted. Checking the vial two days later, large needle-like crystals were observed, and these were twinned crystals suitable for X-ray analysis. The naked hexyl PBTz exhibits a similar sidechain orientation to the alkyl DTP, with an almost perpendicular angle between the PBTz core and the alkyl chain. The fused-ring core itself is completely planar, which is excellent for potential applications in organic electronics. The packing between units is different than the TIPS analogue as expected, with an unusual sulfur-nitrogen interaction occurring between PBTz units in their sheet-like orientation. This interaction consists of two nitrogen atoms coordinating to opposite sides of the sulfur atom from its C-S bonds, taking advantage of the fact that electron density is pulled toward the carbons in those bonds. Overall, this structure is the most significant of the crystallographic results, as it is the first solved structure for the naked PBTz, fulfilling a total and complete comparison of PBTz to DTP.

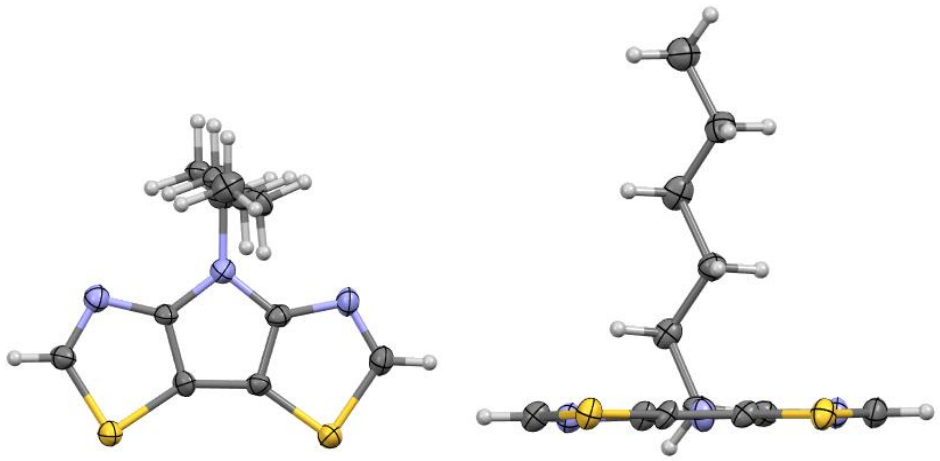

Figure 3.7. Face- and side views of the hexyl PBTz **3.6b** with ellipsoid probability set at 50%

3.6 Attempted Synthesis of N-Acyl PBTz

A direct comparison of the DTP **3.3** to the alkyl PBTz **3.6** was accomplished. However, the PBTz unit still has not been directly compared to **3.3b.** The successful synthesis of acyl PBTz **3.8** (Scheme 3.6) would provide a fused-ring monomer that could feature a HOMO level potentially stabilized beyond that of **3.3b**, combining both the electron deficiency of thiazole with the inductive effect of the acyl sidechain. This would expand the tunability of the frontier orbital levels even further. Depending on the extent of stabilization, the LUMO of **3.8** could reside deep enough to allow application as electron-transporting n-type materials for organic electronics.

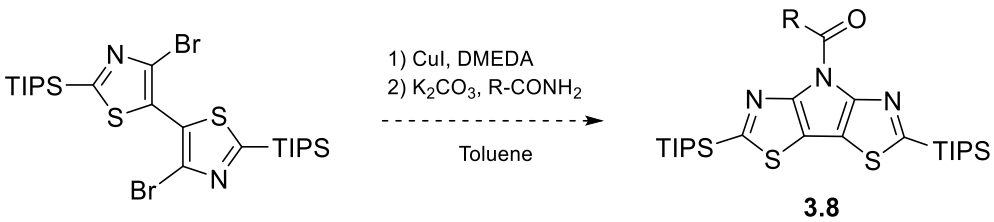

Scheme 3.6. Attempted synthesis of **3.8**

Attempts to synthesize the acyl PBTz **3.8** had been undertaken previously using conditions applied from the synthesis of **3.3b** (Scheme 3.6). They were revisited with a plethora of new reaction conditions, including the use of palladium catalyst and different ligands. As summarized in Table 3.3, all attempts to synthesize **3.8** were unsuccessful and returned starting material. Occasionally a small fraction of debrominated bisthiazole was returned, showing that reductive elimination could be the hindering step in the catalytic cycle. This factor may be explained by thiazole's electron deficiency. Steric crowding from the TIPS ligands was discounted from preventing the amination: attempts were made to synthesize the acyl PBTz with deprotected **3.4** and no product was observed.

Table 3.3. Summary of conditions utilized in to synthesize **3.8**

Solvent	Base	Catalyst	Ligand	Yield
Toluene	K_2CO_3	CuI	DMEDA	0
Xylenes	NaOtBu	CuI	DMEDA	0
Xylenes	NaOtBu	CuI	TMEDA	0
Xylenes	NaOtBu	Pd	(dppf)	0
Xylenes	K_2CO_3	Pd	(dppf)	0
Xylenes	$CsCO_3$	CuI	DMEDA	0
Xylenes	$CsCO_3$	Pd	(dppf)	0

3.7. Conclusions

With the goal of exploring alternative ways to tune the optical and electronic properties of the fused-ring DTP system, the full characterization of the thiazole-based PBTz unit was explored. Four new PBTz analogues were synthesized, including the first reported aromatic N-functionalized units. It was found that the alkyl PBTz units were able to be synthesized in higher yield than their aromatic counterparts, although the deprotection yields were not significantly

affected. Attempts to forgo use of the TIPS group did not result in successful synthesis of the PBTz core.

Concerning the optical and electronic properties of the PBTz unit, it was found that TIPS protection allowed a reversible oxidation and a destabilized HOMO level compared to the naked monomer. The oxidation potentials of the PBTz were found to be more positive than both the first and second generation DTP systems, showing a HOMO stabilized beyond acyl DTPs.. The absorption profile was similar to DTP, but the molar absorptivity values were significantly reduced compared to both the first- and second generation DTPs, which may limit PBTz as a material for organic photovoltaic devices. Greater molar mass contribution of chromophoric PBTz core to sidechain was found to increase extinction coefficient as expected.

As a further goal, synthesis of N-Acyl PBTz species were attempted, but no success was had. Overall, the synthesis of the PBTz unit was further optimized, and direct comparison to both first- and second- generation DTPs was accomplished. With selection of both side-chain and fused-ring functionality, this study showed that the HOMO of the fused-ring bithiophene family can be incrementally tuned by approximately 0.1 eV in a range from -5.6 to -6.1 eV.

3.8. Experimental

General Considerations: All reactions were carried out under nitrogen atmosphere. TIPSCl was purchased from Alfa Aesar. $ZnCl_2$ and $CuCl_2$ were dried in vacuo, and all other materials were reagent-grade and used without further purification. The solvents diethyl ether, xylenes, and tetrahydrofuran were distilled over sodium/benzophenone. All glassware was oven-dried, assembled hot, and cooled under N_2 atmosphere. Chromatography was performed using standard methods, with 230-400 mesh silica gel in 1-inch diameter columns. Melting points were obtained with a digital thermocouple, accurate to 0.1 °C resolution. HRMS (ESI-TOF) was

performed in-house. Electrochemistry was performed on a Bioanalytical Systems BAS 100B/W in CH_2Cl_2 using a Pt disc working electrode, a Pt wire counter electrode, and Ag/Ag+ (0.10M $AgNO_3$ in CH_3CN) reference electrode, and resulting data was calibrated to the ferrocene/ferrocene$^+$ redox couple. NMR spectroscopy was performed on a Bruker 400 mHz spectrometer in $CDCl_3$, with all spectra obtained at 25 °C. All NMR spectra are referenced to the chloroform resonance at 7.26 ppm, and multiplicity is as follows: s = singlet, d = doublet, dd= doublet of doublets. UV-vis spectroscopy was performed on a Cary 500 UV-vis-NIR spectrophotometer, with chloroform as a solvent.

2,2',4,4'-Tetrabromo-5,5'-bisthiazole **(3.6):** A 125 mL addition funnel was attached to a 250 mL three-necked round-bottom flask and placed under N_2 atmosphere. 2,4-dibromothiazole (3.61 g, 15 mmol) and $ZnCl_2$ (2.46 g, 18 mmol) were added to the addition funnel segment. 75 mL THF was added to the round-bottom flask, which was cooled to 0 °C. Diisopropylamide (2.55 mL, 18 mmol) and butyllithium (7.2 mL of 2.5 M soln. in hexanes, 18 mmol) were added to the flask, and the solution stirred for 30 min at 0 °C. Meanwhile, 75 mL THF was added to the addition funnel segment, dissolving the solids. The LDA solution was lowered to -78 °C and the contents of the addition funnel were added dropwise. The resulting bright-yellow solution was stirred for 1 h 45 min. The flask was then warmed to room temperature over 15 min to ensure complete formation of thiazoylzinc chloride. The solution was then cooled once more to -78 °C. $CuCl_2$ was added (2.42 g, 18 mmol) and the solution stirred for 30 min. Dry air was bubbled into the reaction for 2 min, and the flask was left in the cryogenic bath overnight, warming slowly to room temperature. The following day, saturated aqueous NH_4Cl was added to the reaction mixture, and the organic portion separated. The remaining organic product in the aqueous layer was extracted with chloroform, and the combined organic fractions dried over $MgSO_4$. The

combined organic fractions were evaporated *in vacuo*. The resulting brown solid was washed repeatedly with methanol, affording 2,2',4,4'-tetrabromo-5,5'-bisthiazole as a lightly tan solid in 82-88% yield. mp: 224.1-225.6 °C. ^{13}C NMR 138.0, 126.5, 125.4

4,4'-Dibromo-2,2'-bis(triisopropylsilyl)-5,5'-bisthiazole **(3.3)**: To a 500 mL three-necked round-bottom flask was added 2,2',4,4'-tetrabromo-5,5'-bisthiazole (1.45 g, 3.0 mmol). The flask was placed under N_2 atmosphere and 250 mL THF added, followed by triisopropylsilyl chloride (1.41 mL, 6.6 mmol). The solution was immersed in an acetone/CO_2 bath and the temperature dropped to -78 °C. Butyllithium (2.64 mL, 2.5 M soln in hexanes, 6.6 mmol) was added, and the solution stirred at -78 °C for 2 h. The reaction was allowed to warm to room temperature overnight. Saturated aqueous NH_4Cl was poured into the reaction mixture, and the organic portion separated. The remaining organic product was extracted from the aqueous portion with chloroform, and the combined organic layers were dried over $MgSO_4$ and evaporated *in vacuo*. The resulting brown oily solid was purified via column chromatography with 20% chloroform in hexanes to yield 4,4'-dibromo-2,2'-bis(triisopropylsilyl)-5,5'-bisthiazole as a yellow crystalline solid in 75-80% yield. mp: 109.7-110.9 °C. ^{1}H NMR: δ 1.48 (sept, 6 H, *J* = 7.5 Hz) 1.18 (d, 36H, *J* = 7.5 Hz) ^{13}C NMR 172.5, 130.3, 125.0, 18.4, 11.6.

General procedure for the synthesis of 2,6-bis(triisopropylsilyl)-4H-pyrrolo[2,3-d:5,4-d']bisthiazoles: To a 50 mL round-bottom flask equipped with reflux condenser was added sodium *tert*-butoxide (0.461 g, 4.8 mmol), $Pd_2(dba)_3$ (0.045 g, 5 mol %), 4,4'-dibromo-2,2'-bis(triisopropylsilyl)-5,5'-bisthiazole (0.636 g, 1.0 mmol), and racemic BINAP (20 mol %, 0.125 g, 0.2 mmol). Dry xylenes (25 mL) were added, and the solution stirred for 20 min, turning dark violet. The appropriate amine was added (1.5 mmol), and the dark brown solution heated to reflux for 20 h. Water was added, and the organic portion separated. The remaining organic

product was extracted from the aqueous layer with diethyl ether. The combined organic layers were dried over $MgSO_4$ and evaporated *in vacuo,* and the resulting oils purified via column chromatography in hexanes to afford the protected PBTz.

4-Octyl-2,6-bis(triisopropylsilyl)-4H-pyrrolo[2,3-d:5,4-d']bisthiazole (**3.4a**): 65-68% yield. mp: 58.4-60.3 °C. ^{1}H NMR: δ 4.61 (t, *J* = 6.7 Hz, 2H), 2.05 (quint., *J* = 6.7 Hz, 2H) 1.46 (sept., *J* = 7.4 Hz, 6H), 1.31 (m, 4H), 1.21 (m, 6H) 1.18 (d, *J* = 7.4 Hz, 36H) 0.85 (t, *J* = 6.7 Hz , 3H). ^{13}C NMR: δ 166.4, 158.5, 106.7, 45.3, 31.8, 29.8, 29.13, 29.11, 26.8, 22.7, 18.6, 14.1, 11.8. HRMS: m/z 606.3767 calcd for $C_{32}H_{59}N_3S_2Si_2$ $[M]^+$, 606.3776 found.

4-Hexyl-2,6-bis(triisopropylsilyl)-4H-pyrrolo[2,3-d:5,4-d']bisthiazole (**3.4b**): 59-64% yield. mp: 74.9-76.0 °C. ^{1}H NMR: 4.62 (d, *J* = 6.7 Hz, 2H) 2.04 (quint., *J* = 6.7 Hz, 2H), 1.47 (sept., *J* = 7.5 Hz, 6H), 1.28 (m, 6H), 1.19 (d, *J* = 7.5 Hz, 36H), 0.90 (t, *J* = 6.7 Hz, 3H). ^{13}C NMR: δ 166.4, 158.5, 106.7, 45.3, 31.3, 29.7, 26.4, 22.5, 18.6, 14.0, 11.8.

4-Dodecyl-2,6-bis(triisopropylsilyl)-4H-pyrrolo[2,3-d:5,4-d']bisthiazole (**3.4c**): 55-60% yield. mp: 36.8-37.1 °C. ^{1}H NMR: 4.61 (d, *J* = 6.7 Hz, 2H), 2.04 (quint., *J* = 6.7 Hz, 2H) 1.48 (sept., *J* = 7.5 Hz, 6H), 1.28 (p, 18H), 1.19 (d, *J* = 7.5 Hz, 36H), 0.90 (t, *J* = 6.7 Hz, 3H). ^{13}C NMR: δ 166.4, 158.5, 106.7, 45.3, 31.9, 29.8, 29.68, 29.65, 29.64, 29.5, 29.4, 29.1, 26.7, 22.7, 18.6, 14.1, 11.8.

4-tert-Butyl-2,6-bis(triisopropylsilyl)-4H-pyrrolo[2,3-d:5,4-d']bisthiazole (**3.4d**): Synthesized using the methods described above, but substituting tri-*tert*-butylphosphine tetrafluoroborate catalyst for BINAP. 60-63% yield. mp: 82.4-84.1 °C. ^{1}H NMR: δ 2.01 (s, 9H), 1.45 (sept., *J* = 7.4 Hz, 6H), 1.18 (d, *J* = 7.4 Hz, 36H). ^{13}C NMR: δ 164.8, 158.2, 107.5, 59.3, 30.5, 18.6 , 11.7. HRMS: m/z 550.3141 calcd for $C_{28}H_{51}N_3S_2Si_2$ $[M]^+$, 550.3166 found.

4-Phenyl-2,6-bis(triisopropylsilyl)-4H-pyrrolo[2,3-d:5,4-d']bisthiazole (**3.4e**): 45-58% yield. mp: 87.7-89.2 °C. ^{1}H NMR: δ 8.55 (d, *J* = 8.7 Hz, 2H), 7.60 (t, *J* = 7.6 Hz, 2H), 7.34 (t, *J* = 7.6 Hz, 1H), 1.52 (sept., *J* = 7.4 Hz, 6H) 1.22 (d, *J* = 7.4 Hz, 36H). ^{13}C NMR: δ 167.2, 157.1, 138.7, 128.9, 124.6, 120.9, 109.7, 18.6, 11.8. HRMS: m/z 570.2828 calcd for $C_{30}H_{47}N_3S_2Si_2$ $[M]^+$, 570.2833 found.

4-(4-Hexylphenyl)-2,6-bis(triisopropylsilyl)-4H-pyrrolo[2,3-d:5,4-d']bisthiazole (**3.4f**): 40-48% yield. mp: 36.3-36.8 °C. ^{1}H NMR: δ 8.57 (d, *J* = 8.7 Hz, 2H), 7.34 (d, *J* = 8.7 Hz, 2H) 2.67 (quint., *J* = 7.7 Hz, 2H), 1.69 (sept., *J* = 7.7 Hz, 6H), 1.50 (m, 10H), 1.19 (d, *J* = 7.7 Hz, 36H), 0.90 (t, *J* = 7.7 Hz, 3H). ^{13}C NMR: δ 167.0, 157.1, 139.3, 136.4, 128.7, 120.7, 109.4, 35.6, 31.8, 31.5, 28.9, 22.6, 18.6, 14.1, 11.8. HRMS: m/z 654.3767 calcd for $C_{36}H_{59}N_3S_2Si_2$ $[M]^+$, 654.3792 found.

General procedure for the deprotection of 2,6-bis(triisopropylsilyl)-4H-pyrrolo[2,3-d:5,4-d']bisthiazoles: To a 50 mL round-bottom flask under N_2 atmosphere was added the protected PBTz (0.4 mmol) and dry THF (25 mL). Tetrabutylammonium fluoride (1.6 mL of 1.0 M in THF soln, 1.6 mmol,) was added, and the reaction stirred at room temperature for 2 h. The reaction was washed with brine solution and product in the aqueous layer extracted with diethyl ether, the organic layer dried under $MgSO_4$ and concentrated *in vacuo*, and the resulting solid purified via column chromatography in hexanes with 5% diethyl ether to afford the PBTz in 91-97% yield.

4-Octyl-4H-pyrrolo[2,3-d:5,4-d']bisthiazole (**3.7a**): 96-97% yield. mp: 69.1-69.9 °C. ^{1}H NMR: δ 8.60 (s, 2H), 4.57 (t, *J* = 7.4 Hz, 2H), 2.02 (quint., *J* = 7.4 Hz, 2H) 1.35 (m, 4H) 1.25 (m, 6H) 0.85 (t, *J* = 7.4 Hz, 3H) ^{13}C NMR: δ 154.7, 149.0, 103.9, 45.6, 31.7, 30.1, 29.14, 29.12, 26.8, 22.6, 14.1. HRMS: m/z 294.1099 calcd for $C_{14}H_{20}N_3S_2$ $[M + H]^+$, 294.1089 found.

4-Hexyl-4H-pyrrolo[2,3-d:5,4-d']bisthiazole (**3.7b**): 93-96% yield. mp: 82.6-83.6 °C. ^{1}H NMR: δ 8.59 (s, 2H), 4.57 (t, *J* = 7.3 Hz, 2H) 2.02 (quint., *J* = 7.3 Hz, 2H), 1.31 (m, 8H), 0.85 (t, *J* = 7.3 Hz, 3H). ^{13}C NMR: δ 154.7, 149.0, 103.9, 45.6, 31.3, 30.1, 26.5, 22.5, 14.0.

4-Dodecyl-4H-pyrrolo[2,3-d:5,4-d']bisthiazole (**3.7c**): 94-95% yield. mp: 48.6-48.8 °C. ^{1}H NMR: δ 8.59 (s, 2H), 4.57 (t, *J* = 7.2 Hz, 2H) 2.02 (quint., *J* = 7.2 Hz, 2H), 1.34 (m, 5H), 1.22 (m, 13H), 0.88 (t, *J* = 7.2 Hz, 3H) ^{13}C NMR: δ 154.7, 149.0, 103.9, 45.6, 31.9, 30.1, 29.6 (two carbons), 29.53, 29.47, 29.3, 29.2, 26.8, 22.7, 14.1.

4-tert-Butyl-4H-pyrrolo[2,3-d:5,4-d']bisthiazole (**3.7d**): 95-96% yield. mp: 168.4-169.9 °C (dec)**.** ^{1}H NMR: δ 8.56 (s, 2H), 2.01 (s, 9H). ^{13}C NMR: δ 154.6, 147.6, 104.8, 59.7, 30.4. HRMS: m/z 238.0473 calcd for $C_{10}H_{12}N_3S_2$ $[M + H]^+$, 238.0464 found.

4-Phenyl-4H-pyrrolo[2,3-d:5,4-d']bisthiazole (**3.7e**): 92-94% yield. mp: 129.1-131.6 °C. ^{1}H NMR: δ 8.69 (s, 2H), 8.21 (d, *J* = 7.9 Hz, 2H), 7.57 (t, *J* = 7.9 Hz, 2H), 7.35 (t, *J* = 7.5 Hz, 1H). ^{13}C NMR: δ 153.8, 149.6, 137.4, 129.4, 126.2, 122.3, 106.4. HRMS: m/z 258.1060 calcd for $C_{10}H_{12}N_3S_2$ $[M + H]^+$, 258.1064 found.

4-(4-Hexylphenyl)-4H-pyrrolo[2,3-d:5,4-d']bisthiazole (**3.7f**): 91-93% yield. mp: 68.9-70.3 °C. ^{1}H NMR: δ 8.67 (s, 2H), 8.03 (d, *J* = 8.5 Hz, 2H), 7.37 (d, *J* = 8.5 Hz, 2H), 2.68 (t, *J* = 7.7 Hz, 2H) 1.65 (quint., *J* = 7.7 Hz, 2H), 1.31 (m, 6H) 0.89 (t, *J* = 7.7 Hz, 3H). ^{13}C NMR: δ 153.8, 149.5, 141.2, 134.9, 129.3, 122.4, 106.0, 35.6, 31.8, 28.9, 22.7, 18.1, 14.1. HRMS: m/z 342.1099 calcd for $C_{18}H_{20}N_3S_2$ $[M + H]^+$, 342.1082 found.

3.9. References

1. Friend, R. H.; Greenham, N. C. *In Handbook of Conducting Polymers*, 2nd Ed.; Skotheim, T. A., Elsenbaumer, R. L., Reynolds, J. R., Eds.; Marcel Dekker, Inc: New York, 1998; pp 823-880.

2. Cui, T.; Liu, Y. In *Organic Electronics and Photonics: Electronic Materials and Devices*, Nalwa, H. H., Ed.; American Scientific: Stevenson Ranch, 2008; Vol. 1, pp 263-303.
3. Grimsdale, A. C.; Chan, K. L.; Martin, R. E.; Jokisz, P. G.; Holmes, A. B. *Chem. Rev.* **2009**, 109, 897-1091.
4. Ogawa, K.; Rasmussen, S. C. *Macromolecules* **2006**, 39, 1771-1778.
5. Roncali, J. *Chem. Rev*. **1997**, 173-205.
6. Gunes, S.; Neugebauer, H. Sariciftci, S. *Chem. Rev.* **2007**, *107*, 1324−1338.
7. Mishra, A.; Ma, C.-Q.; Bauerlie, P. *Chem. Rev.* **2009,** *109*, 1141–1276.
8. Mishra, A.; Ma, C-Q.; Segura, J.; Bauerle, P. In *Handbook of Thiophene-Based Materials: Applications in Organic Electronics and Photonics*; Perepichka, I., Perepichka, D., Eds.; Wiley: West Sussex, U. K., 2009; Vol. 1, pp 1-157.
9. Rasmussen, S.C.; Evenson, S. J.; McCausland, C. B. *Chem. Commun.* **2015**, 51, 4528-4543.
10. Radke, K. R.; Ogawa, K.; Rasmussen, S. C. *Org. Lett.* **2005**, *7*, 5253-5256.
11. Balaban, A. T.; Oniciu, D. C.; Katritzky, A. R. *Chem. Rev*. **2004**, *104*, 2777−2812.
12. Zanirato, P.; Spagnolo, P.; Zanardi, G. *J Chem. Soc. Perkin. Trans. 1* **1983**, 2551-2554.
13. Gronowitz, J. E.; Skramstad, J.; Eriksson, B.; *Ark. Kemi.* **1967**, *28*, 99-107.
14. Berlin, A.; Pagani, G.; Zotti, G.; Schiavon, G. *Makromol. Chem*. **1992**, *193*, 399-409.
15. Ogawa, K.; Radke, K. R.; Rothstein, S. D.; Rasmussen, S. C. *J. Org. Chem.* **2001**, *66*, 9067-9070.
16. Kenning, D. D.; Ogawa, K.; Rothstein, S. D.; Rasmussen, S. C. *Polym. Mater. Sci. Eng.* **2002**, *86*, 59-60.
17. Ogawa, K.; Rasmussen, S. C. *J. Org. Chem.* **2003**, *68*, 2921-2928.

18. Nozaki, K.; Takahashi, K.; Nakano, K.; Hiyama, T.; Tang, H.; Fujiki, M.; Yamaguchi, S.; Tamao, K. *Angew. Chem. Int. Ed.* **2003**, *42*, 2051-2053.

19. Evenson, S. J.; Rasmussen S. C. *Org. Lett.* **2010**, *12*, 4054-4057.

20. Koeckelberghs, G.; De Cremer, L.; Vanormelingen, W.; Dehaen, W.; Verbiest, T.; Persoons A.; Samyn, C. *Tetrahedron* **2005,** *61*, 687-691.

21. Mitsudo, K.; Shimohara, S.; Mizoguchi, J.; Mandai, H.; Suga, S.; *Org. Lett.*, **2012**, *14*, 2702–2705

22. Evenson ,S. J.; Mumm, M. J.; Konstantin, P. I.; Rasmussen, S. C. *Macromolecules* **2011**, *44*, 835-841.

23. Price, S.; Stuart, A.; You, W. *Macromolecules* **2010**, *20*, 123-124.

24. Yue, W.; Zhao, Y.; Shao, S.; Tian, H.; Xie, Z.; Geng, Y.; Wang, F. *J. Mater. Chem.* **2009**, *19*, 2199-2206.

25. Steckler, T. T.; Zhang, X.; Hwang, J.; Honeyager, R.; Ohira, S.; Zhang, X.-H.; Grant, A.; Ellinger, S.; Odom, S. A.; Sweat, D.; Tanner, D. B.; Rinzler, A. G.; Barlow, S.; Bredas, J.-L.; Kippelen, B.; Marder, S. R.; Reynolds, J. R. *J. Am. Chem. Soc.* **2008**, *131*, 2824-2826.

26. Liu, J.; Zhang, R.; Sauve, G.; Kowalewski, T.; McCullough, R. *J. Am. Chem. Soc.* **2008**, *130*, 13167-13176.

27. Blouin, N.; Michaud, A.; Gendron, D.; Wakim, S.; Blair, E.; Neagu-Plesu R.; Belletete, M.; Durocher, G.; Tao, Y. Leclerc, M. *J. Am. Chem. Soc.* **2008**, 130, 732-742.

28. Evenson, S. J; Pappenfus, T. M.; Ruiz Delgado, M. C.; Radke-Wohlers, K. R.; Lopez Navarrete, J. T.; Rasmussen, S. C. *Phys. Chem. Chem. Phys*., **2012**, *14*, 6101–6111.

29. Uzelac, E. J.; Rasmussen, S. C. *Eur. J. Inorg. Chem.* **2017**, *33*, 3878-3883.

30. Lin, Y.; Fan, H.; Li, Y.; Zhan, X. *Adv. Mater.* **2012**, *24*, 3087-3106.

31. Al-Hashimi, M.; Labram, G. J.; Watkins, S.; Motevalli, M.; Anthopoulos, T. D.; Heeney, M. *Org. Lett*. **2010**, *12*, 5478−5481.

32. Getmaneko, Y. A.; Singh, S.; Sandhu, B.; Wang, C.-Y.; Timofeeva, T.; Kippelen, B.; Marder, S. R. *J. Mater. Chem. C,* **2014**, *2*, 124-131.

33. Patra, D.; Lee, J.; Lee, J.; Sredojevic, D. N.; White, A. J. P.; Bazzi, H. S.; Brothers, E. N.; Heeney, M.; Fang, L.; Yoon, M.-H.; Al-Hashimi, M. *J. Mater. Chem. C*, **2017**, *5*, 2247-2258.

34. Schnürch, M.; Spina, M.; Khan, A. F.; Mihovilovic, M. D.; Stanetty, P. *Chem. Soc. Rev.* **2007**, *36*, 1046−1057.

35. Getmaneko, Y. A.; Risko, C.; Tongwa, P.; Kim, E.-J.; Li, H.; Sandhu, B.; Timofeeva, T.; Bredas, J.-L.; Marder, S. R. *J. Org. Chem.* **2011**, *76*, 2660-2671.

36. Stangeland, E. L.; Sammakia, T. *J. Org. Chem.* **2004**, *69*, 2381-2385.

37. Greene, T. W.; Wuts, P. G. M. *Protective Groups in Organic Synthesis*, 3rd ed. John Wiley & Sons: New York, 1991.

38. Stangeland, E.; Sammakia, T. *J. Org. Chem.* **2004**, *69*, 2381-2385.

39. Soderquist, J. A.; Rivera, I.; Negron, A. *J. Org. Chem.* **1989**, *54*, 4051-4055.

40. Alfa Aesar. https://www.alfa.com/en/. Accessed 10-1-17

41. Sigma Aldrich. https://www.sigmaaldrich.com/united-states.html. Accessed 9-30-17

42. Panek, J. S.; Prock, A.; Eriks, K.; Giering, W. P. *Organometallics* **1990**, *9*, 2175-2176.

43. Bock, H. Siedl, H. *J. Am. Chem. Soc.* **1968**, *90*, 5694-5700.

44. Cardona, C. M.; Li, W.; Kaifer, A. E.; Stockdale, D.; Bazan, G. C. *Adv. Mater.* **2011**, *23*, 2367-2371.

45. Braude, E.; *J. Chem. Soc.* **1950**, 379-384

46. Katritzky, A.; Pozharskii, A. *Handbook of Heterocyclic Chemistry*, 2nd. Ed. Pergamon, New York, NY, 2000, pp 101

47. Spingler, B.; Schnidrig, S.; Todorova, T.; Wild, F. *Cryst. Eng. Comm*, **2012**, *14*, 751-757.

48. Yassin, A.; Leriche, P.; Roncali, J. *Macromol. Rapid Commun.* **2010**, *31*, 1467-1472.

49. Pappenfus, T. M.; Burand, M. W.; Janzen, D. E.; Mann, K. R.; *Org. Lett.* **2003**, *5*, 1535-1539.

CHAPTER IV. A NEW SERIES OF ARYL-EXTENDED PYRROLO[2,3-*d*:5,4-*d'*]BISTHIAZOLE OLIGOMERS

4.1. Introduction

Over the past few decades there has been considerable advancement in the field of organic electronics, which utilize organic materials that combine electronic properties typical of inorganic semiconductors with the flexibility and low production costs of plastics.[1] Thiophene-based materials are thought to be one of the most versatile classes of materials for organic electronics, and oligothiophenes have received special attention. Featuring highly-tunable conjugation lengths and low molecular weights, these molecules are able to be solvent-cast like polymers, or deposited via vacuum sublimation.[2-5] The ease of processing combined with tunable optoelectronic properties has led to oligothiophene use in OLEDs, OPVs, and OFETs.[6-10] Examples of oligothiophenes in literature showcase how their versatility leads to multiple applications. Linear oligothiophene materials have been documented to absorb across the UV and visible regions with simple synthetic modifications, as exemplified by the ter- and hexathiophene oligomers developed by Pappenfus and coworkers (Figure 4.1.).[11] Capping with tricyanovinyl groups has a dramatic, yet controllable, effect on the absorbance wavelengths of the compounds, a feature more difficult to control in polymeric systems.

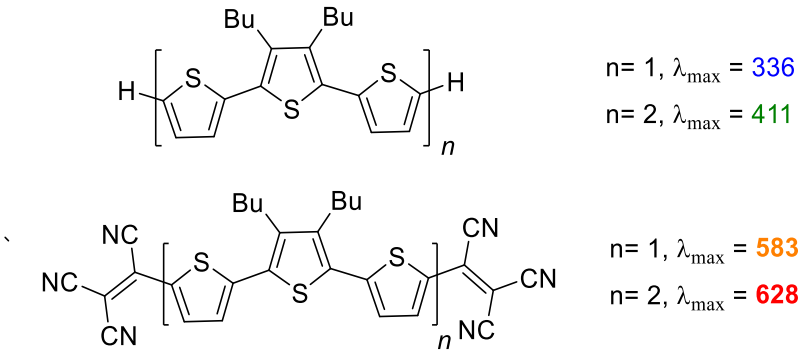

Figure 4.1. Linear oligothiophene systems capped with tricyanovinyl groups to tune absorption

In addition to linear oligothiophenes, fused-ring variants are attractive for the aforementioned applications due to the optoelectronic properties bestowed by their increased planarity and electron delocalization (Figure 4.2). The charge-carrying mobilities and π-stacking interactions are enhanced in fused-ring oligothiophenes such as DTP which allows them to act as ambipolar units in OFETs as opposed to simple *p*- or *n*- type transistors.[12] As a significant example, Kippelen and coworkers extended the conjugation of electron-rich DTP with two electron-poor naphthalene diimide units to produce an organic transistor that acts as both a hole and electron transporting unit.[13] In the same vein, DTP oligomers with cyanovinyl groups have also been reported by Pappenfus and Rasmussen,[14] and also by Zhu.[15]

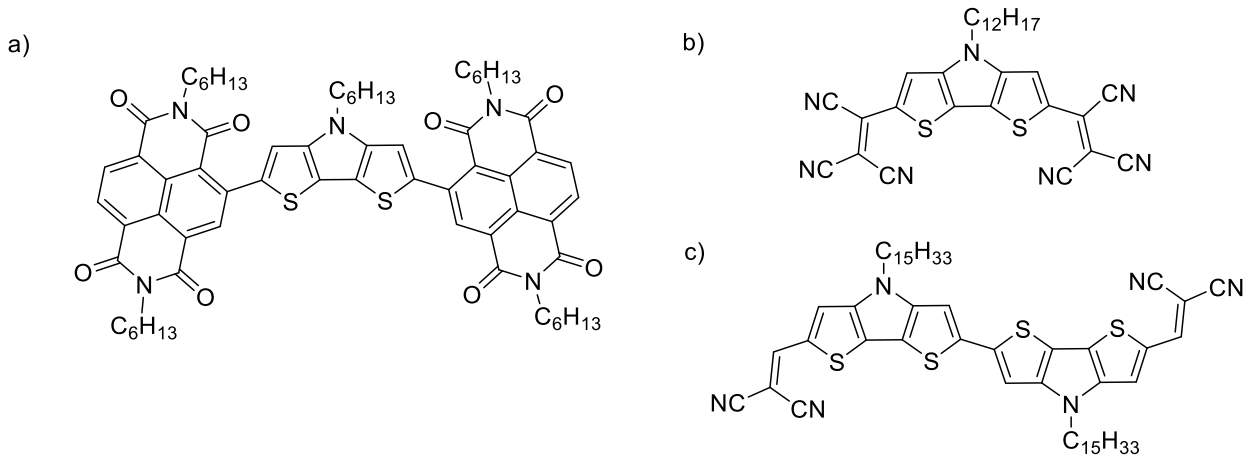

Figure 4.2. Examples of DTP oligomers for OFET use developed by Kippelen (a),[13] Pappenfus (b),[14] and Zhu (c)[15]

Although widely used in materials as described above, the first examples of DTP oligomers were developed by the Rasmussen group. After publishing their new synthetic route to DTP in 2003,[16] Rasmussen and coworkers reported the first examples of aryl-extended DTP oligomers in 2005 as model compounds for a series of planned DTP polymers (Figure 4.3).[17] The first series of oligomers were both mono- and diarylated (**4.3a**) with pendent thiophenes, showing that each additional pendent ring provided 40-50 nm of bathochromic shift in

absorption wavelength. The monomers were N-functionalized with octyl groups, providing good solubility in organic solvents despite the increased conjugation. A further study in 2007 reported N-functionalization with *tert*-butyl groups and expanded the array of substituents on the pendant aromatic rings,[15] which allowed further control of optical and electronic properties. Additionally, a new material property was discovered during these studies: although DTP itself exhibits poor fluorescence, the aryl extended oligomers **4.3** showed excellent photophysical properties with solution fluorescent quantum yields of 0.65 for **4.2b**.[15]

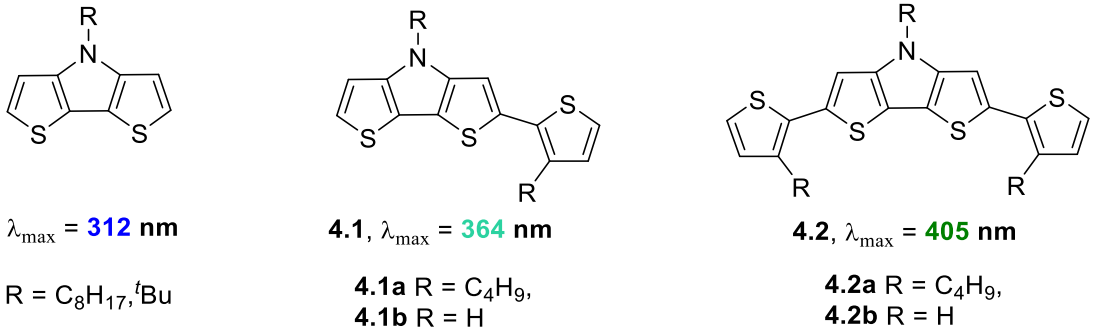

Figure 4.3. Select examples of mono- and diarylated DTP oligomers[15] showing how additional aromatic units bathochromically shifts absorption λ_{max}

X-ray crystallography was performed on single crystals of the *tert*-butyl DTP oligomers. The data revealed that the oligomers exhibited slipped π-stacking of two varieties (Figure 4.4), one with close molecular contacts between the pendent thiophene rings, and another with the molecules eclipsed over the DTP core. Each orientation suggests good electron delocalization, and close intermolecular contacts showed effective π-stacking. Overall, the fused-ring system enhanced the DTP fluorescence properties compared to analogous linear oligothiophenes making aryl-extended DTPs prime candidates for OLED application.

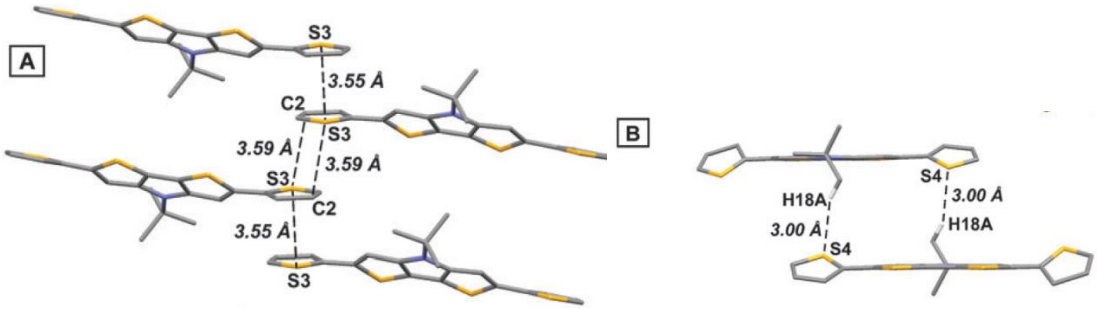

Figure 4.4. Crystal packing of a ^{t}Butyl DTP oligomer, showing slip-stacking over the external thiophenes (a) and approximately one-half of the molecular plane (b). Adapted from ref. 15

With the goal in mind of examining how the "second-generation" acyl DTPs behaved with aryl extension, the Rasmussen group synthesized a new series of quarterthiophene DTP oligomers in 2010.[19] Utilizing acyl and benzoyl N-functionalities (**4.3c,d** and **4.4c,d**), the optoelectronic properties of the entire series of DTP oligomers (Figure 4.5) was compared. It was found that the acyl and benzoyl oligomers did not show the expected bathochromic shift in solution, due to the carbonyl's effect on the polarizability of the oligomer and thus different conformations in solution compared to the alkyl analogues. However, their solid state absorbances were redshifted, and quantum yields generally increased over the alkyl analogues, with a very high fluorescent quantum yield of 0.93 for the phenyl-extended benzoyl DTP **4.4d**. The frontier orbitals were also stabilized with the acyl modifications, with the benzoyl sidechain showing the greatest stabilization by up to 250 mV over the alkyl analogue.[19]

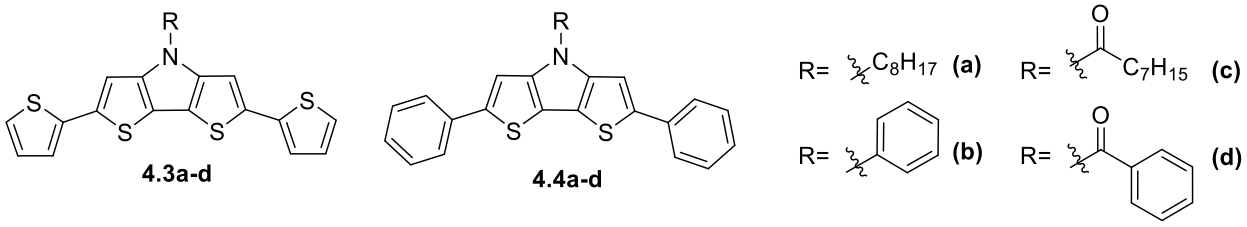

Figure 4.5. Series of first- and second- generation aryl-extended DTP oligomers

The Rasmussen group's 2010 study showed that precise tuning of optical and electronic properties of DTP quarterthiophenes is attainable through both aryl-extension and N-functionalization. There remained one major area of the oligothiophene system to modify, however: the fused-ring core itself. With the synthesis and characterization of a new PBTz monomer family accomplished as detailed in Chapter III, performing aryl-extension to forge a series of PBTz oligomers akin to the DTP family was undertaken (Figure 4.6).

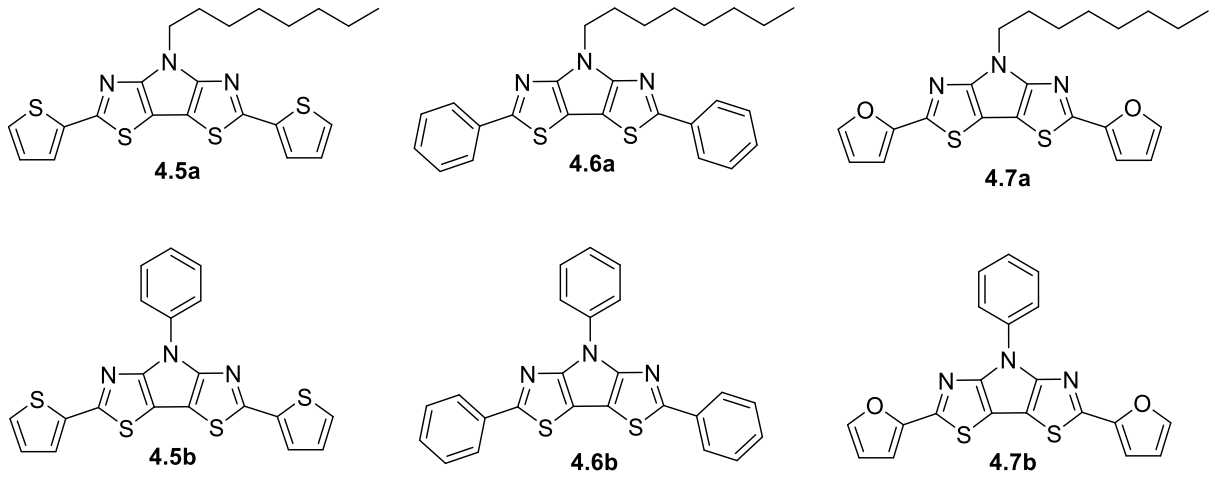

Figure 4.6. Series of thienyl-, phenyl-, and furyl-extended PBTz oligomers with alkyl and aromatic sidechains

There were a few key reasons for this study. A prominent goal was to explore how extending the conjugation path impacts the optoelectronic properties of the PBTz. Since the PBTz monomers exhibited significantly reduced molar absorptivities which can limit their use in devices, it was critical to know if aryl functionalization could mitigate this major hinderance. Additionally, discovering if aryl-extended PBTz behaved similarly to DTP would allow further comparison of the two units. Finally, the furyl-extended analogues provide a synthetic modification that has not been performed on a DTP-based system and a new research direction for the Rasmussen group.

4.2. Synthesis of Aryl-Extended PBTz Oligomers

The synthetic pathway towards the PBTz oligomers began with the PBTz monomer, of which octyl and phenyl extended units were chosen to provide the most accurate comparison to the DTP oligomers **4.3a-b** and **4.4a-b**. To form the carbon-carbon bonds via Stille or Suzuki coupling, both a brominated and metallated aryl group are needed.[19] In the case of first-generation DTP precursors, metalation with an organotin species was undertaken and the resulting molecule paired with a bromothiophene or bromobenzene, as the highly electron-rich DTP was oxidatively unstable upon bromination. For the acyl and benzoyl DTP analogues, bromination of the DTP was facile and the unit was paired with a stannylarene. For the current study, bromination of the PBTz was chosen over metalation due to the stabilized HOMO levels. Bromination of both PBTz monomers to produce **4.8** and **4.9** proceeded smoothly, although in lower yield than the DTP analogues (Scheme 4.1). The reaction can be performed in both chloroform and DMF, and a visible diminishing of luminescence due to the heavy atom effect[20] was noted as the reaction proceeded and used as a visual cue to monitor progress.

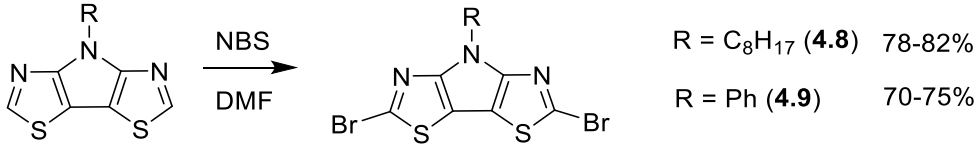

Scheme 4.1. Bromination of PBTz monomers to produce precursors for cross-coupling

Using the methods developed by Evenson and Rasmussen,[19] the synthesis of PBTz oligomers was then undertaken. The cross-coupling conditions for the acyl DTP analogues (**4.3c,d** and **4.4c,d**.) were chosen due to the close energetic relation of acyl DTPs to PBTz: Stille coupling for the thiophene-extended analogue, and Suzuki couplings for the phenyl-extended analogues. However, issues were noted with both methods when applied to PBTz. Synthesis of

4.5a was attempted first via Stille coupling of the brominated PBTz and tributylstannyl-thiophene, but a mixture of mono- and di-coupled oligomer was produced as well as a slight recovery of starting material (Scheme 4.3a). Even after 24 h of reflux with toluene, the desired oligomer **4.11** was only produced in approximately half the ratio as monocoupled oligomer. Adding further stoichiometric excess of the other reaction components did not make a significant difference in the ratio of products or their yields.

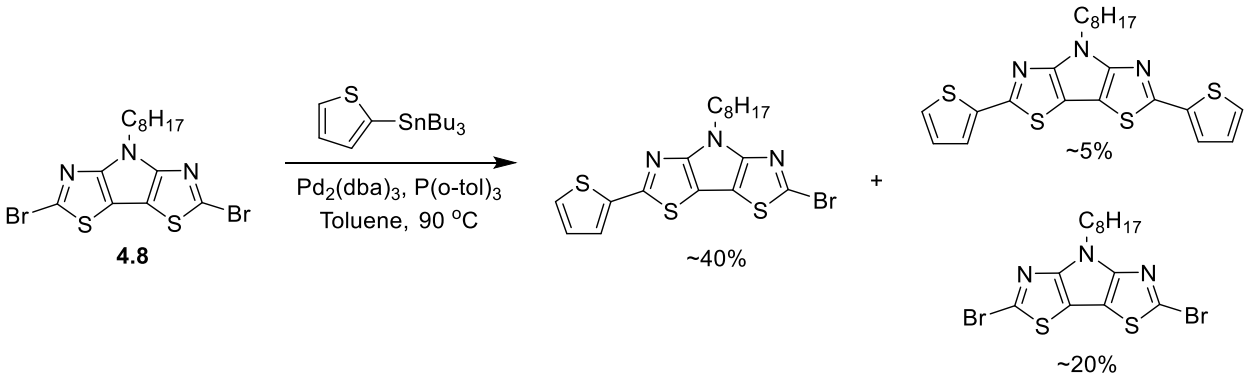

Scheme 4.2. Attempts at synthesis of **4.5a** with direct conditions from DTP analogues

Meanwhile, Suzuki coupling was employed in the same manner as Rasmussen and coworkers' 2010 study to produce the phenyl-extended oligomers **4.5b** and **4.6b**. As opposed to the thienyl analogue, only a trace amount of monocoupled product was synthesized, and only a small portion of starting material was returned. A black film corresponding to decomposed PBTz was observed on the reaction vessel during each attempt. With the slight success of the Stille coupling route for the thienyl-extended analogue, 2-tributylstannyl benzene was prepared and Stille coupling conditions were attempted. While success was greater using these conditions than the Suzuki coupling, most of the product was monocoupled PBTz in a very similar manner to the thienyl analogue.

The lack of success prompted a recollection of the synthesis of the PBTz monomers family, in which a significant difference between the methods employed to synthesize PBTz and the DTP synthesis was involved. Whereas the Buchwald-Hartwig amination of the DTPs could be carried out in toluene, attempts to synthesize any PBTz in toluene failed. The thiazole ring may have disfavored the reductive elimination of the palladium center at the lowered temperatures, as this would require the transfer of electrons from the already electron-deficient thiazole to the metal. Xylenes, with its higher boiling point, provided the necessary thermal energy for PBTz synthesis. Thus, synthesis of the **4.5a** was attempted with xylenes as a solvent, and the results were successful. The product was predominately dicoupled, with a small fraction of monocoupled oligomer and a trace of starting material. These new conditions were successful with both phenyl and octyl PBTz, and produced **4.5a,b-4.6a,b** in 40-55% yield. Purification of the oligomer was performed via column chromatography, although excess arylstannane was found to have a similar R_f value to the oligomers in all feasible solvent systems and contaminated the oligomer even after multiple runs through the column. Washing the octyl oligomers with 10% HCl and the phenyl oligomers with cold hexanes removed the impurities.

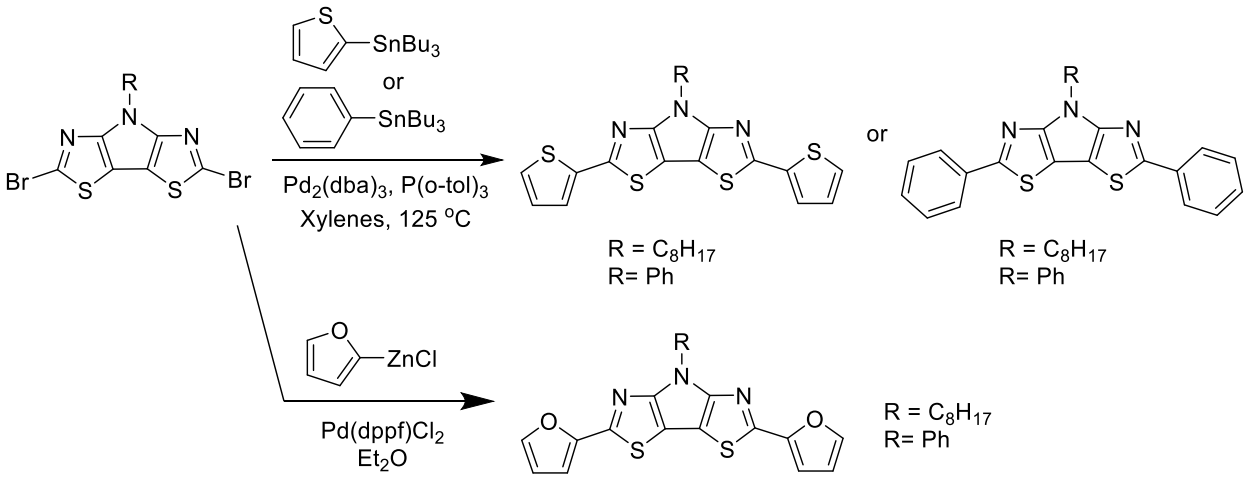

Scheme 4.3. Successful synthesis of **4.5** and **4.6** series oligomers via modified Stille conditions, and **4.7** series via Negishi coupling

Attempts to synthesize the new furyl oligomers **4.7a** and **4.7b** through Stille coupling methods failed, as the tributylstannyl-furan would readily decompose upon heating in xylenes. As an alternative method, a double Negishi coupling was attempted due to the gentle, room-temperature reaction conditions.[21] Synthesis of the furylzinc chloride intermediate was successful as evidenced by thin-layer chromatography (TLC) and a white solution appearance, and addition of the brominated PBTz resulted in the same appearance of bright fluorescence observed during Stille conditions. The Negishi method was a success and produced **4.7a** and **4.7b** in good yields. (Scheme 4.3).

Obtaining NMR spectra of the phenyl N-functionalized oligomers came with a set of challenges not observed in the thiophene counterparts. Whereas the octyl N-functionalized oligomers were readily soluble in $CDCl_3$ solvent, the phenyl analogues were only slightly soluble. Other solvents such as dimethyl sulfoxide-d_6 and benzene-d_6 contained solvent peaks in the range of expected signals for the oligomers and were not used. Sufficient quantities of **4.5b** and **4.7b** to perform carbon NMR were able to be dissolved in $CDCl_3$ at 40 °C, but **4.6b** proved to be the least soluble. The maximum scanning temperature of 50 °C was not able to fully dissolve the sample. Consequently, interesting resonances appeared in the carbon spectrum. The resonances corresponding to the PBTz core each had a duplicate which appeared close by, as well as the resonances corresponding to the external phenyl ring. A dimeric, off-centered π-stack between two oligomers, *analogous to the DTP packing observed in Figure 4.2*, may be causing this change at high concentrations (Figure 4.7), as this would provide a different chemical environment for seven carbons in each molecule.[22] The NMR experiment was repeated at low concentrations (7 mg **4.14** in 700 μL $CDCl_3$). The expected number of carbon resonances appeared, further supporting the hypothesis of dimeric interactions at high concentration.

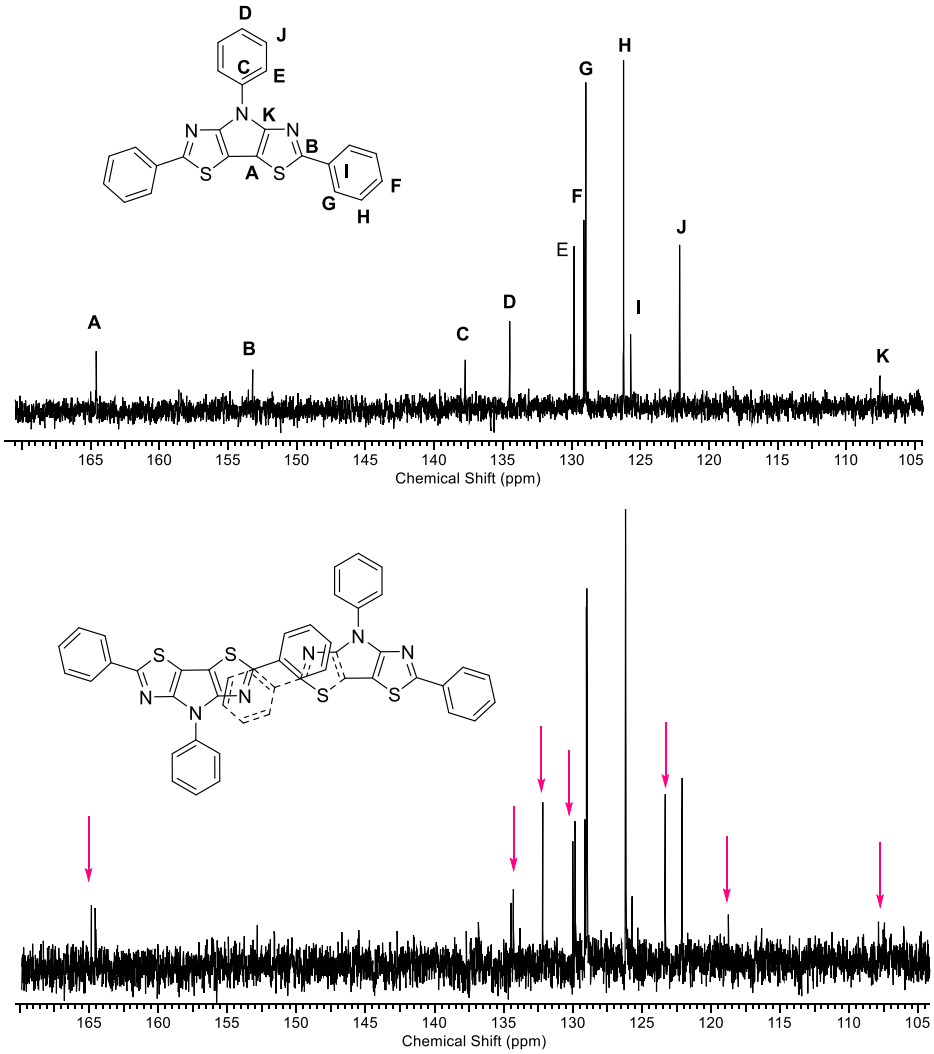

Figure 4.7. Potential dimeric, π-stacked configuration of two **4.6b** oligomers at high concentrations, with pink arrows showing the seven additional peaks

4.3. Electrochemical Characterization of PBTz Oligomers

To determine the HOMO energy levels for the series of PBTz oligomers and compare them to the DTP analogues, cyclic voltammetry was performed. As with their DTP analogues, all of the PBTz oligomers exhibited a quasi-reversible initial redox couple corresponding to the single-electron oxidation of the HOMO, as well as a second, irreversible oxidation (Figure 4.8).[19] The phenyl-extended oligomers typically exhibit reversible redox couples because their radical cations are expected to π-stack but not couple, as evidenced by x-ray structures of a similar

oligothiophene.[23] Observing a reversible oxidation is unusual for thienyl-extended oligothiophenes, as the radical is often localized on the alpha-position of the peripheral thiophene units, allowing fast radical coupling between units which is observable as shifting oxidation potentials in the voltammogram.[24] The reversible oxidation for the DTP and PBTz species implies that the radical cation formed via oxidation of the HOMO is localized on the fused-ring core, which lowers α-radical contribution and thus reduces the kinetic rate of radical coupling. This proposal was supported by calculations performed on the electron-spin density of DTP oligomers.[19]

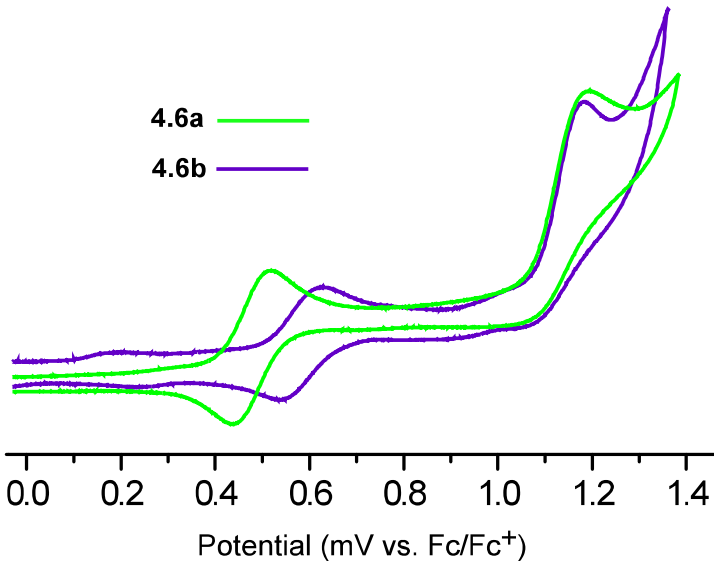

Figure 4.8. Representative PBTz oligomer voltammograms comparing the alkyl and aromatic N-functionalization

Table 4.1 shows the oxidation potentials of the PBTz oligomers, as well as the first- and second-generation DTP oligomers. Some notable trends arise from these data. Phenyl-capped oligomers generally show a stabilized HOMO compared to the thienyl oligomers, which is well-documented and due to the increased aromaticity of the benzene ring, which hinders conjugation across the backbone.[19] The new furyl-extended oligomers showed the most destabilized HOMO,

which may result from their electron-rich nature. Comparing the HOMO values for the **4.5** and **4.6** series oligomers, the first oxidation corresponding to $0/^{+}1$ for all of the PBTz species occur at more positive potentials than the alkyl DTP analogues, showing stabilization of the HOMO comparatively. In addition, the $0/^{+}1$ oxidation couple always occurs at a more positive potential than the corresponding acyl DTP oligomer. This trend shows that the HOMO levels of the new PBTz oligomers are more stabilized than both generations of DTP, the entirety of series **4.3** and **4.4**. This behavior is a match to the trends seen in the corresponding PBTz monomers. The inductive effect of the acyl sidechain could be weaker than the electron-withdrawing effects of thiazole substitution, providing further stabilization for the DTP series. This stabilization is similar in magnitude compared to the corresponding monomers, with increased anodic potentials of 250-350 mV going from alkyl DTP to PBTz and 150-250 mV from acyl DTP to PBTz**.**

Table 4.1. Electrochemical properties of PBTz oligomers and comparison to DTP analogues

Oligomer	E_{pa} (mV)	$E_{1/2}^{0/+1}$ (mV)	$E_{pa}^{+1/+2}$ (mV)	E_{HOMO} (eV)
C_8ThPBTz (**4.5a**)	490	450	1020	-5.55
C_8PhPBTz (**4.6a**)	650	610	1300	-5.71
C_8FuPBTz (**4.7a**)	480	-	630	-5.5
PhThPBTz (**4.5b**)	590	550	1040	-5.65
PhPhPBTz (**4.6b**)	960	690	1290	-5.79
PhFuPBTz (**4.7b**)	520	-	1250	-5.5
C_8ThDTP (**4.3a)**	-	300	930	-5.29
C_8ThADP (**4.3c**)	-	470	860	-5.43
C_8PhDTP (**4.4a**)	-	380	1050	-5.37
C_8PhADTP (**4.4c**)	-	580	1130	-5.56
PhThDTP (**4.3b**)	-	360	1060	-5.35
PhThADTP (**4.3d**)	-	510	1090	-5.46
PhPhDTP (**4.4b**)	-	470	1090	-5.45
PhPhADTP (**4.4d**)	-	620	1130	-5.60

*Potentials referenced to (Fc/Fc^{+}) for PBTz and (Ag/Ag^{+}) for DTP

The second oxidations (+1/+2) for the new **4.5** and **4.6** series PBTz oligomers continue the trend seen in the oxidation of their HOMO. The new PBTz oligomers generally exhibit a second oxidation at a more positive potential than their DTP analogues. The radical cation generated at the PBTz core appears to be stabilized compared to DTP. If the electron density on the peripheral thiophenes is decreased to stabilize the polaron, oxidation would be more difficult. A distinct diradical character was observed in electrochemical studies on the previous oliogmers,[19] and if the second oxidation does correspond to formation of another radical, the external thiophenes would be a logical center for the second oxidation and the argument is supported.

Overall, the electrochemical characterization of the new series of phenyl- and thienyl-extended PBTz oligomers finds that HOMO is stabilized more than that of the first and second generation DTP oliogomers, and the incremental tunability of the HOMO via both N-functionalization and aryl-extension holds true for PBTz in a similar manner to DTP. The furyl-extended oligomers **7a** and **7b** were found to have destabilized HOMO levels compared to series **4.5** and **4.6**. as evidenced by the more negative oxidation potentials for the 0/+1 couple. As furan is even less aromatic than thiophene,[27,28] better electron delocalization may be occurring across the oligomer backbone, destabilizing the HOMO. Both the alkyl and aromatic furan PBTz oligomers displayed this destabilization.

The $0/^{+}1$ oxidation for the furan PBTz was found to be irreversible in both **4.7a** and **4.7b.** With the thought that scanning to the $^{+}1/^{+}2$ couple may result in decomposition of the oligomer and thus little material to reduce, the scanning potential window was narrowed to the first oxidation only. Nevertheless, the transition proved to be irreversible. In addition to this abnormality, the second oxidation for **4.7a** occurred directly after the first, with approximately

150 mV separating them. Scanning was taken to 1800 mV to probe for additional peaks, but none appeared. The working electrode's surface was coated with a red-black material as well. A explanation for these observations could lie in greater radical density localized on the furyl pendent rings due to the reduced furan aromaticity. This increased radical localization could increase the propensity for radical coupling. However, **4.7b** did not display a second oxidation at such negative potentials, though, falling in line with the other phenyl N-functionalized oligomers. The phenyl ring could possibly stabilize the radical cation through resonance, allowing the material to stay intact long enough for a second oxidation to occur.

4.4. UV-vis Characterization of PBTz Oligomers

The series of PBTz oligomers was analyzed via UV-vis spectrometry to determine their absorption profile. The oliogomers show a large and broad $\pi \rightarrow \pi^*$ transition similar to the PBTz monomers. The λ_{max} of the $\pi \rightarrow \pi^*$ transition is bathochromiacally shifted approximately 100-130 nm in comparison to the PBTz monomers. This fits in well with the accepted correlation of increasing conjugation length to bathorchromic shift of energy transition and a decrease in the HOMO-LUMO gap.[25] There is also a noticeable difference in the shape of the absorption bands between the PBTz monomers and oligomers: while the monomers have a broad and featureless band, the oligomeric units have a distinct shoulder in the low-energy range of the band. The distances between the λ_{max} of the band and the shoulder are consistent between the PBTz series, and are all around 21-23 nm in distance. This corresponds to a vibrational separation of around 1200 cm^{-1}, which was shown to be consistent with the ring-breathing modes of thiophene and pyrrole which occur at vibrational spacings of 1100-1500 cm^{-1}.[26] If the breathing modes of thiazole are close to thiophene, it can be argued that the excitation of the PBTz core is not

distinct from the aryl rings, and the HOMO should be spread over the entirety of the oligomer's conjugated backbone as consistent with the DTP analogues.

Within the PBTz oligomer series itself, an additional trend appears. The absorbances of the thienyl-extended analogues are redshifted from the phenyl analogues by circa 20-25 nm (Figure 4.9). Multiple factors could be causing this redshift, which correlates to a decreased HOMO-LUMO gap. Thiophene is less aromatic than benzene,[27,28] and so electron delocalization across the molecular backbone would be comparatively enhanced. Additionally, Rasmussen and coworkers found through DFT calculations that there exists a 7° greater torsional deviation between the fused-ring plane and the pendent rings for phenyl extension over thienyl, limiting orbital overlap to a greater degree. Examining the structure of **4.4a**, a potential factor in this deviation could be from the spacial proximity of the DTP core C-H group with the phenyl's ortho C-H, akin to a 1,6-diaxial interaction between the two hydrogens. This interaction would be absent in the PBTz case, because the nitrogen's lone pair occupies this same space.

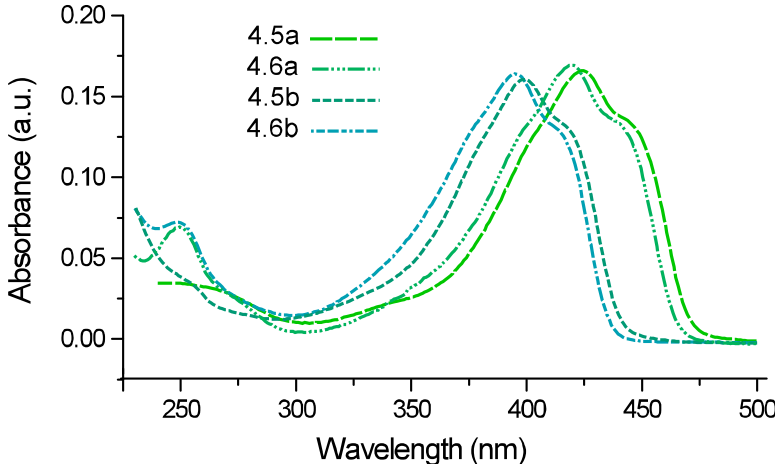

Figure 4.9. Absorption bands of the phenyl- and thienyl- extended PBTz oligomers with line colors corresponding to emission color

Concerning the furyl-extended analogues, the absorbance behavior is more similar to the phenyl-extended series than the thienyl-extended series. The furyl analogues exhibit only a slight

(~5 nm) redshift from the phenyl. While thiophene is less aromatic than benzene, furan is even less aromatic than both heterocycles and has the lowest electron confinement potential of the three.[27,28] Conventional thought would lead to the conclusion that the furan-extended PBTz oligomers would exhibit better electron delocalization and a redshift in absorption wavelengths, but this was not observed. Others who have developed dyes,[29] polymers,[30,31] and oligomers[30] functionalized with furan have noticed that substitution of thiophene for furan in conjugated materials generally leads to a hypsochromic shift in absorption, a destabilization of the HOMO for oligomers, and an overall increase in bandgap for polymers. Authors have explained this effect in terms of reduced molecular aggregation due to the small heteroatom in furan,[31] but this would apply to solid-state measurements. An explanation of the observed trends could lie in the profound electronegativity of the oxygen atom. Oxygen is less polarizable than sulfur, which could lead to localization of electron density on each furan ring and a blueshift in absorption. Another characteristic of the furyl analogues, though is that they exhibit the most well-defined shoulder of the series.

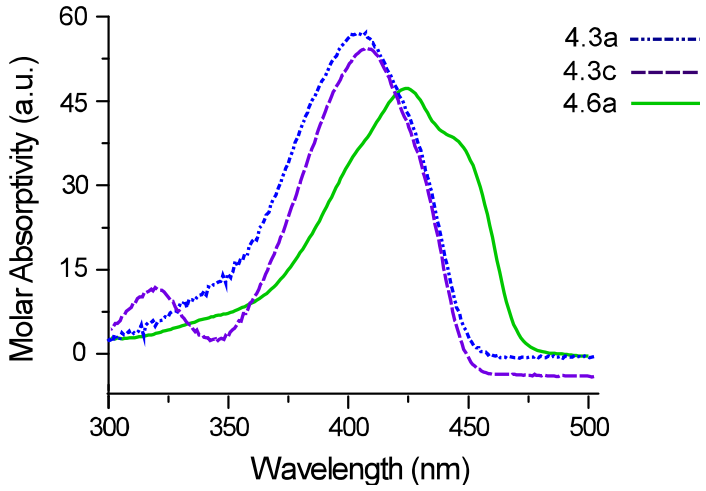

Figure 4.10. UV-vis absorbance profile of thienyl-extended DTP, ADTP, and PBTz

Comparing the absorbance profiles of the PBTz oliogmers to the DTP analogues shows additional trends in the data. Foremost, the solution λ_{max} for every one of the PBTz oligomers are bathochromically shifted from both its first and second generation DTP counterparts. This may be an effect of the increased intermolecular contacts evidenced by the affinity for π-dimerization seen in the NMR spectra. A similar redshift would be seen for the acyl oligomers, but as stated by Rasmussen and coworkers the solution conformation of those molecules could be vastly different than the alkyl analogues due to differences in solvation energy or polarizability induced by the acyl chain.[19] The PBTz absorption profiles may resemble what the acyl DTP oligomers would appear like without these effects.

Films of the PBTz oligomers were drop-cast onto glass substrates to measure solid-state absorption. The PBTz solid-state absorptions are all broadened from their solution counterparts as expected, due to increased delocalization of electron density via enhanced π-π interactions.[19] However, the PBTz oligomers do not appear to follow the same trends as the DTPs. Whereas the phenyl-extended DTPs exhibit blueshifted absorption maxima upon entering the solid state, all but **5.6a** and **5.7b** appeared to blueshift. There are also noticeable shoulders at lower-energy transitions in all of the PBTz analogues, which extend beyond the ranges of the DTPs.

Table 4.2. Optical properties of PBTz, DTP, and ADTP oligomers

Oligomer	Soln. λ_{max} (nm)	ε (M^{-1} cm^{-1})	Solid λ_{max} (nm)
C_8ThPBTz (**4.5a**)	423	46,600	435, (463)
C_8PhPBTz (**4.6a**)	399	39,000	399, (420), (448)
C_8FuPBTz (**4.7a**)	406	48,700	395, (431), (454)
PhThPBTz (**4.5b**)	421	33,100	406, (445)
PhPhPBTz (**4.6b**)	396	38,600	395, (413), (441)
PhFuPBTz (**4.7b**)	406	40,000	426, (451)
C_8ThDTP (**4.3a)**	400	56,000	404, (434)
C_8ThADP (**4.3c**)	396	54,000	417, (444)
C_8PhDTP (**4.4a**)	399	61,000	393, (420)
C_8PhADTP (**4.4c**)	398	43,200	406, (430)
PhThDTP (**4.3b**)	381	45,100	409, (439)
PhThADTP (**4.3d**)	380	44,000	409, (430),(460)
PhPhDTP (**4.4b**)	378	58,400	354, (414)
PhPhADTP (**4.4d**)	380	45,500	381, (419)

Since PBTz monomers had been shown to follow the electronic trends of the acyl DTPs, it was expected that the molar absorptivites would be reduced for the PBTz oligomers. However, the PBTz oligomers combine the N-functionality of the first-generation DTPs with the stabilized frontier orbitals of the second-generation DTPs, and thus determining if the trends in their optical data followed one series more than the other became an important question. Thus, the molar absorptivity values for the PBTz oligomers were obtained and can be compared to the DTP analogues. A general trend appears with the first-generation DTP series, with alkyl N-functionalized analogues showing a higher extinction coefficient than the aromatic counterparts, and phenyl-extended analogues showing a higher molar absorptivity than their thienyl-extended cousins. Concerning the second generation DTPs, a pattern between the four molecules is not as evident, but the extinction coefficients are generally reduced compared to the first-generation series.

For the PBTz oliogmers, the general trend more closely follows the first-generation DTPs as shown in Table 4.2. The alkyl N-functionalized analogues generally have a higher molar absorptivity than aromatic counterparts, but **5.6a** does not exhibit the highest overall ε of the series as opposed to **4.4a**. The new furyl-extended oligomer **5.7b** exhibited the highest overall molar absorptivites for the phenyl N-functionalized series, despite contributing to a smaller photoactive surface than benzene. The phenyl-extended oligomers do generally exhibit higher extinction coefficients than thienyl-extended analogues, but cross-sectional area is also larger for benzene than thiophene.[19] The furan functionality must thus affect the oscillator strength of the transition and increase the allowedness to give furan the highest ε in the case of **4.7b**. These data obtained via UV-vis spectroscopy are significant overall, as they show that the differences between molar absorptivity across the fused-ring oligomers are diminished somewhat, helping to overcome the limitation expressed for the PBTz monomers.

4.5. Fluorimetry Studies

With the DTP oligomer series exhibiting excellent quantum yields of fluorescence, comparing the luminescent properties of PBTz series will discern another important effect of substitution of thiophene with thiazole. The PBTz series was dissolved in chloroform and analyzed via fluorescence spectroscopy, in which it was found that the emission pattern exhibits broad shoulders analogous to the absorption. However, the emission wavelengths were unable to be verified with the current instrumental setup, although comparison of **5.6b** to its DTP analogue found similar emission wavelengths when measured. The **5.7** series is expected to show high quantum yields of fluorescence, as substitution of the sulfur atom for oxygen can limit the heavy-atom effect and disfavor non-radiative decay pathways from the excited state.[32] Fluorimetry studies are ongoing at the time of this dissertation's writing.

4.6. Conclusions

Oligothiophenes have been at the forefront for application in organic electronic devices due to advantages not easily attainable in their polymer counterparts, such as functionalizable peripheral units, improved solubility, and tunable conjugation length. The fused-ring DTP unit has been shown to be a promising material for fluorescent applications such as OLED devices, and aryl-extension of the DTP unit has produced materials with some of the highest recorded quantum fluorescent yields for oligothiophenes.

As further analogues of the DTP materials, a new series of aryl-extended PBTz oligomers were synthesized with simple modifications to the synthetic conditions employed for the DTP cousins. The PBTz oligomers were functionalized with phenyl, thienyl, and furyl groups, representing the first incorporation of furan into the Rasmussen group's DTP family. The oligomers were shown to have a HOMO that was stabilized beyond the level of both the alkyl- and acyl DTP oligomers, matching the trend seen in the PBTz monomer studies. Once again, the HOMO of fused-ring bithiophenes was shown to be tunable in increments, with the same patterns emerging for the oligomers as monomers. The furyl-extended oligomers were the most destabilized of the series, and showed irreversible oxidations. The optical properties of the PBTz oligomers were evaluated via UV-vis spectroscopy, and the absorption maxima were found to be more redshifted in the solution state and solid state than both DTP units. Additionally, the HOMO-LUMO gap of the furyl oligomers were found to lie between the phenyl and thienyl analogues. Fluorimetry on the PBTz series is underway, as well as attempts to grow single crystals.

4.7. Experimental

General Considerations: All reactions were carried out under nitrogen atmosphere. $ZnCl_2$ was dried in vacuo, and all other materials were reagent-grade and used without further purification. The solvents diethyl ether and xylenes were distilled over sodium/benzophenone. Dry DMF, $CHCl_3$, and CH_2Cl_2 were obtained via drying over $MgSO_4$ and filtering through a silica get plug. All glassware was oven-dried, assembled hot, and cooled under N_2 atmosphere. Chromatography was performed using standard methods, with 230-400 mesh silica gel in 1-inch diameter columns. Melting points were obtained with a digital thermocouple, accurate to 0.1 °C resolution. HRMS (ESI-TOF) was performed in-house. Electrochemistry was performed on a Bioanalytical Systems BAS 100B/W in CH_2Cl_2 using a Pt disc working electrode, a Pt wire counter electrode, and Ag/Ag^+ (0.10M $AgNO_3$ in CH_3CN) reference electrode, and resulting data was calibrated to the ferrocene/ferrocene$^+$ redox couple. A 0.1 M solution of $TBAPF_6$ in DCM was used for the electrochemical measurements. NMR spectroscopy was performed on a Bruker 400 mHz spectrometer in $CDCl_3$ solvent, with acquisition at 25 °C unless noted. All NMR spectra are referenced to the chloroform resonance at 7.26 ppm, and multiplicity is as follows: s = singlet, d = doublet, dd= doublet of doublets, quint. = quintet, m = multiplet. UV-vis spectroscopy was performed on a Cary 500 UV-vis-NIR spectrophotometer, with chloroform as a solvent.

General procedure for bromination of PBTz monomers: Phenyl PBTz or Octyl PBTz (1 mmol) were added to a 125 mL 3-neck flask and placed under nitrogen atmosphere. 30 mL dry DMF was added, followed by NBS (4 mmol). The solution was stirred for 2 h at room temperature, as a color change from yellow to deep red was noted. Saturated $NaHCO_3$ was added, followed by 100 mL diethyl ether. The organic layer was separated and washed with 100

mL portions of deionized water to remove DMF. The remaining organics were dried over $MgSO_4$, concentrated in vacuo, and the oily product was purified via column chromatography with 10% chloroform in hexanes to give the brominated PBTz in 70-83%.

2,6-Dibromo-4-octyl-4H-pyrrolo[2,3-d:5,4-d']bisthiazole (**4.8**): 76-83% yield. mp: 80.8-82.1 °C. ^{1}H NMR: δ 4.44 (dd, *J* = 7.2 Hz, 2H), 1.95 (quint., *J* = 7.0 Hz, 2H), 1.28 (m, 10H) 0.87 (t, *J* = 6.6 Hz, 3H). ^{13}C NMR: δ 150.1, 132.0, 106.6, 45.7, 31.7, 30.0, 29.1, 29.0, 26.6, 22.6, 14.1. HRMS: m/z 448.9231 calcd for $C_{14}H_{17}N_3S_2Br_2$ $[M^{79,79}]^+$, 448.9203 found. 450.9210 calcd for $C_{14}H_{17}N_3S_2Br_2$ $[M^{79,81}]^+$, 450.9201 found.

2,6-Dibromo-4-phenyl-4H-pyrrolo[2,3-d:5,4-d']bisthiazole (**4.9**): 70-75% yield. ^{1}H NMR: δ 8.04 (d, *J* = 7.6 Hz, 2H), 7.54 (t, *J* = 7.1 Hz, 2H), 7.35 (t, *J* = 7.1 Hz, 1H) ^{13}C NMR: δ 179.2, 136.4, 132.7, 129.5, 126.8, 122.7, 108.8. HRMS: m/z 415.8349 calcd for $C_{12}H_5N_3S_2Br_2$ $[M^{79,81}]^+$, 415.8357 found.

General Procedure for synthesis of Phenyl- or Thienyl- extended PBTz Oligomers: Thiophene or bromobenzene (5 mmol) were dissolved in 100 mL diethyl ether in a 250 mL 3-neck flask, and the solution placed in a dark environment. The solution was immersed in an ice bath and cooled to 0 °C. BuLi (2.4 mL, 2.5M soln in hexanes, 6 mmol) was added, and the solution stirred for 1 h. Tributylstannyl chloride (1.63 mL, 6 mmol) was added, and the solution gradually turned opaque and white. After warming to room temperature over the course of 30 min, water was poured into the solution, upon which the solution became clear and colorless. The organic layers were separated, and the aqueous layer extracted with 100 mL diethyl ether. The combined organic layers were dried over $MgSO_4$, filtered into an aluminum-foil covered flask, and concentrated in vacuo, keeping the solution near room temperature. The product was collected as a clear oil, and used without further purification.

Meanwhile, a Schlenk flask was prepared and placed under nitrogen atmosphere. $Pd_2(dba)_3$ (0.010 g, 0.01 mmol), the appropriate stannyl species (1.2 mmol) tri-*o*-tolyl phosphine (0.012 g, 0.04 mmol) and the proper brominated PBTz (0.5 mmol) were added. 20 mL xylenes was added, and the solution refluxed overnight. A bright blue or green fluorescence gradually appeared as the reaction proceeded and product was formed. The next day, the solution was cooled and poured into water. 50 mL diethyl ether was added and the organic layers separated. Another 50 mL diethyl ether was used to extract product from the aqueous layer, and the organic layers were combined, dried over $MgSO_4$, and filtered. The product was concentrated in vacuo and separated via column chromatography to give the PBTz oligomer in 40-54% yield.

2,6-Di(2-thienyl)-4-octyl-4H-pyrrolo[2,3-d:5,4-d']bisthiazole (**4.5a**): 54% yield. mp: 147.4-148.2 °C. ^{1}H NMR: δ 7.53 (dd, *J* = 3.8, 1.1 Hz, 2H), 7.38 (dd, *J* = 5.1, 1.1 Hz, 2H), 7.09 (dd, *J* = 3.8, 5.1 Hz, 2H), 4.53 (t, *J* = 7.2 Hz, 2H) 2.06 (quint., *J* = 7.0, 2H) 1.38 (3H, m) 1.26 (m, 7H) 0.85 (t, *J* = 6.6 Hz, 3H). ^{13}C NMR: δ 157.4, 153.8, 138.5, 127.8, 127.0, 125.4, 104.6, 45.4, 31.8, 29.8, 29.1, 29.0, 26.6, 22.6, 13.9. HRMS: m/z 457.077 calcd for $C_{22}H_{23}N_3S_4$ $[M]^+$, 457.0769 found.

2,6-Diphenyl-4-octyl-4H-pyrrolo[2,3-d:5,4-d']bisthiazole (**4.6a**): 50% yield. mp: 125.5-127.3 °C. ^{1}H NMR: δ 8.02 (d, *J* = 7.6 Hz, 4H), 7.44 (t, *J* = 7.1 Hz, 4H), 7.08 (t, *J* = 7.1 Hz, 2H), 4.59 (t, *J* = 7.3 Hz, 2H), 2.11 (m, 2H), 1.40 (m, 2H), 1.26 (m, 8H), 0.85 (t, *J* = 5.7 Hz, 3H). ^{13}C NMR: δ 164.0, 154.3, 134.7, 129.6, 128.9, 126.1, 105.1, 45.3, 31.9, 29.9, 29.2, 29.1, 26.7, 22.7, 14.1. HRMS: m/z 445.1646 calcd for $C_{26}H_{27}N_3S_2$ $[M]^+$, 445.1642 found.

2,6-Di(2-thienyl)-4-phenyl-4H-pyrrolo[2,3-d:5,4-d']bisthiazole (**4.5b**): 43% yield. mp: 266.4-267.2 °C (dec). ^{1}H NMR: δ 8.02 (d, *J* = 7.6 Hz, 4H), 7.44 (t, *J* = 7.1 Hz, 4H), 7.08 (t, *J* = 7.1 Hz, 2H), 4.59 (t, *J* = 7.3 Hz, 2H), 2.11 (m, 2H), 1.40 (m, 2H), 1.26 (m, 8H), 0.85 (t, *J* = 5.7

Hz, 3H). ^{13}C NMR: δ 158.0, 152.4, 138.2, 137.4, 129.2, 128.0, 127.6, 125.9, 122.1, 106.9. HRMS: m/z 420.9836 calcd for $C_{20}H_{11}N_3S_4$ $[M]^+$, 420.9819 found.

2,4,6-Triphenyl-4H-pyrrolo[2,3-d:5,4-d']bisthiazole (**4.6b**): 40% yield. mp: 269.1-270.0 °C. ^{1}H NMR (*Obtained at 45 °C):* δ 8.46 (d, *J* = 7.8 Hz, 2H), 8.05 (d, *J* = 7.1 Hz, 4H), 7.60 (t, *J*= 7.8 Hz, 2H), 7.45 (m, 6H), 7.35 (t, *J* = 7.3 Hz, 1H). ^{13}C NMR (*Obtained at 45 °C*): δ 164.6, 153.2, 137.8, 134.5, 129.8, 129.1, 128.9, 126.2, 125.7, 122.1, 107.6. HRMS: m/z 410.0786 calcd for $C_{24}H_{16}N_3S_2$ $[M + H]^+$, 410.0796 found.

General Procedure for Synthesis of Furyl-extended PBTz Oligomers: 30 mL diethyl ether was added to a 125 mL round bottom flask. The flask was cooled to 0 °C and furan (0.07 mL, 1 mmol) was added, followed shortly by BuLi (0.4 mL, 2.5 M soln. in hexanes, 1 mmol). The clear solution was stirred for 30 min, and then $ZnCl_2$ (0.136 g, 1 mmol) was added. The solution was removed from the ice bath and allowed to warm to room temperature over the course of 1 h. After that time, the brominated PBTz (0.25 mmol) was added, followed by $Pd(dppf)Cl_2$ (0.010 g, 5 mol%). The solution was stirred overnight, and water was then added, and the organic layers separated. The aqueous layers were extracted with diethyl ether, and the organic layers combined. The organic layers were dried over $MgSO_4$, concentrated in vacuo, and purified via column chromatograph in hexanes to afford the furyl-extended PBTz oligomer.

2,6-Di(2-furyl)-4-phenyl-4H-pyrrolo[2,3-d:5,4-d']bisthiazole: (**4.7a**): 39% yield. ^{1}H NMR: δ 8.31 (d, *J* = 8.0 Hz, 2H), 7.56 (m, 4H), 7.60 (t, *J* = 7.3 Hz, 2H), 7.35 (t, *J* = 3.3 Hz, 1H), 7.06 (t, *J* = 7.3 Hz, 2H), 6.56 (dd, *J* = 1.6 Hz, 2H). ^{13}C NMR: δ 154.1, 153.2, 149.5, 143.4, 137.4, 129.2, 125.9, 122.4, 112.4, 109.0, 106.9. HRMS: m/z 390.0321 calcd for $C_{22}H_{12}N_3S_2O_2$ $[M +H]^+$, 390.0323 found.

***2,6-Di(2-furyl)-4-octyl-4H-pyrrolo[2,3-d:5,4-d']bisthiazole* (4.7b):** 58% yield: ^{1}H NMR: δ 7.53 (t, *J* = 7.1 Hz, 4H), 7.00 (t, *J* = 7.1 Hz, 2H), 6.57 (t, *J* = 7.3 Hz, 2H), 4.55 (m, 2H), 2.05, 1.36 (m, 2H), 1.24 (m, 8H), 0.85 (t, *J* = 5.7 Hz, 3H) ^{13}C NMR: δ 154.2, 153.6, 149.5, 143.3, 112.4, 108.7, 104.6, 45.3, 31.8, 29.9, 29.2, 29.1, 26.7, 14.1. HRMS: m/z 426.1310 calcd for $C_{22}H_{24}N_3S_2O_2$ $[M + H]^+$, 426.1305 found.

4.8. References

1. Rasmussen, S. C. In *Encyclopedia of Polymeric Nanomaterials*; Müllen, K. Ed.; Springer-Verlag: Berlin, 2013; pp 1-13.
2. Izumi, T.; Kobashi, S.; Takimiya, K.; Aso Y.; Otsubo, T. *J. Am. Chem. Soc.*, **2003**, *125*, 5286-5287.
3. Bao, Z. *Adv. Mater*., **2000**, *12*, 227-230.
4. Noma, N.; Tsuzuki, T.; Shirota, Y. *Adv. Mater*., **1995**, *7*, 647-648.
5. Barbarella, G.; Favaretto, L.; Sotgiu, G.; Zambianchi, M.; Fattori, V.; Cocchi, M.; Cacialli, F.; Gigli, G.; Cingolani, R. *Adv. Mater*., **1999**, *11*, 1375-1379.
6. Nguyen T.; Destruel, P. In *Handbook of Luminescence, Display Materials, and Devices*, Nalwa, H., Rohwer, L. Eds; American Scientific Publishers, Stevenson Ranch, CA, 2003, Vol. 1, p. 5.
7. Rasmussen, S. C.; Ogawa, K.; Rothstein, S. D. In *Handbook of Organic Electronics and Photonics*, Nalwa, H. Ed.; American Scientific Publishers, Stevenson Ranch, CA, 2008, Vol. 1, Ch. 1.
8. Roncali, J. *Chem. Rev*., **1992**, *92*, 711.

9. Mishra, A.; Ma, C-Q.; Segura, J.; Bauerle, P. In *Handbook of Thiophene-Based Materials: Applications in Organic Electronics and Photonics*; Perepichka, I., Perepichka, D., Eds.; Wiley: West Sussex, U. K., 2009; Vol. 1, pp 1-157.
10. Friend, R. H.; Gymer, R. W.; Holmes, A. B.; Burroughes, J. H.; Marks, R. N.; Taliani, C.; Bradley, D. D. C.; Dos Santos, D. A.; Bredas, J.-L.; Loglund ,M.; Salaneck, W. R. *Nature* **1999**, *397*, 121-128.
11. Pappenfus, T. M.; Burand, M. W.; Janzen, D. E.; Mann, K. R. *Org. Lett.* **2003**, *5*, 1535-1539.
12. Sirringhaus, H. *Adv. Mater.* **2014**, *26*, 1319–1335.
13. Polander, L. E.; Tiwari, S. P.; Pandey, L.; Seifried, B. M.; Zhang, Q.; Barlow, S.; Risko, C.; Bredas, J.-L.; Kippelen, B.; Marder, S. R. *Chem. Mater*. **2011**, *23*, 3408–3410.
14. Pappenfus, T. M.; Hermanson, B. J.; Helland, T. J.; Lee, G. G. W.; Drew, S.; Mann, K.; McGee, K.; Rasmussen, S. C. *Org. Lett.* **2008**, *10*, 1553-1556.
15. Lin, G.; Qin, L.; Guan, Y.; Xu, H.; Xu, W.; Zhu, D. *RSC Adv*., **2016,** *6*, 4872–4876.
16. Ogawa, K.; Rasmussen, S. C. *J. Org. Chem.* **2003**, *68*, 2921-2928.
17. Radke, K. R.; Ogawa, K.; Rasmussen, S. C. *Org. Lett*. **2005**, *7*, 5253-5256.
18. Ogawa, K.; Mo, H.; Radke, K. R.; Rasmussen, S. C. *Polymer Preprints* **2007,** *48*, 40-41.
19. Evenson, S. J; Pappenfus, T. M.; Ruiz Delgado, M. C.; Radke-Wohlers, K. R.; Lopez Navarrete, J. T.; Rasmussen, S. C. *Phys. Chem. Chem. Phys*., **2012**, *14*, 6101–6111.
20. Turro, N. J.; Ramamurthy, V. Scaiano, J. C. In *Modern Molecular Photochemistry of Organic Molecules.* Viva Books: Delhi, India, 2017; Ch. 4.
21. Amb, C. M.; Rasmussen, S. C. *Eur. J. Org. Chem*. **2008**, 801–804
22. Jenekhe, S. A.; Osaheni, J. A. *Science*, **1994**, *265*, 765-768.

23. Graf, D. D.; Campbell, J. P.; Miller, L. L.; Mann, K. R. *J. Am. Chem. Soc*., **1996**, *118*, 5480-5481.

24. Heth, C. L.; Tallman, D. E.; Rasmussen, S. C. *J. Phys. Chem. B*, **2010**, *114*, 5275-5282.

25. Becker, R.;. de Melo, S.; Macanita, A.; Elisei, F. *J. Phys. Chem.*, **1996**, *100*, 18683-18695.

26. Katritzky, A. R.; Pozharskii, A. F. *Handbook of Heterocyclic Chemistry*, 2nd ed.; Pergamon: Oxford, 2000; pp 70–71.

27. Balaban, A. T.; Oniciu, D. C.; Katritzky, A. R. *Chem. Rev*. **2004**, *104*, 2777−2812.

28. Del Zoppo, M.; Zerbi, G. *Phys. Rev. B*, **1994**, *50*, 9815-9823.

29. Gidron, O.; Dadvand, A.; Shenynin, Y.; Bendikov, M.; Perepichka, D. F. *Chem. Commun*., **2011**, *47*, 1976–1978.

30. Li, R.; Lv, X.; Shi, D.; Cheng, Y.; Zhang, G.; Wang, P. *J. Phys. Chem. C*. **2009**, *113*, 7469–7479.

31. Lee, S.; Lee, H.; Han, A.; Lee, J.; Oh, J.; Yang, C. *ACS Appl. Mater. Interfaces*, **2017**, *9*, 15652–15661.

32. Rasmussen, S. C.; Evenson, S. J.; McCausland, C. B. *Chem. Commun.* **2015**, *51*, 4528-4543.

CHAPTER V. A NEW SERIES OF π-EXTENDED METAL THIAZOLEDITHIOLENES EXHIBITNG STABILIZED FRONTIER ORBITALS

5.1. Introduction

Independently reported by both Schrauzer and Gray in 1962,[1,2] metal dithiolenes have generated significant interest over the last few decades because of their electronic and magnetic properties. Such characteristics, coupled with their bulk solid-state packing, have led to properties such as superconductivity, ferromagnetism, and non-linear optical response.[3-9] Consequently, they have been widely studied as building blocks for crystalline molecular materials. Metal dithiolenes can also exhibit liquid crystalline properties, allowing field-induced absorbance switching.[10]

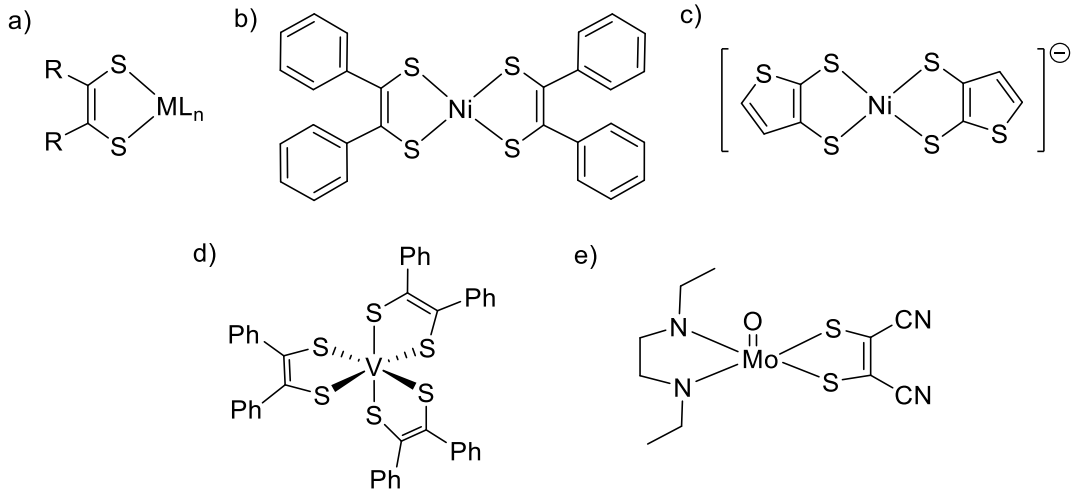

Figure 5.1. General configuration of a metal dithiolene (a),[3] the first reported literature example (b),[2] fused-ring thiophenedithiolene (c),[13] octahedral vanadium dithiolene (d)[12], and asymmetric molybdenum dithiolene (e)[11]

In its simplest form, a metal dithiolene consists of a metal center coordinated to at least one bidentate sulfide ligand conjugated by a carbon-carbon double bond (Chart 5.1a). Although square-planar metal dithiolenes are the focus of this study, many octahedral and asymmetrical

dithiolenes have been reported (Figure 5.1d,e).[11,12] Transition metals occupy the center of the inorganic complex, with known examples including Ni, Au, Pt, Pd, Co, Cu, and Fe.[3-5,10] Complexes with symmetric dithiolene ligands enveloping the metal center, such as square-planar or octahedral species, exhibit mixed-valence states which lead to interesting redox behavior. These molecules can exist in neutral and anionic forms depending on the oxidation state of the metal and the ligands. A dithiolene in a charged state will exist as a salt, which allows tuning of certain properties through counterion choice. The counterion affects solubility of the resulting complex in addition to intermolecular interactions. For example. aromatic cations such as pyridinium can lead to semiconducting behavior in dithiolenes through enhanced π-interactions, and alkyl cations such as tetra-N-butyl ammonium bromide allow dithiolenes to be soluble in organic solvents of varying polarity.[10]

However, the delocalization of electrons from the metal to the ligands is one of the most desirable properties of metal dithiolenes, and can be exploited by tuning of the ligands in the same manner as other classes of conjugated organic materials to afford varying optical and electronic properties. Fusing aromatic rings to the dithiolene core enhances electron delocalization onto the ligands via increased molecular planarity and enhanced orbital overlap, which are themes common to molecular tuning in conjugated materials. Such examples of fused rings include benzene,[11] thiophene,[10,13,14], pyridine,[15] quinoxaline,[16] and other heterocycles[17]

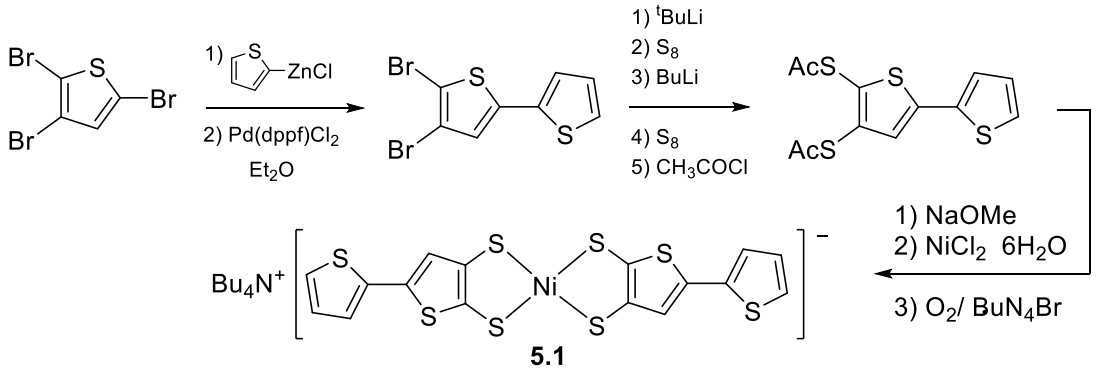

Scheme 5.1. Rasmussen and Amb's synthesis of π-extended nickel thiophenedithiolenes[13]

With the goal of producing new hybrid materials that combine the characteristics of metal dithiolenes and oligothiophenes,[14] the Rasmussen group has previously focused on extending the conjugation of thiophenedithiolenes via coupling of a pendant aryl group to the 5-position of the thiophene ring.[10,13] The regioselective coupling developed by Rasmussen and Amb led to the thiophene extended complex **5.1** (Scheme 1), and a new class of π-extended dithiolenes, which exhibited a bathochromic shift of the intervalence charge transfer (IVCT) band by 100-200 nm from the "parent" thiophenedithiolene complex **5.2** (Figure 5.1)**.**[18] The extent of the redshift depended on the functionalization of the new aryl ring, with aryl units containing electron-donating groups generally causing a greater redshift.[10]

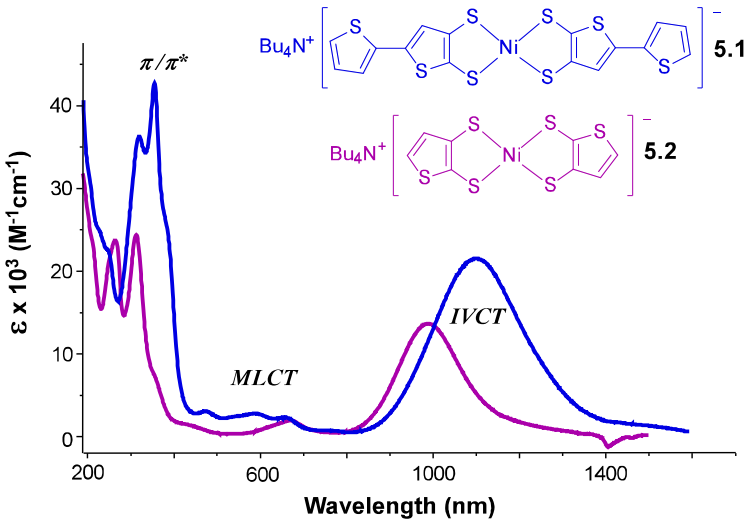

Figure 5.2. UV-vis-NIR absorption profile of **5.1** compared to the parent complex **5.2**[15]

As stated previously, the ligands in metal dithiolenes are mixed valence, and noninnocent, which means that the oxidation state of each ligand is unclear.[1-3] The IVCT band in dithiolenes exemplified this non-innocence and is attributed to transfer of the unpaired electron from one ligand to another, with the singly-occupied molecular orbital (SOMO) playing an important role.[19,20] The charge-transfer occurs via electronic transition of a paired electron from a lower-energy doubly-occupied orbital below the SOMO (SOMO^{-1}) to the SOMO itself,[10] which results in an unpaired electron on the opposing ligand as shown in Figure 5.3. Thus, the oxidation state of each participating ligand is instantaneously switched.

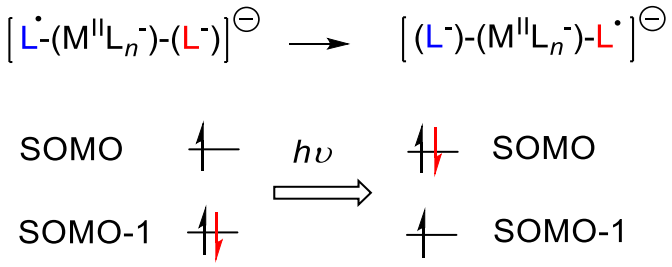

Figure 5.3. Interpretation of the IVCT transition upon photon absorption

The metal dithiolenes would not exhibit the IVCT if it were not for the metal itself. The metal mediates communication between the dithiolate ligands and thus the IVCT itself. This is best shown by the MO diagrams calculated for **5.1**.[10] As can be seen in Figure 5.4, the SOMO and SOMO^{-1} are both delocalized across the fused-ring thiophenedithiolene core. However, the metal itself contributes *only* to the SOMO, and not the SOMO^{-1}. Thus, the metal mediates inter-ligand communication through this interruption of conjugation in the SOMO^{-1}, which must be overcome by low-energy NIR radiation. The IVCT is therefore distinct from a normal $\pi \rightarrow \pi^*$ transition.

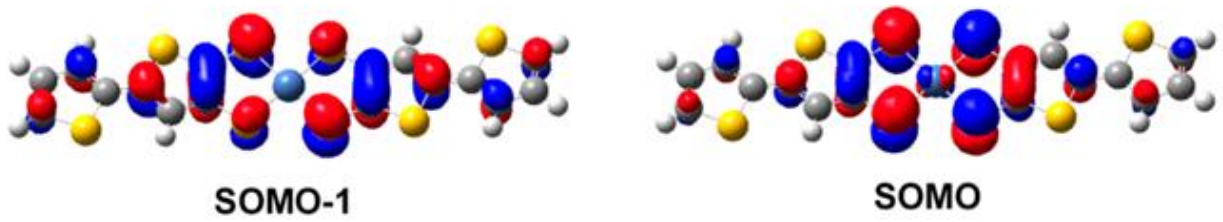

Figure 5.4. Molecular orbital diagram showing the orbitals that participated in the IVCT for **5.1**. Adapted from reference 10.

The materials produced via Rasmussen and Amb's work exhibited enhanced electron delocalization with ICVT transitions pushed far into the NIR region, absorbing from 1076-1160 nm.[10,13] This unique NIR absorption proved to be a more compelling material property to focus on than the magnetic properties that the Rasmussen group originally planned the metal dithiolene project around. Since such a low energy absorbance is rare amongst thiophene materials, the π-extended metal dithiolene system can be applied as a donor unit to donor-acceptor polymeric frameworks to theoretically utilize a larger portion of the solar spectrum, a characteristic that would be valued for application in organic photovoltaics.[23] Between the retained dithiolene characteristics of rich electrochemistry, good solid-state intermolecular contacts, and attainable

semiconducting properties, the applications for π-extended metal thiophenedithiolenes are expansive.

Yet, metal thiophenedithiolenes exhibit a hinderance common to conjugated organic materials. Many organic semiconductors, including the p-type DTP units discussed in Chapters III and IV, exhibit elevated frontier orbital levels, in this case the HOMO and LUMO. This electron-rich character limits device performance and matching with common components in organic electronics.[15] The SOMO levels of the π-extended metal thiophenedithiolenes exhibit this constraint as well. To address this issue, development of analogous materials was initiated in which the fused thiophene in the metal dithiolene is replaced with the more electron-deficient thiazole. The thiazole ring's electron density is concentrated on the sulfur to a greater extent than in thiophene, while the electronegative nitrogen atom not only removes electron density from the ring via increased electron affinity, but also decreases aromaticity through the same effect.[22] It was theorized that the metal dithiolene complex's SOMO should be stabilized by the thiazole ring, while the unique IVCT band should not significantly shift wavelengths, as the simple change from thiophene to thiazole should not result in the LUMO being independently tuned from the SOMO.

There were originally two reports in the literature of metal thiazoledithiolenes (Figure 5.5), but both reports did not satisfy the research questions and goals of the current study. In 1988, Kibbel and coworkers reported a series of phenyl-extended nickel thiazoledithiolenes in a communication.[25] The described solution color, crystal appearance, and electrochemical behavior of Kibbel's compounds were reminiscent of the known metal dithiolenes, with reversible redox character noted and resulting potentials near the expected values for π-extended metal thiazoledithiolenes. However, no confirmation of product identity was given whatsoever, nor

was any synthetic detail reported, and the NIR absorption was not investigated. Recently, Lorcy and coworkers reported 2-alkylthio-capped gold thiazoledithiolenes,[26,27] but their synthetic methods do not allow variability in functionality at the 2-position and are solely limited to the alkylthio derivatives.

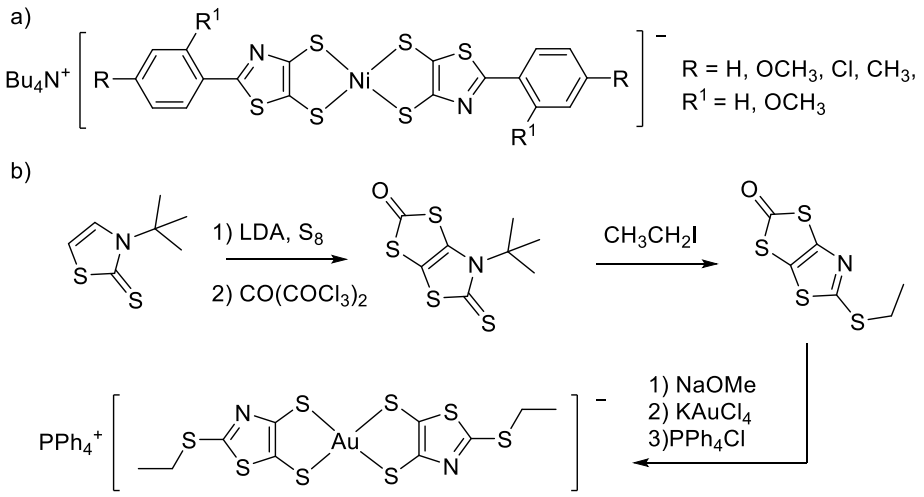

Figure 5.5. Examples of the first reported metal thiazoledithiolenes, with phenyl-extended nickel thiazoledithiolene[25] (a) and route to thioether-extended gold thiazoledithiolene[26] (b)

In the interest of precisely tuning the optical and electronic properties of the dithiolene system, a new family of π-extended metal thiazoledithiolenes (**5.3-5.5**) were synthesized and characterized (Figure 5.6). The thienyl- and phenyl-extended analogues provide direct comparison to the properties of the metal thiophenedithiolene family and show the effect of the thiazole ring. In particular synthesis of **5.4** using the Rasmussen group's conditions allow its full characterization and verification of the properties reported by Kibbel and coworkers.[18] The furyl analogue **5.5** is a new direction for dithiolene chemistry, as no existing compounds feature either π-extension with furan, or furyl-fusion to the dithiolene core. Furan provides an electron-rich heterocycle that is even less aromatic than thiophene,[28,29] perhaps producing the strongest dipole

between the pendent heterocycle and thiazole out of the series. Portions of this work have recently been published in the *European Journal of Inorganic Chemistry*.[30]

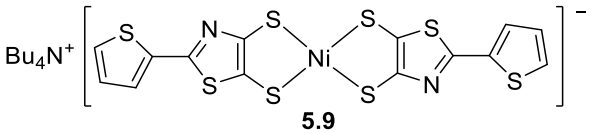

5.9

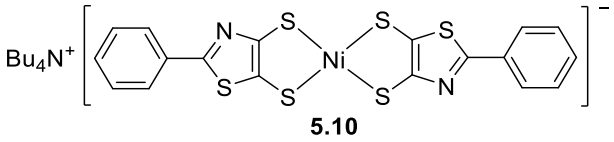

5.10

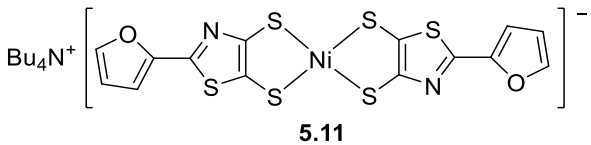

5.11

Figure 5.6. New π-extended metal thiazoledithiolenes

5.2. Synthesis of Metal Thiazoledithiolene Ligand Precursors

To produce the family of π-extended metal thiazoledithiolenes, the thiazole heterocycle must first be incorportated into the ligand precursors (Scheme 5.2). The synthetic procedures used for the formation of the cross-coupled brominated thiazole and subsequent protection with thioacetate groups were developed by Rasmussen and Amb for their work on thiophene-based systems.[10,18,31] To incorporate the thiazole core, tribromothiazole was used in place of tribromothiophene for the Negishi coupling reaction. Synthesis of tribromothiazole was accomplished using conditions outlined in Chapter II.[32] The first ligand precursor synthesized was **5.6.** Overall, the electron deficiency of the thiazole ring did not significantly affect yields for the Negishi coupling, as yields for the product are similar to the thiophene analogue in the 60% range. Thioacetate protection of the brominated precursor using *tert*-butyllithium proceeded smoothly as well, with slightly lower yields observed compared to the analogous thiophene compound.

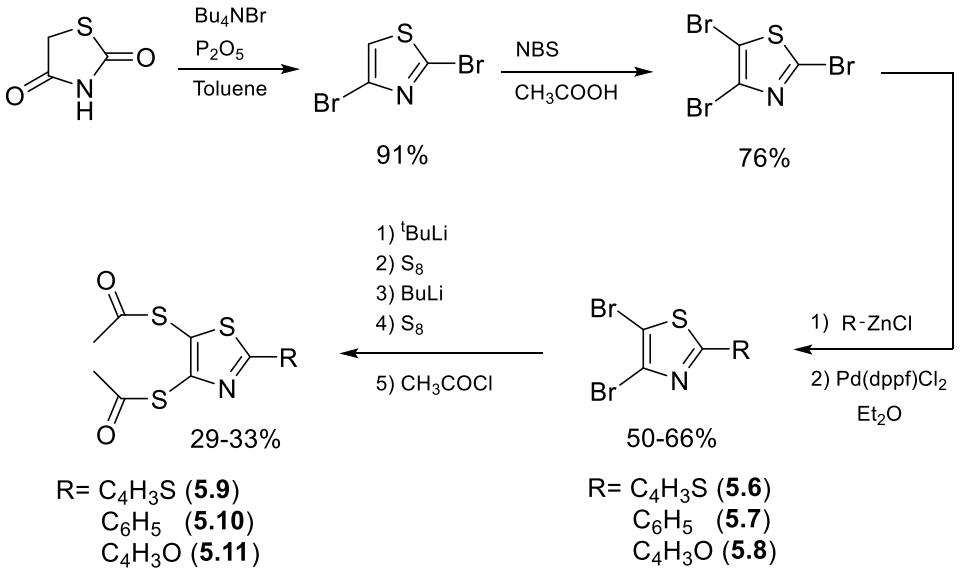

Scheme 5.2. General synthesis of thioacetate-protected ligand precursors

Upon the successful synthesis of **5.9**, π-extension of the brominated ligand precursor with different aromatic rings were undertaken. Synthesis of the brominated furan and phenyl-extended ligand precursors **5.7** and **5.8** were successfully accomplished using the same conditions, albeit with some minor variations. It was found that the phenylzinc chloride produced via transmetallation of 2-lithiobenzene with $ZnCl_2$ was not as stable as the furyl- and thienylzinc chlorides. Decomposition of the opaque solution to a clear mixture with residue on the reaction vessel was observed, and carrying out the reaction did not lead to a sufficient yield of coupled product **5.7**. The decomposition occurred in both THF and diethyl ether, and mixes thereof. This decomposition was not observed in the other analogues, but immediate addition of tribromothiazole and catalyst upon formation of the opaque phenylzinc chloride solution resulted in decent yield. Despite the higher likelihood of furan compounds to ring-open versus their thiophene counterparts (observed in Chapter IV), the lithiation of furan at 0 °C was facile and no darkening of solution or precipitate was observed on the reaction vessel. The furyl systems thus

behaved in a similar manner to the thienyl, and no special conditions were required for the synthesis of **5.8**.

All three of the brominated π-extended ligand precursors **5.6**-**5.8** were able to be acylated as per Scheme 5.2. *Tert*-butyllithium was employed once more to generate the desired lithiated intermediates and avoid the halogen dance.[33] It was anticipated that the basic strength of this reagent would deprotonate and ring-open the furan, but this was not observed to be the case based upon the consistent yields amongst **5.9**-**5.11**. Looking at the data obtained for the new organic molecules, an interesting trend occurs. The melting point for the brominated compounds **5.6** and **5.7** were found to be lower than the thiophene analogues, but **5.8** exhibited a melting point much higher. The greater dipole between the electron-deficient thiazole and electron-rich furan could be causing this increase. Interestingly, the thioacetate ligand precursors **5.10** and **5.11** showed melting points much higher than the thiophene analogues. A large, combined dipole from the electron-withdrawing thioacetate groups and thiazole may cause the disparity. Overall, the synthesis of analogous ligand precursors proceeded smoothly, showing that the Rasmussen group's synthetic conditions can be applied to different functional groups.

5.3. Synthesis of π-Extended Metal Thiazoledithiolenes

The first metal thiazoledithiolene planned for synthesis was the thienyl-extended **5.3**, with the goal of direct comparison of material properties to **5.1.** The initial deprotection, complexation, and oxidation of **5.9** to produce **5.3** was carried out in an identical manner to **5.1,** but a mixture of the desired metal thiazoledithiolene and a second product was found (**5.12**), in which two of the coordinating sulfurs were doubly-oxidized to sulfonyl species. There have been literature reports of sulfur-oxidized dithiolenes with similar configurations,[34-38] but these compounds were produced with radical oxidation via peroxides. Only two species were able to

be oxidized with O_2 in a similar manner to **5.3.**[37,38] Considering that this oxidation was not observed for **5.1**, but occurred for **5.3** in such a simple manner with O_2, shows that the ligand electronics have been significantly modified by replacement with thiazole.

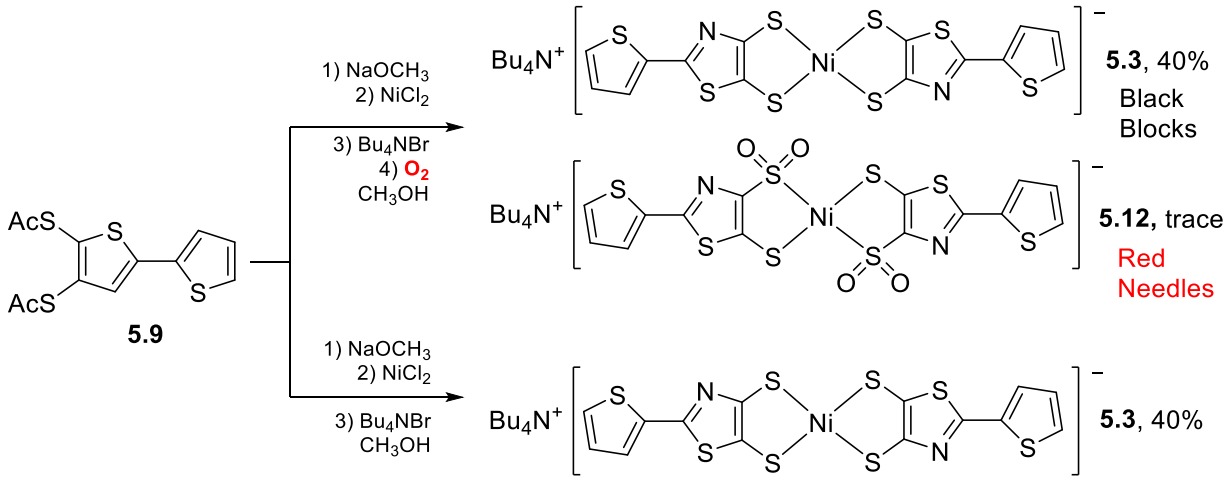

Scheme 5.3. Synthesis of thaizoledithiolene **5.3** and oxidized analogue

The direct reaction of dithiolenes with molecular oxygen is thought to occur with oxygen adducts that can form via approach of the electron-deficient sulfur (Scheme 5.4).[35] Since the formation of the sulfonyls are only observed for dithiolenes which contained an electron-deficient fused-ring system such as benzothiadiazole,[38] it can be proposed that the thiazole ring pulls electron density from the coordinated sulfur atoms, allowing the approach of O_2 and the formation of an adduct which can undergo decomposition to form the observed sulfonyls (Figure 5.7). The electron-rich oxygen could approach the electron poor sulfur, coordinating to the molecule through the π-bond as shown in Figure 5.7a. The sulfur can then participate in backbonding, which leads to a three-coordinate resonance structure. Finally, the three-coordinate structure shift to 3-membered ring between the oxygens and sulfur, which breaks the σ-bond to oxidize the sulfur. This reactivity was only observed on the thiophene-extended metal thiazoledithiolene, and has not been noted for other metal thiazoledithiolenes. Eliminating the

bubbling of air was found to inhibit formation of the sulfonyl complex, allowing the selective isolation of **5.3**. Exposing the reaction mixture to air and adding non-deoxygenated water was found to allow the one-electron oxidation of all of the π-extended metal thiazoledithiolenes, forming a dark-green solution upon filtration.

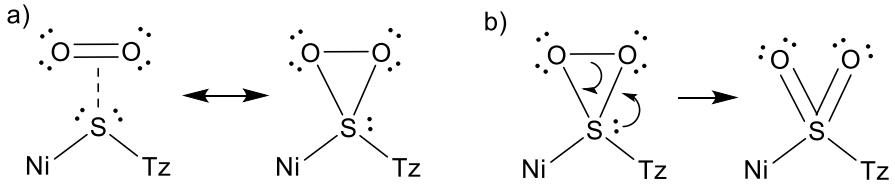

Figure 5.7. Proposed mechanism of the oxidation of a ligand sulfur via addition of molecular oxygen a) followed by decomposition of the three-membered ring (b)

For synthesis of **5.3**, the yield was slightly lower than the thiophene analogue with an overall synthetic yield is 9.4% for **5.3**, versus 11.9% for **5.1**. Overall, the consistency of reactivity and yield between the thiophene and thiazole species shows that the synthetic methods used were not affected to a large degree by the electronic differences between the two heterocycles. Synthesis of the dithiolenes **5.4** and **5.5** proceeded similarity to thienyl with the conditions outlined in Scheme 5.3, but with reductions in yield compared to the thienyl analogue. It is possible that basic attack on the furan's α-position for **5.8** may be occurring in the strongly alkaline conditions and contributing to a reduction in yield.

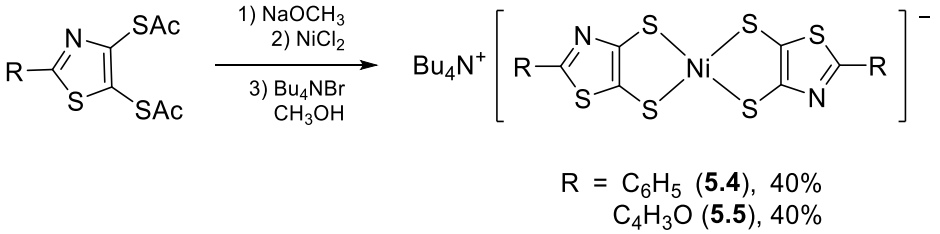

Scheme 5.4. General Synthesis of π-extended metal thiazoledithiolenes

5.4. X-ray Crystallography of π-Extended Metal Thiazoledithiolenes

Single crystals of both **5.3** and **5.12** were grown from a green solution of the synthesized mixture. The method used was vapor diffusion,[39] with an acetonitrile/diethyl ether solvent and antisolvent mix. The green solution produced two crystal types- large black block-type crystals and a small fraction of red needle-type crystals. X-ray diffraction of the black crystals resulted in the anticipated structure of **5.3**, which agrees well with the structure of **5.1**. The two metal thiazoledithiolene ligands adopt the lower-energy trans configuration commonly observed in dithiolenes, and Ni-S bond lengths range from 2.160 to 2.176 Å which is similar to **5.1**.[10] Also, the thiazole rings exhibit bond lengths that agree fairly well with the bond lengths seen in the parent thiazole,[40] with a small amount of asymmetry seen that is characteristic of fused five-membered heterocycles.[3]

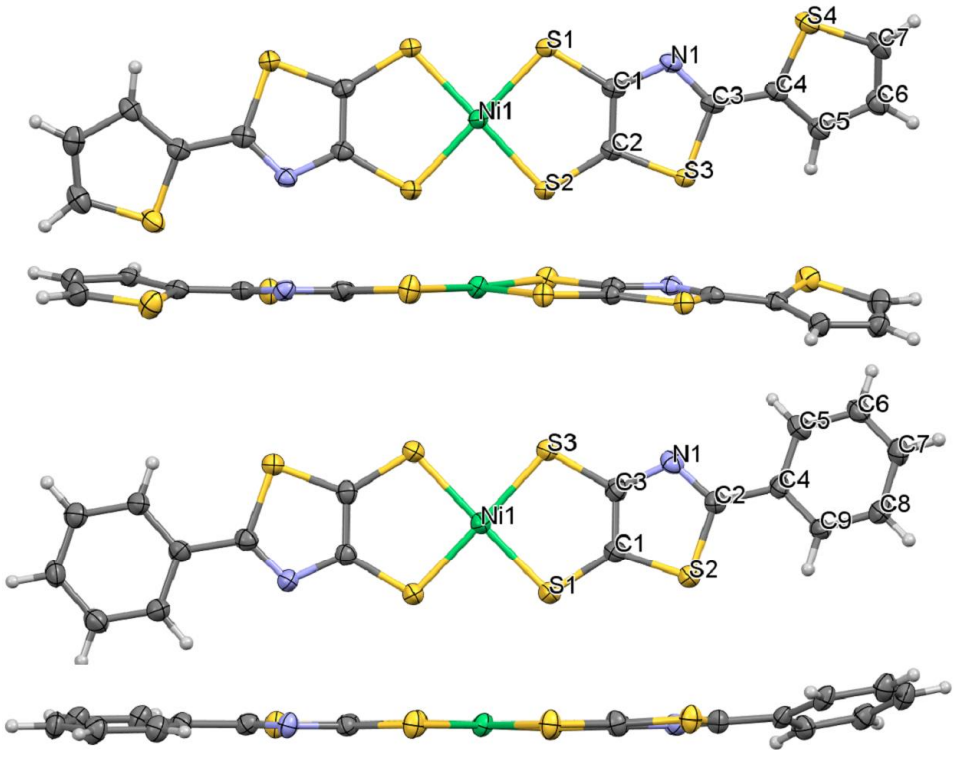

Figure 5.8. Crystal structure of **5.3** and **5.4** showing front-facing and planar views with ellipsoids set at 50% probability

The metal thiazoledithiolene **5.3** is not completely planar as can be seen in Figure 5.8, and these deviations are the result of twists of 12.7° and 14.0° about the C3-C4 bonds between the pendent thiophenes and metal thiazoledithiolene core. Since a small fraction of the complex lies in the tetrahedral configuration which is typical for square-planar metal dithiolenes,[3] the slight twist along the complex's long axis shows this contribution to the ellipsoid plot. The interannular C3-C4 bonds between the thiazole and thiophene rings have an average length of 1.44 Å, which is in good agreement with the interannular bond of **5.1** and shows good conjugation across the two heterocycles (Table 5.1).[10] The phenyl-extended analogue **5.4** is also shown in Figure 5.2. It exhibits less twisting about the interrannular bonds (C2-C4) with torsion angles of 5.3° and 8.9° , and shows less tetrahedral character in the dithiolene core. The thiazole ring's bond lengths are largely consistent with **5.3**, showing a maximum deviation of 0.005 Å. However, the C2-C4 interranular bond for **5.4** is longer than the comparable bond in **5.3** (1.469 Å vs 1.441), which is a sign of reduced conjugation between the two units.

Table 5.1. Selected bond lengths of **5.1**, **5.3**, and **5.4**

Parameter	Thiazole[27]	**5.5**[3]	**5.3**	**5.4***
Ni-S1	-	2.175	2.1762	2.170
Ni-S2	-	2.170	2.1656	2.172
S1-C1	-	1.708	1.733	1.739
S2-C2	-	1.733	1.717	1.712
C1-C2	1.367	1.396	1.376	1.371
C2-S3	1.713	1.748	1.728	1.732
C1-N1	1.372	-	1.378	1.373
N1-C3	1.304	-	1.310	1.306
S3-C3	1.724	1.746	1.754	1.752
C3-C4	-	1.472	1.441	1.469

*Analogous bonds to **5.3** shown

As with previous π-extended nickel thiophenedithiolenes, **5.1** and **5.3** exhibit close S-S and CH-S contacts between neighboring molecules, resulting in edge-to-edge sheets. These sheets form a herringbone packing arrangement with the cations separating sheets in parallel. The packing structure shown in Figure 5.9 also confirms the monoanionic character of **5.3**, as the ratio of tetrabutylammonium cations to dithiolenes is 1:1.

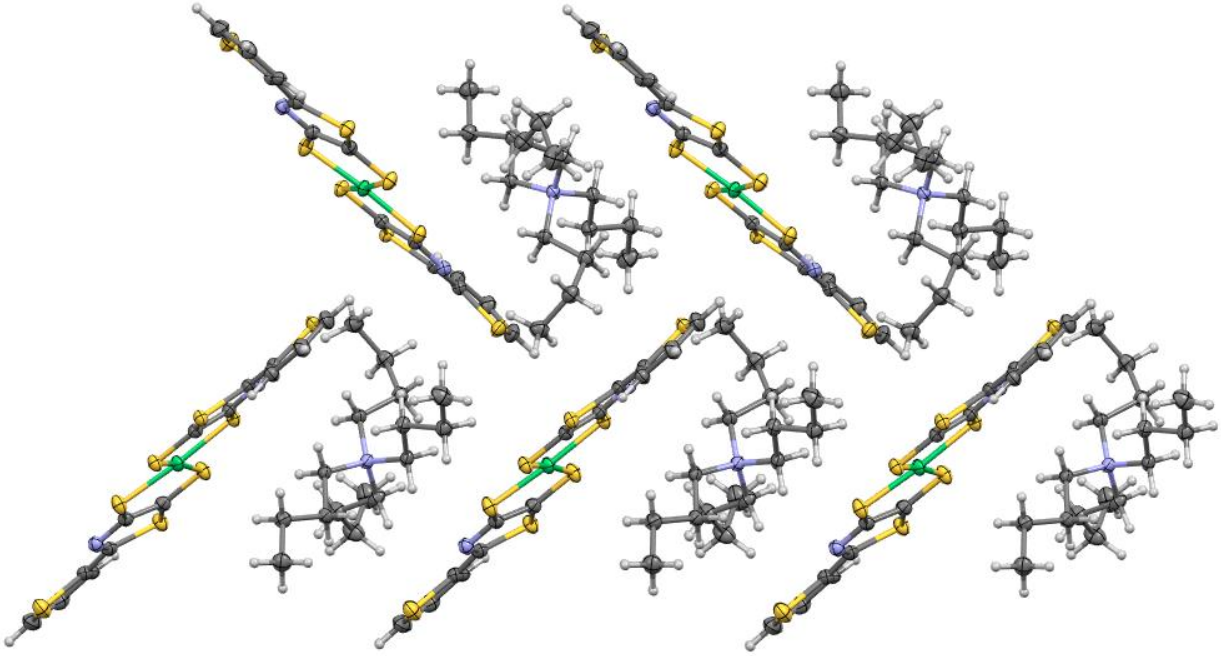

Figure 5.9. Packing arrangement of **5.3** showing the unit cell and monoanionic character

The red needle-like crystals were that of the sulfonyl-containing **5.12**. As apparent in the structure shown in Figure 5.10, the oxidized sulfurs exhibit a *trans* configuration to each other. The ellipsoid plots show that the calculated structure of **5.12** has more uncertainty than that of **5.3**, but interesting data can be gleaned from the structure. The oxidized sulfur exhibits a Ni-S bond length agreeable to those in **5.3**, but the other Ni-S bonds are significantly elongated. Additionally, the dithiolene's C-S bonds are both elongated while the C1-C2 bond is considerably shortened. The C3-C4 interannular bond between the metal thiazoledithiolene core

and pendent thiophene is also elongated. Considering that bond elongation in the X-ray structure is due to increased single-bond character and the shortening due to increased double-bond character, it is quite clear from the crystal structure that the conjugation across **5.12** is quite reduced and does not resemble typical dithiolenes. Even the planarity of the structure is affected, with an s-shape evident in the dithiolene center.

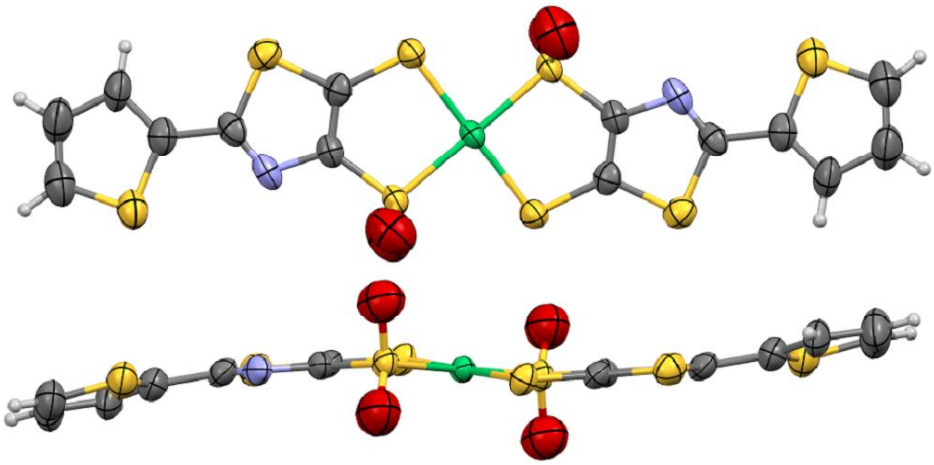

Figure 5.10. Crystal structure of the S-oxidized metal thiazoledithiolene with ellipsoids set at 50% probability

5.5. Electrochemical Characterization of π-Extended Metal Thiazoledithiolenes

In order to elucidate the electronic properties of the metal thiazoledithiolene core in comparison to compound **5.1**, electrochemistry was performed on the three new metal thiazoledithiolenes. Foremost, a comparison of **5.1** to **5.3** shows that molecule exhibits redox behavior similar to the reported dithiolenes (Figure 5.11).[10,18] **5.1** features two quasireversible redox couples corresponding to the oxidation from the dianonic to monoanionic states (-2/-1) and from the monoanion to netural states (-1/0), with an irreversible third oxidation representing the neutral to cationic state (0/n+). The peaks for the -1/0 couple of **5.1** show more reversible

character than for **5.3**, which could represent decreased aggregation of the neutral species due to greater solubility of **5.3**.

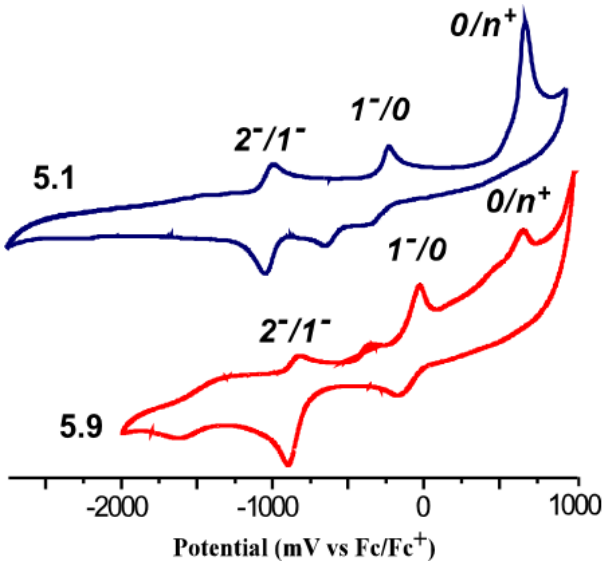

Figure 5.11. Voltammograms of **5.1** and **5.3** obtained in 0.1M Bu_4NPF_6

As predicted, the electron-deficient thiazole shifts the -2/-1 and -1/0 redox couples to more positive potentials (Table 5.2). The $E_{1/2}$ of the -2/-1 couple is shifted by 140 mV from -1.00 to 0.86 V vs. ferrocene, and the -1/0 couple is shifted by 140 mV from -0.24 to -0.10 V. These values correspond to a stabilization of the SOMO from -4.86 to -5.00 eV,[41] which is estimated using the vacuum potential of the Fc/Fc^+ oxidation. The energy level is still slightly higher than the optimal energy matching for electrode workfunctions in organic electronic devices, exemplified in Leclerc's calling for an optimal HOMO of -5.2 eV for OPVs.[42] However, it is an improvement over dithiolene **5.1**.

Table 5.2. Electrochemical data for metal thiazole- and thiophenedithiolenes, with abbreviations signifying thiazole (TzDT) or thiophene (ThDT) cores

Dithiolene	$E_{1/2}$ -2/-1 (V)	$E_{1/2}$ -1/0 (V)	E_{pa} $0/n^+$ (V)
ThThDT **5.1**	-1.00	-0.24	+0.69
ThTzDT **5.3**	-0.86	-0.10	+0.67
PhThDT[10]	-1.00	-0.26	+0.73
PhTzDT **5.4**	-0.92	-0.18	+0.65
FuTzDT **5.5**	-0.91	-0.15	+0.85

The other new metal thiazoledithiolenes **5.4** and **5.5** also exhibited redox behavior under the conditions employed for cyclic voltammetry and the resulting voltammograms are shown in Figure 5.12. Table 5.2 shows the redox potentials of the new metal thiazoledithiolenes and a comparison to the thiophene analogues. Some trends are evident in the data, namely that the phenyl- and thienyl-extended metal thiazoledithiolenes exhibit stabilization of their SOMO levels compared to thiophene analogues **5.1** and **5.13**.[10] The extent of stabilization is different, however, as each redox couples is shifted positively by 140 mV for **5.1**, and by 180 mV for **5.4** compared to their thiophene analogues. It is clear that thienyl extension stabilizes the SOMO to a greater extent then phenyl extension, which can be attributed to decreased electron delocalization of the phenyl ring due to its greater degree of aromaticity and increased steric interactions between the thiazole and larger six-membered ring.

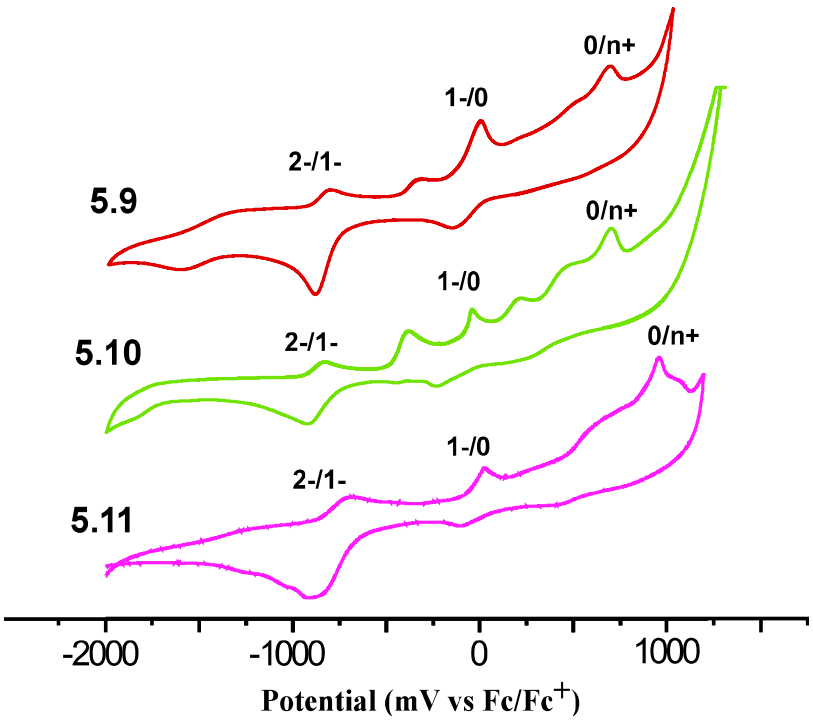

Figure 5.12. Voltammograms of the three new π-extended metal thiazoledithiolenes

The new furyl complex **5.5** exhibits stabilization between that of **5.3** and **5.4**. This trend is similar to what was observed with the new series of PBTz oligomers discussed in Chapter IV. Although furan is less aromatic than thiophene, the profound electronegativity of the oxygen atom could be creating a local dipole that disrupts electron delocalization across the complex. Obtaining a crystal structure of **5.5** would show the bond lengths within the ligands, and longer interannular bonds would support this claim.

One issue that must be noted lies in the comparison between our data obtained for **5.4** and the original communication by Kibbel and coworkers.[25] The communication reported the -1/-2 redox couple for **5.4** occurring at -0.48 V and the –1/0 couple at +0.1 V. They reported their data as $E_{1/2}$, implying that the couples were reversible. These data are quite different than what was obtained on our instruments, but could be possibly be explained by the extra peaks observed in our voltammogram (Figure 5.6). The voltammogram obtained for **5.4** did have a prominent extra

peak with E_{pa} = -0.42 V which had a slightly visible couple. Although it would be a stretch to call this quasireversible, adding the reduction peak E_{pc} would give an $E_{1/2}$ for this couple of -0.46 V, which is close to what was reported by Kibbel. Another extra peak appears at approximately 0.17 V, but also appears irreversible. Although conjecture once more, if reversible behavior was observed for this couple it would lie nearer to the $E_{1/2}$ of 0.1 V reported by Kibbel. Since cyclic voltammetry is a diffusion-controlled process, aggregation of the species or increased π-stacking interactions could result in further stabilization of the frontier orbitals via enhanced electron delocalization and extra peaks in the voltammogram upon oxidation. Since the 1988 communication did not show voltammograms, there is no frame of comparison to our data. Nevertheless, the data obtained by Rasmussen and Amb for the thiophenedithiolene series is consistent and thereby the basis for the reported potentials for **5.4**.[10]

5.6. Optical Characterization of π-Extended Metal Thiazoledithiolenes

UV-vis-NIR spectroscopy was initially utilized to compare absorbance properties of **5.1** and **5.3** (Figure 5.13) and elucidate any effect from thiazole substitution. The higher-energy absorptions are attributed to π-π* transitions in the UV, which appear similar to those of **5.1** but with a slight bathochromic shift.[10] As seen in Chapters III and IV, the other new thiazole-based materials also show redshifts in their π-π* transitions. The absorptions in the visible region are assigned as ligand-to-metal charge transfer (LMCT) bands, and **5.3** shows more prominent LCMT character than **5.1** which may be a cause for its deep-green color in solution. As the most prominent feature of the spectrum, the large IVCT band appeared at 1110 nm for **5.3**. This is virtually unchanged from **5.3**, in which the same band appeared at 1108 nm. This supports our hypothesis that no charge-transfer character would occur upon substitution of the thiophene to the thiazole heterocycle. Additionally, the lack of red- or blueshift in the IVCT band shows that

the SOMO to SOMO^{-1} transition has similar energetic spacing as with **5.1**, implying that the stabilization of each participating molecular orbital is the same upon incorporation of the thiazole heterocycle.[10]

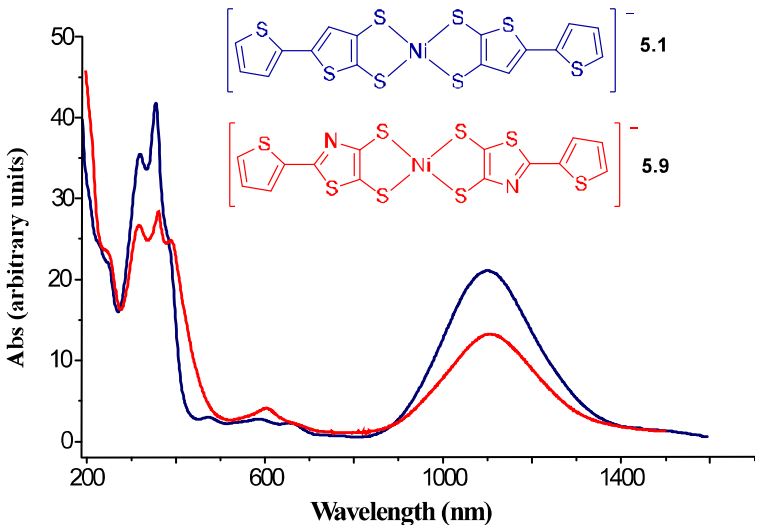

Figure 5.13. UV-vis-NIR absorption profile of **5.1** and **5.3**

The most significant difference in the optical properties lie in each transition's molar absorptivites (ε). The π-π* transitions of complex **5.3** feature ε values around 27,100 M^{-1} cm^{-1} in acetonitrile. This ε value is roughly 33% lower than the ε of 40,000 M^{-1} cm^{-1} for **5.1**, although the broader vibrational character seen in **5.3** could mitigate this difference somewhat. The ε_{IVCT} was 14,600 M^{-1} cm-1 for **5.3**, which is lower than the 21,000 M^{-1} cm^{-1} for compound **5.1**. However, the IVCT band of **5.3** is also broader than **5.1**, which requires the oscillator strength (*f*) to be examined. It was found that $f = 0.14$ for **5.3** and $f = 0.18$ for **5.1**, which is still a 25% decrease in ε. While both transitions for **5.3** experience reduced molar absorptivities compared to **5.1**, the IVCT appears to be less affected by the incorporation of thiazole than the π-π* transition.

To show that the IVCT transitions were a Class III type and fully delocalized,[44] the two compounds were analyzed in a variety of solvents with various coordinating strengths. The three

critera for a Class III transition are intense absorbance with ε over 5000, narrow bandwidths of $\Delta\nu_{1/2} \leq 2000$ cm^{-1}, and solvent independence of the transition. Small changes of approximately 20 nm in the IVCT energy were observed (Table 5.3) with solvent changes. The prevailing thought is that increased ability of the donor solvent to coordinate to the empty sites on the square-planar complexes are been correlated to a decrease in transition energy,[43] and the results obtained generally agree with this statement. Additionally, the two dithiolenes **5.1** and **5.3** exhibited similar trends in energy shift, with chloroform/pyridine causing the largest stabilization and acetone the least. The measured molar absorptivities were similar for both **5.1** and **5.3** across the tested solvents, with the prominent exception of pyridine. For both dithiolenes, pyridine significantly lowered the strength of the IVCT band, as well as the higher-energy $\pi \rightarrow \pi^*$ transition. Being aromatic and a strong coordinator, pyridine could be disrupting orbital overlap by encouraging more tetrahedral character in solution. Overall, the data collected show that the IVCT transitions fit within the Class III criteria.[44]

Table 5.3. Optical data for IVCT band of **5.1** and **5.3** with bandwidth displayed

Solvent	λ_{max} (nm)	ε (M^{-1} cm^{-1})	$\Delta\nu_{1/2}$	λ_{max} (nm)	ε (M^{-1} cm^{-1})	$\Delta\nu_{1/2}$
Acetone	1100	14,700	2020	1097	22,200	1970
THF	1101	15,300	2030	1107	24,200	1960
CH_3CN	1108	14,600	2020	1108	21,000	2010
DMF	1112	15,100	2050	1115	23,300	2030
Pyridine	1118	8000	2020	1120	16,500	2010
$CHCl_3$	1118	13,800	2040	1120	19,200	2030

Because an explanation for the observed differences in molar absorptivity has not been published in the literature, we examined both factors which determine the allowedness of an electronic transition: the oscillator strength and chromophore cross-sectional area.[45] The decrease of molar absorptivity when incorporating thiazole into photoactive molecules has been noted by

other authors,[46,47] and personally observed with our studies concerning PBTz species discussed in Chapters III and IV. Computational studies performed showed that extent of the ε drop appears to be related to the proportion of thiazole to the photoactive surface area of the molecule, with greater thiazole contribution resulting in a greater decrease of molar absorptivity due to the continued decrease of transition oscillator strength. This property was also observed in the parent heterocycles, with thiazole itself having an ε of 3,700 M^{-1} cm^{-1} compared to thiophene's 7,400 M^{-1} cm^{-1}.[38] Although the electronic differences between thiazole and thiophene could affect the transition's allowedness, it has also been established in the literature that the thiazole ring is smaller than thiophene.[38] This results in an objectively smaller cross-sectional chromophore area which can be verified in the obtained crystal structure for **5.3**, in which the thiazole ring causes the overall molecule to be shorter and cross-sectional area reduced.

To further support this reasoning, we examined the π-π* molar absorptivites of the brominated ligand precursors functionalized with thiophene (**5.3**), phenyl (**5.4**), and furyl (**5.5)**. These data are shown in Table 5.3 alongside ε values for their parent aromatic rings. It can be seen that the molar absorptivites for the cross-coupled ligands are much higher than the parent heterocycles, due to the extra cross-sectional chromophoric area introduced by the thiazole. Also, the trends in ε for the parent rings tend to reflect the cross-coupled counterparts, with thiophene exhibiting the lowest ε and furan the highest.

Table 5.4. Molar absorptivities of parent aromatic units and cross-coupled dibromothiazole ligand precursors

Aromatic System	**λ_{max} (nm)**	**ε (mol^{-1} cm^{-1})**
Thiophene	215, 231	6300, 7400
Furan	208	7900
Benzene	203, 254	7400, 100
Thiazole	207, 233	2600, 3700
Thienothiazole **5.6**	-	16,800
Furylthiazole **5.8**	-	22,800
Phenylthiazole **5.7**	-	17,100

The absorption spectra of the phenyl- and furyl-extended metal thiazoledithiolenes were compared to **5.3**. The increasing aromaticity of **5.4** hypsochromically shifted the IVCT. These results are consistent with the phenyl-extended thiophenedithiolene.[10] The furyl-extended **5.5** showed an even greater blueshift of the IVCT band than **5.4,** with a λ_{max} 21 nm lower than **5.4** and 57 nm lower than **5.3**. Large dipoles between the electron-deficient thiazole and the pendent ring may be destabilizing the SOMO to a greater extent than the $SOMO^{-1}$ in these cases.[43] The pendent furan must therefore provide the either largest destabilization to the SOMO relative to the $SOMO^{-1}$, or the largest stabilization to the $SOMO^{-1}$ relative to the SOMO, to produce the largest hypsochromic shift seen in the new metal thiazoledithiolene family.

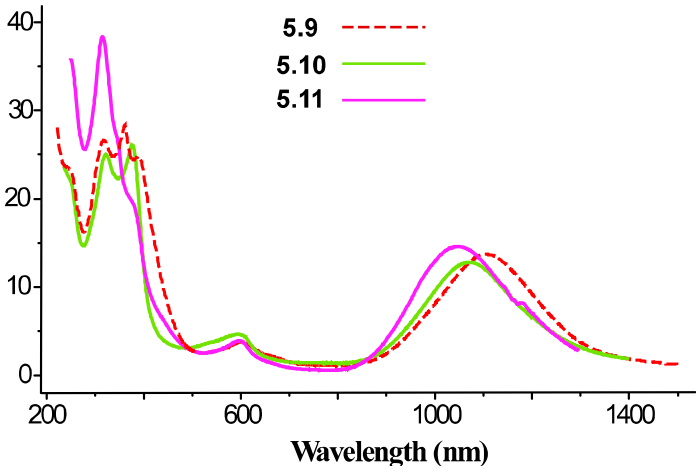

Figure 5.14. UV-vis-NIR absorption profile of **5.3**, **5.4**, and **5.5**

Overall, the effects of aryl functionalization are quite apparent for the new thiazoleditihiolenes, and are summarized in Table 5.5. The π-π* ε values for **5.3**-**5.5** shown in Table 5.4 are all within 60-65% of the π-π* values observed in their respective dithiolene complexes (Table 5.5), signifying that the major contribution to the dithiolene's π→π* transition is from the aromatic ligands. The reduction in ε values for the phenyl-extended dithiolenes are consistent across thiophene or thiazole cores. **5.5** exhibits the highest ε of the series for both transitions.

Table 5.5. Optical properties of π-extended metal thiazoledithiolenes (TzDT) and thiophenedithiolenes (ThDT) with ε values in acetonitrile

Metal thiazoledithiolene	**λ_{max} (nm)**	**ε (mol^{-1} cm^{-1})**	**λ_{max} (nm)**	**ε (mol^{-1} cm^{-1})**
ThThDT **5.1**	362	41,800	1110	21,000
ThTzDT **5.3**	365	27,100	1108	14,600
PhThDT[10]	329	39,800	1076	19,800
PhTzDT **5.4**	377	26,300	1072	13,500
FuTzDT **5.5**	316	38,200	1051	15,100

5.7. Synthesis and Characterization of a Methyl-functionalized Metal Thiazoledithiolene

The new π-extended metal thiazoledithiolenes provided a new direction for dithiolene chemistry and a comparison to the electronic properties of the thiophene analogues. With these advances in mind, the effect of thiazole substitution on the thiophenedithiolene core itself had not been quantified. Therefore, attempts were made to synthesize the metal thiazoledithiolene parent complex (Figure 5.15) in order to provide a comparison to the full thiophenedithiolene family and specifically compound **5.2**.

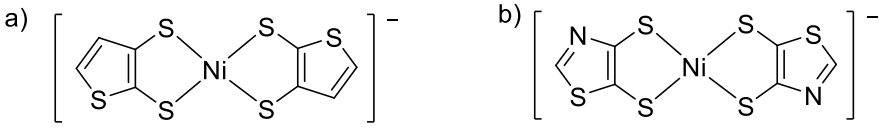

Figure 5.15. Thiophenedithiolene parent compound and its planned thiazole analogue

The initial route towards the metal thiazoledithiolene parent was planned to begin with 4,5-dibromothiazole **5.14**, selectively prepared as described in Chapter II (Scheme 5.5).[32] The Rasmussen group's conditions were anticipated to directly work for 4,5-dibromothiazole because lithium-halogen exchange was favored over deprotonation in ethereal solvents, despite the more acidic proton in thiazole's 2-position.[48] The presence of the proton itself was an advantage, too, as the halogen dance would be mitigated from the more unstable 4-position.[31,32] Thus, the only plausible halogen dance migration without basic attack on the 2-position should occur from the 4- to the 5-position. Yet during the reaction, a black film coated the reaction vessel upon raising the lithiated species to ambient temperature after addition of S_8, alluding to ring-opening of the lithiated thiazole species. This could be explained by a portion of the **5.14** in solution undergoing basic attack due to the sheer strength of *tert*-butyllithium. Thus, attempts to directly convert **5.14** to the thioacetate protected species were not successful.

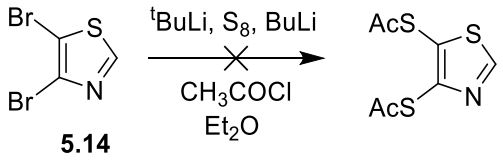

Scheme 5.5. Unsuccessful synthesis of thioacylated ligand precursor from **5.14**

The next attempt involved blocking the 2-position to prevent deprotonation (Scheme 5.6). Looking back to our studies with PBTz in Chapters III and IV, the triisopropylsilyl (TIPS) group was employed. Initially, tribromothiazole **5.15** was debrominated with BuLi in diethyl ether in the presence of TIPSCl, with the thought that substitution of the lithiated thiazole would take place before the halogen dance.[32] Yet, the resulting product was primarily 2,4-dibromo-5-triisopropylsilylthiazole **5.16**, instead of the desired **5.17**, and it was determined that the rate of halogen dance exchange surpassed reaction with TIPSCl. Attempting the reaction in the same manner as synthesis of **5.14** but with TIPSCl as a quenching agent instead of methanol was unsuccessful, producing **5.16**. The steric bulk of the TIPS group may hinder substitution no matter the conditions and solvent, allowing the favoring of the kinetic product as the temperature rises.

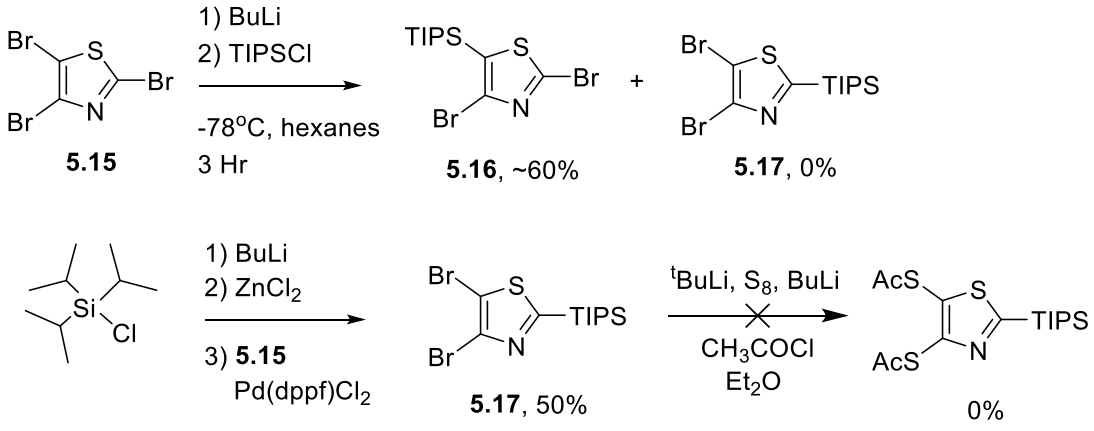

Scheme 5.6. Attempted synthesis of TIPS protected precursors to the parent metal thiazoledithiolene

An alternate path towards **5.17** was planned based on our Negishi cross-coupling pathway to ligand precursors **5.3-5.5.** The use of Pd(dppf)Cl_2 provided a sterically bulky ligand on the catalysts which prevented oxidative addition at the crowded 4- and 5- positions of **5.15**. Therefore, performing the Negishi coupling with triisopropylsilyl zinc chloride selectively protected the 2-position without decomposition. Using this method, **5.17** was produced in approximately 50% yield (Scheme 5.6). Unfortunately, acylation of this molecule was not successful, as the reaction produced a complex mixture of thiazole species with peaks in the ^{1}H-NMR corresponding to the naked 2-position (circa 8.5-9.0 ppm). There was evidence that one position was thioacylated, but diacylation was not observed and the species could not be carried on to the dithiolene synthesis. It was theorized that the *tert*-butyllithium reagent was strong enough to deprotonate the isopropylsilyl groups and lead to further chemistry. Considering that our previous studies outlined in Chapter III established that the TIPS group is the optimal protecting group for thiazoles, this route towards the parent metal thiazoledithiolene was set aside.

Our next plan involved synthetically altering the thiazole ring with a functional group that would preserve the optical and electronic properties of the naked ring to the best ability possible while protecting the 2-position. A methyl group was chosen due to these reasons, as it would be more difficult to deprotonate in solution, and only alter the electronic properties of the thiazole ring with slight electron-donating character. Our synthetic conditions to produce **5.14** were employed as first attempt to synthesize 4,5-dibromo-2-methylthiazole **5.18**. Quenching with iodomethane versus methanol was theorized to produce **5.18**, but a complex mixture of various debrominated thiazoles were obtained, showing that the halogen dance once again occurred at a faster rate than quenching.

Following the pattern of logic used for the TIPS route towards **5.17**, Negishi coupling with methylzinc chloride was attempted (Scheme 5.7). A reaction of methyliodine with magnesium to produce methylmagnesium iodide was successful, and the resulting Grignard reagent was successfully reacted with $ZnCl_2$ to produce a cloudy white solution akin to the ones observed for aryl analogues. However, addition of **5.15** did not result in product and only starting material was returned. Since production of the methyl Grignard was successful, a Kumada coupling was then attempted, which produced **5.18** successfully in 53% yield. Addition of CuO aided the reaction and raised the yield to 73%.[48] **5.18** was able to be thioacylated and carried through to the methyl-capped parent thiazoledihiolene **5.20**, although yields for the final step were quite low at around 16-20%.

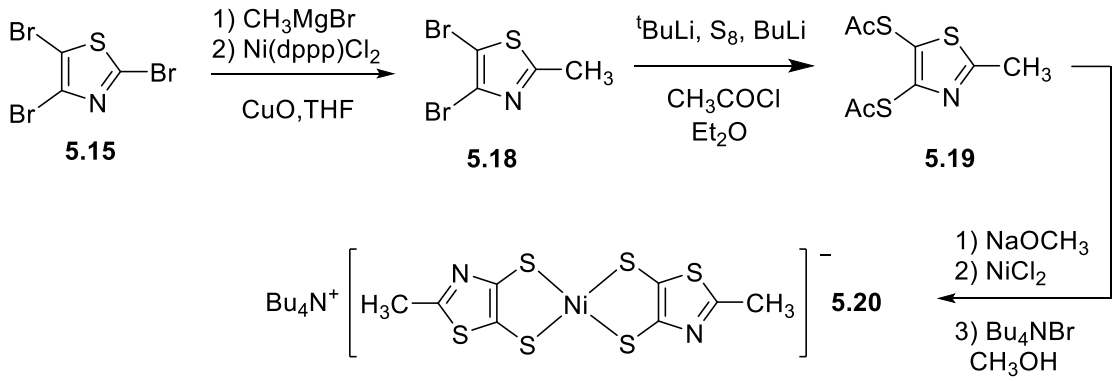

Scheme 5.7. Synthetic route to **5.20**, the methyl-capped metal thiazoledithiolene

The optical properties of **5.20** were compared to **5.2**, and it was found that the trends with the thiazole analogues were maintained. The IVCT band was redshifted by approximately 24 nanometers, from 990 to 1014 nm, which is typical of increased electron-donating character on the ligands.[10] The MLCT bands were also diminished compared to **5.2**, apparent in the medium-brown appearance of **5.20** *in situ* versus the bright green of the other dithiolenes. Finally, the IVCT molar absorptivity was reduced to a greater degree for **5.20** versus the π-extended metal

thiazoledithiolenes, showing once more that increasing proportion of thiazole content leads to lower ε values.

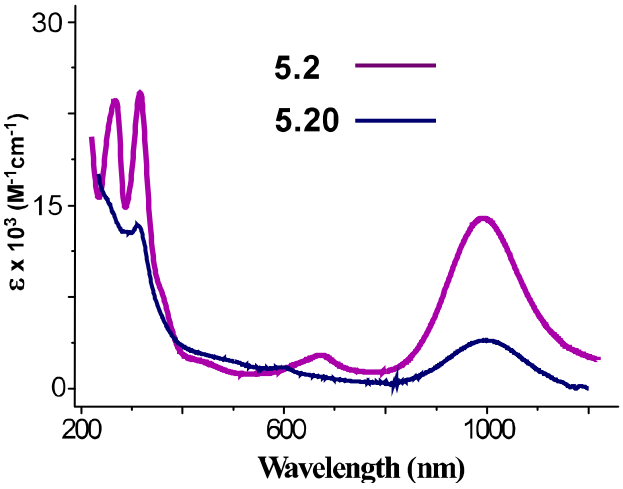

Figure 5.16. UV-vis-NIR absorption of **5.20** compared to **5.2**

Finally, the electronic properties of **5.20** were compared to **5.2**. It was found that only one of the oxidation potentials was significantly shifted to more positive potentials upon incorporation of the thiazole into the dithiolene core, with approximately 50 mV of stabilization for the -2/-1 couple and approximately 280 mV for the -1/0 couple. The reduced stabilization for the -2/-1 couple shows that electron-electron repulsion disfavors the reduction of the SOMO in a similar manner across the thiophene and thiazole, whereas increased delocalization of the π-extended metal thiazoledithiolenes lowers the energy barrier to reduction and stabilizes the -2/-1 couple to a greater extent that the thiophene analgoue. The -1/0 couple of **5.20** appeared to be almost irreversible, perhaps pertaining to the increased diffusion ability of **5.20** thanks to its increased solubility. Nevertheless, **5.20** features a SOMO that is stabilized compared it its thiophene analogue, and exemplifies the trend seen in the other metal thiazoledithiolenes. Additionally, our new methods for Kumada coupling alkyl groups onto the 2-position of thiazole can be applied to a wide variety of functional groups and various lengths of alkyl chain.

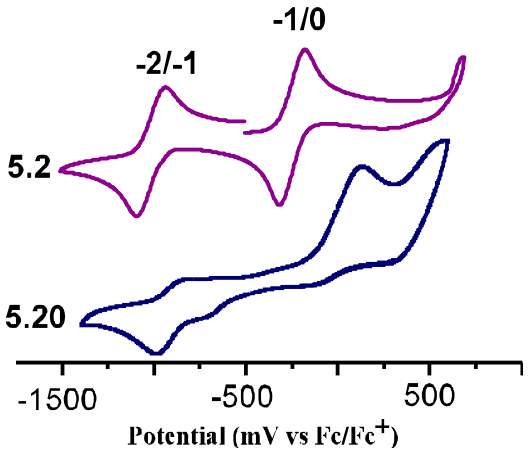

Figure 5.17. Voltammogram of **5.13** and **5.2**

5.8. Progress Towards a Metal-Coordinating Metal Thiazoledithiolene

Upon synthesis of the first verifiable family of π-extended metal thiazoledithiolenes, our interests turned to another aspect of the new series of molecules with potential applications. The nitrogen atom on each thiazole ring could form a five-membered ring with a metal center, provided the aryl group used for π-extension also has a nitrogen with which to coordinate. Coordination to other metal centers along the dithiolene backbone would allow inter-dithiolene communication through the metal center and potentially shift the IVCT band even further into the NIR region through enhanced electron delocalization. Two planned species are shown in Figure 5.18, both of which could form coordination complexes with two additional metal centers.

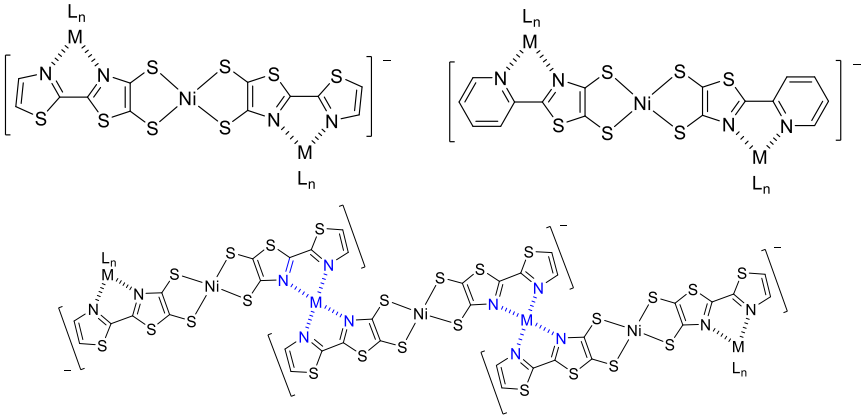

Figure 5.18. Proposed coordinating metal thiazoledithiolenes

To be brief, synthesis of the brominated pyridyl precursor was unsuccessful with standard methods of Negishi and Kumada couplings. Table 5.4 summarizes the various solvent, catalyst, additive, and temperature conditions attempted to synthesize **5.21**. Reaction of 2-lithiopyridine with $ZnCl_2$ resulted in an insoluble white powder *in situ*, which was able to be collected and analyzed via NMR spectroscopy. The observed peaks were distinct from both 2-bromopyridine and pyridine itself, providing evidence that it was an arylzinc species. However, it did not react with the tribromothiazole under any conditions, and solvent choice did not affect reactivity either. Attempts to synthesize **5.21** using Kumada coupling did not prove to be any more fruitful despite additives such as TMEDA. Overall, no synthetic tuning produced any trace of **5.21**.

Table 5.6. Reaction conditions utilized in an attempt to synthesize **5.21**

Entry	Solvent	Catalyst	MX	Order of Addition	Temperature	Additive	Yield
1	Et_2O	$Pd(dppf)Cl_2$	$ZnCl_2$	SM, BuLi, $ZnCl_2$	-78 °C → rt	-	-
2	Et_2O	$Pd(dppf)Cl_2$	IPrMgCl	SM, IPrMgCl	rt → reflux	-	-
3	THF	$Pd(dppf)Cl_2$	IPrMgCl	SM, IPrMgCl	rt → reflux	-	-
4	THF	$Ni(dppp)Cl_2$	IPrMgCl	SM, IPrMgCl	rt → reflux	-	-
5	Et_2O	$Ni(dppp)Cl_2$	Mg	SM, Mg	0 °C → rt → reflux	I_2	-
6	THF	$Ni(dppp)Cl_2$	Mg	SM, Mg	0 °C → rt → reflux	EtBr	-
7	Et_2O	$Pd(dppf)Cl_2$	Mg, $ZnCl_2$	SM, Mg, $ZnCl_2$	0 °C → rt	I_2	-
8	Et_2O	$Pd(dppf)Cl_2$	Mg, $ZnCl_2$	SM, Mg, $ZnCl_2$	0 °C → rt → reflux	I_2	
9	Et_2O	$Pd(dppf)Cl_2$	$ZnCl_2$	BuLi, $ZnCl_2$, SM	-78 °C → rt	-	-
10	Et_2O	$Pd(dppf)Cl_2$	$ZnCl_2$	BuLi, SM, $ZnCl_2$	-78 °C → rt	-	-
11	THF	$Ni(dppp)Cl_2$	IPrMgCl	IPrMgCl, SM	0 °C → reflux	TMEDA	-
12	THF, Et_2O	$Pd(dppf)Cl_2$	IPrMgCl, $ZnCl_2$	IPrMgCl, SM, $ZnCl_2$	0 °C → reflux	TMEDA	-

After a long hiatus, a new plan to synthesize **5.21** was inspired by the route to the PBTz oligomers in Chapter IV. Instead of using Kumada or Negishi coupling, Stille coupling could provide the necessary carbon-carbon bond formation. It was theorized that the pyridylstannane species would not aggregate *in situ* due to both the increased solubility and steric hinderances

from the butyl chains. The reaction was carried out with **5.15** and CuO as an additive,[49] which produced **5.21** in desirable yields of 85%. Progress towards thioacyl protection and subsequent dithiolene formation are ongoing.

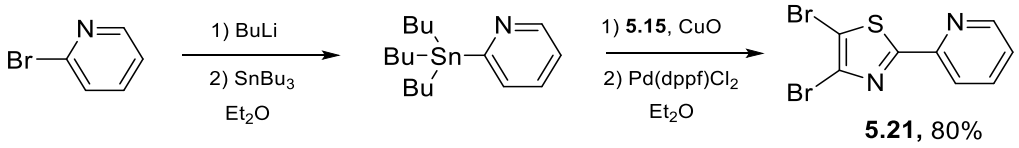

Scheme 5.8. Successful synthesis of pyridyl-extended ligand precursor **5.21**

5.9. Conclusions

Metal thiophenedithiolenes have been well-studied for their magnetic and superconducting properties. However, current efforts are focused on metal dithiolenes as NIR photodetectors, which provide a coveted low-energy absorption unique amongst thiophene-based materials. The thiophenedithiolene core has been modified to incorporate thiazole, and a series of π-extended metal thiazoledithiolenes has been synthesized as well as a methyl-capped analogue to compare properties with the thiophenedithiolene core. It was found that the SOMO of every analogue was stabilized by 100-240 mV, with thiophene offering the most stabilization and phenyl the least. The new furyl analogue exhibited SOMO stabilization between that of phenyl and thienyl, but interestingly featured the most hypsochromically shifted IVCT band. As seen with the studies concerning PBTz monomers and oligomers in Chapter III and IV, the molar absorptivities were reduced compared to the thiophene materials, and increasing contribution of thiazole led to lower ε values. Overall, this work experimentally quantifies the optoelectronic effect of thiazole incorporation into a new generation of metal dithiolenes while providing a synthetic toolkit for π- and alkyl-extension of metal thiazoledithiolenes.

5.10. Experimental

General Considerations: Thiophene and Pd(dppf)Cl_2 were purchased from Alfa Aesar and used without further purifications. $ZnCl_2$ was dried in vacuo prior to use. Diethyl ether and THF were distilled over sodium/benzophenone. All other materials were reagent-grade and used without further purification. All glassware was oven-dried, assembled hot, and cooled under N_2 prior to use. Chromatography was performed using standard methods with 230-400 mesh silica gel. Melting points were obtained with a digital thermocouple accurate to 0.1 °C resolution. HRMS (ESI-TOF)was performed in-house and all NMR spectroscopy was performed on a Bruker 400 mHz spectrometer in $CDCl_3$ solvent at 25 °C. All NMR spectra were referenced to the chloroform signal at 7.26 ppm, and multiplicity is as described: s = singlet, d = doublet, dd = doublet of doublets. UV-vis-NIR spectroscopy was performed on a dual-beam scanning Cary 500 UV-vis-NIR spectrophotometer in matching 1 cm quartz cuvettes. Electrochemistry was performed in a three-electrode cell consisting of a Pt disc working electrode, Pt wire auxiliary electrode, and Ag/Ag^+ reference electrode which was calibrated to the ferrocene/ferrocenium redox couple. The electrochemical measurements were obtained in DMF solvent, which was dried via $MgSO_4$ and filtered through silica gel. The electrolyte solution was 0.10 M tetrabutylammonium hexafluorophosphate.

4,5-Dibromo-2-(2-thienyl)-thiazole (**5.3**)*:* A solution of thiophene (0.96 mL, 12 mmol) in 150 mL diethyl ether was brought to 0 °C. BuLi (4.8 mL, 2.5 M soln. in hexanes, 12 mmol) was added dropwise, and the solution allowed to stir 30 min. $ZnCl_2$ (1.640 g, 12 mmol) was added and the solution stirred for 30 min at 0 °C before rising to ambient temperature. The solution was stirred for 1 h at room temperature, becoming opaque and white. 2,4,5-tribromothiazole (3.240 g, 10 mmol) was added, followed shortly by Pd(dppf)Cl_2 (0.184 g, 2.5 mol %). The mixture was

stirred for 3 h and aqueous $NaHCO_3$ was added to quench the reaction. The organic layers were separated, and the aqueous layers extracted with an addition 100 mL diethyl ether. The organic fractions were combined, dried with $MgSO_4$, filtered, and concentrated *in vacuo.* The product was chromatographed on silica gel with 5% diethyl ether in hexanes to give a faintly-yellow solid in 60-66% yield. mp: 73.4-74.6 °C. ^{1}H NMR: δ 7.45 (dd, *J* = 3.8, 1.1 Hz, 1H), 7.44 (dd, *J* = 5.1, 1.1 Hz, 1H), 7.08 (dd, *J* = 3.8, 5.1 Hz, 1H). ^{13}C NMR: δ 162.7, 135.8, 129.1, 128.9, 128.1, 127.3, 105.7 HRMS: m/z 325.8255 calcd for $C_7H_4Br_2NS_2$ $[M + H]^+$, 325.8276 found.

4,5-Dibromo-2-phenylthiazole (**5.4**)*:* A solution of bromobenzene (1.26 mL, 12 mmol) in 150 mL diethyl ether was brought to 0 °C. BuLi (4.8 mL, 2.5M soln. in hexanes, 12mmol) was added and the solution allowed to stir 1 h. $ZnCl_2$ (1.640 g, 12 mmol) was added and the solution was stirred for 15 min at 0 °C. Then, the solution was immersed in a room-temperature water bath, in which it became opaque and white. Formation of the opaque solution was complete with an additional 15 min of stirring, and immediately thereafter, 2,4,5-tribromothiazole (3.240 g, 10 mmol) was added, followed by $Pd(dppf)Cl_2$ (0.204 g, 2.5 mol %). The mixture was stirred overnight, aqueous $NaHCO_3$ was added to quench the reaction. The organic layers were separated, and the aqueous layers extracted with 100 mL diethyl ether. The organic fractions were combined, dried with $MgSO_4$, filtered, and concentrated *in vacuo.* The product was chromatographed on silica gel with 5% diethyl ether in hexanes to give a white solid in 50-54% yield. mp: 62.1-63.5 °C. ^{1}H NMR: δ 7.85 (m, 2H), 7.45 (m, 3H). ^{13}C NMR: δ 132.3, 131.1, 129.5, 129.2, 128.7, 127.3, 127.2, 126.1, 106.8. HRMS: m/z 319.8567 calcd for $C_9H_6Br_2NS$ $[M + H]^+$, 319.8573 found.

4,5-Dibromo-2-(2-furyl)-thiazole (**5.5**): A solution of furan (0.87 mL, 12 mmol) in 150 mL diethyl ether was brought to 0 °C. BuLi (4.8 mL, 2.5 M soln. in hexanes, 12 mmol) was

added dropwise, and the solution allowed to stir 1 h. $ZnCl_2$ (1.640 g, 12 mmol) was added and the solution stirred for 15 min at 0 °C before warming to ambient temperature. The solution was stirred for 15 min at room temperature, becoming opaque and white. 2,4,5-tribromothiazole (3.240 g, 10 mmol) was added, followed shortly by $Pd(dppf)Cl_2$ (0.184 g, 2.5 mol %). The mixture was stirred for 3 h and aqueous $NaHCO_3$ was added to quench the reaction. The organic layers were separated, and the aqueous layers extracted with 100 mL diethyl ether. The organic fractions were combined, dried with $MgSO_4$, filtered, and concentrated *in vacuo.* The product was chromatographed on silica gel with 5% diethyl ether in hexanes to give a white solid in 62-65% yield. mp: 98.9-99.8 °C. ^{1}H NMR: δ 7.51 (dd, *J* = 1.7, 0.6 Hz, 1H), 7.05 (dd, *J* = 3.5, 0.6 Hz, 1H), 6.55 (dd, *J* = 3.5, 1.7 Hz, 1H). ^{13}C NMR: δ 158.8, 147.6, 144.4, 129.4, 112.6, 110.1, 106.2 HRMS: m/z 309.8360 calcd for $C_7H_4Br_2NOS$ $[M + H]^+$, 309.8362 found.

4,5-Dibromo-2-methylthiazole (**5.18**)*:* Mg (0.291 g, 12 mmol) and a single crystal of iodine were added to a 125 mL oven dried round-bottom flask and purged with nitrogen gas. 50 mL diethyl ether was added, and CH_3I (0.40 mL, 6 mmol) was added dropwise over the course of 30 min. A white precipitate formed after Grignard reagent activation. The Grignard reagent was allowed to stir 1 h after addition was complete, and subsequently transferred via cannula to a solution of 2,4,5-tribromothiazole (1.640 g, 5 mmol), CuO (0.397 g, 5 mmol), and $Ni(dppp)Cl_2$ (0.135 g, 5 mol %) in 100 mL diethyl ether. The combined solutions were stirred overnight at ambient temperature, and saturated $NaHCO_3$ was poured into the reaction mixture. The organic layers were separated and the aqueous layers were extracted with diethyl ether. The organic fractions were combined, dried over $MgSO_4$, filtered, concentrated *in vacuo*, and chromatographed on silica gel to afford a clear-yellow oil in 73% yield. ^{1}H NMR: δ 2.67 (s, 3H).

^{13}C NMR: δ 167.5, 127.5, 105.7, 19.9. HRMS: m/z 257.8410 calcd for $C_4H_4Br_2NS$ $[M + H]^+$, 257.8436 found.

General Procedure for synthesis of thioacetate protected ligand precursors: The cross-coupled thiazole species (5.0 mmol) was added to a 250 mL round-bottom flask and purged with nitrogen gas. 100 mL of diethyl ether was added and the solution brought to -78 °C. *tert*-butyllithium (3.2 mL, 1.7 M soln. in pentane, 5.5 mmol) was added via metal syringe, and the solution stirred for 1 h. Sulfur (0.16 g, 5.0 mmol) was added, and the solution stirred for 1 h. An additional solution was prepared by adding *n*-BuLi (5.0 mL of 2.5 M soln. in hexanes, 12.5 mmol) to 150 mL diethyl ether in a 500mL round-bottom flask at -78 °C. Once the second solution was prepared, the initial solution was warmed to room temperature and transferred via cannula into the second. The combined solution was stirred for 2 h, sulfur (0.40 g, 12.5 mmol) added, and stirred for 1 h. The solution was then warmed to ambient temperature, forming a precipitate, and then cooled back to -78 °C. Acetyl chloride (2.1 mL, 30 mmol) was added and the mixture stirred for 15 min. The reaction was warmed to room temperature, sodium bicarbonate was added, and the organic layers were separated. The remaining thioacetate product was extracted from the aqueous layers using 100 mL diethyl ether, and collected. The combined organic layers were dried with $MgSO_4$, filtered, and concentrated in vacuo, resulting in a strongly odiferous, oily product. The oil was chromatographed on silica gel in a mixture of 5% ethyl acetate in hexanes, to afford a yellow solid in 29-33% yield.

4,5-Bis(thioacetate)-2-(2-thienyl)thiazole (**5.6**): 30-33% yield: mp: 100.8-102.1 °C. ^{1}H NMR: δ 7.56 (dd, *J* = 3.7, 1.1 Hz, 1H), 7.45 (dd, *J* = 5.1, 1.1 Hz, 1H), 7.09 (dd, *J* = 5.1, 3.7 Hz, 1H) 2.48 (s, 3H), 2.44 (s, 3H). ^{13}C NMR: δ 191.7, 190.8, 169.6, 165.2, 144.8, 129.1, 128.1,

127.7, 103.0, 30.3, 30.0. HRMS: m/z 315.3594 calcd for $C_{11}H_{10}NO_2S_4$ $[M + H]^+$, 315.9621 found.

4,5-Bis(thioacetate)-2-phenylthiazole (**5.7**) 29-32% yield: mp: 104.1-105.3 °C. ^{1}H NMR: δ 7.92 (m, 2H), 7.44 (m, 3H), 2.48 (s, 3H), 2.45 (s, 3H). ^{13}C NMR: δ 191.9, 190.8, 171.7, 145.4, 132.7, 131.0, 129.1, 129.0, 128.3, 126.6, 126.4, 30.3, 30.0. HRMS: m/z 310.0030 calcd for $C_{11}H_{10}NO_2S_4$ $[M + H]^+$, 310.0007 found.

4,5-Bis(thioacetate)-2-(2-furyl)-thiazole (**5.8**) 30-35% yield. ^{1}H NMR: δ 7.55 (dd, *J* = 0.7, 1.8 Hz, 1H), 7.09 (dd, *J* = 0.7, 3.4 Hz, 1H), 6.55 (dd, *J* = 1.8, 3.4 Hz, 1H) 2.45 (s, 3H) 2.41 (s, 3H). ^{13}C NMR: δ 191.7, 190.7, 161.3, 148.1, 145.3, 144.5, 127.6, 112.5, 110.5, 30.3, 30.0. HRMS: m/z 299.9823 calcd for $C_{11}H_{10}NO_3S_3$ $[M + H]^+$, 247.9821 found.

4,5-Bis(thioacetate)-2-methylthiazole (**5.19**) 31-36% yield. mp: 61.5- 63.0 °C. ^{1}H NMR: δ 2.75 (s, 3H), 2.45 (s, 3H), 2.42 (S, 3H). ^{13}C NMR: δ 192.0, 190.9, 170.5, 144.2, 127.8, 30.2, 29.9, 19.8. HRMS: m/z 247.9874 calcd for $C_4H_4NO_2S_3$ $[M + H]^+$, 247.9869 found.

General Procedure for synthesis of nickel metal thiazoledithiolenes: A 125 mL round bottom flask was filled with 100 mL of methanol and degassed using freeze-pump-thaw procedures. Sodium (4.00 g) was added to the solution at cold temperature and allowed to react for one h. The protected thiazole species (0.64 mmol) was added to the sodium methoxide solution and stirred for 1 h. A separate solution of $Ni(H_2O)_6Cl_2$ (0.076 g, 0.32 mmol) in 5 mL nitrogen-purged methanol was added dropwise, prompting a color change from yellow to red. The mixture was stirred 45 min and Bu_4NBr (0.820 g, 2.54 mmol) was added. To prompt precipitation, 50 mL H_2O was added and the solution was exposed to ambient atmosphere. The solution was filtered and washed with H_2O, methanol, and Et_2O. The precipitate was dissolved in

MeCN and $CHCl_3$ to produce a dark green or dark violet solution, from which the dithiolenes were recrystallized.

Bis(2-(2-thienyl)-4,5-thiazoledithiolato)nickelate(1-) (**5.3**)*:* 40-43% yield. mp: 146.4-146.6 °C. HRMS: 515.7650 calcd for $C_{14}H_6N_2NiS_8$ $[M]^-$, 515.7669 found. E.A. for $C_{14}H_6N_2NiS_8$ x 0.25 eq $CHCl_3$: C 46.36, H 5.40, N 5.36 calcd; C 46.54, H 5.00, N 5.12 found.

Bis(2-phenyl-4,5-thiazoledithiolato)nickelate(1-) (**5.4**)*:* 36-40% yield. mp: 181.0-181.7 °C. HRMS: 503.8522 calcd for $C_{18}H_{10}N_3NiS_6$ $[M]^-$, 503.8534 found.

Bis(2-(2-furyl)-4,5-thiazoledithiolato)nickelate(1-) (**5.5**)*:* 37-42% yield. HRMS: 483.8107 calcd for $C_{14}H_6N_2O_2NiS_6$ $[M]^-$, 483.8123 found.

Bis(2-methyl-4,5-thiazoledithiolato)nickelate(1-) (**5.20**)*:* 16-22% mp: 126.5-127.2 ^oC.

5.11. References

1. Eisenberg, R.; Gray, H. B. *Inorg. Chem.* **2011**, *50*, 9741-9751.
2. Schrauzer, G. N.; Mayweg, V. *J. Am. Chem. Soc.*, **1962**, *84*, 3221–3221.
3. Stiefel, E. I., Karlin, K. D. Eds.; *Dithiolene Chemistry: Synthesis, Properties, and Applications.* Progress in Inorganic Chemistry, Vol. 52, John Wiley and Sons: Hoboken, NJ, 2004.
4. Cassoux, P. *Coord. Chem. Rev.* **1999**, *185*, 213-232.
5. Robertson, N.; Cronin, L. *Coord. Chem. Rev.* **2002**, *227*, 93–127.
6. Kato, R. *Chem. Rev*. **2004**, *104*, 5319-5346.
7. Dalgleish, S.; Robertson, N. *Coord. Chem. Rev.* **2002**, *227*, 93-127.
8. Belo, D.; Almeida, M. *Coord. Chem. Rev.* **2010**, *254*, 1479-1492.
9. Rasmussen, S. C.; Amb, C. M. In *Chemical Crystallography;* Connelly, B. L. Ed.; Nova Publishers, Hauppage, NY, 2010, Ch. 2.

10. Amb, C. M.; Heth, C. L.; Evenson, S. J.; Pokhodnya, K. I.; Rasmussen, S. C. *Inorg. Chem*. **2016**, *55*, 10978-10989.
11. Sugimoto, H.; Siren, K.; Tsukube, H.; Tanaka, K. *Eur. J. Inorg. Chem.* **2003**, 2633-2638
12. Milsmann, C.; Kuma Patra, G.; Bill, E.; Wehermuller, T.; DeBeer, S.; Wieghardt, G.; Weighardt, K. *Inorg. Chem.* **2009**, *49*, 5241–5261.
13. Schlindwein, S. H.; Bader, K.; Sibold, C.; Frey, W.; Neugebauer, P.; Orlita, M.; van Slageren, J.; Gudat, D. *Inorg. Chem.* **2016**, *55*, 6186-6194.
14. Alves, H.; Almeida, M.; Belo, D. *Chem. Commun.* **2015**, *51*, 13117-13119.
15. Shibihara, S.; Kitigawa, H.; Kubo, T.; Nakasuji, K.; *Inorg. Chem. Commun.* **2007**, *10*, 860-862
16. Kishore, R.; Das, S. K. *Polyhedron* **2013**, *50*, 612−621.
17. Aragoni, M. C.; Arca, M.; Cassano, T.; Denotti, C.; Devillanova, F. A.; Frau, R.; Isaia, F.; Lelj, F.; Lippolis, V.; Nitti, L.; Romaniello, P.; Tommasi, R.; Verani, G. *Eur. J. Inorg. Chem.* **2003**, 1939−1947.
18. Amb, C. M.; Rasmussen, S. C. *Synth. Met.* **2009**, *159*, 2390-2393.
19. Petrenko, T.; Ray, K.; Wieghardt, K. E.; Neese, F. *J. Am. Chem. Soc.* **2006**, 4422–4436.
20. Ray, K.; Weyhermuller, F.; Neese, K. *Inorg. Chem.* **2005**, *44*, 5345-5360.
21. Skotheim, T. A., Reynolds, J. R., Eds. *Handbook of Conducting Polymers*, 3rd ed.; CRC Press: Boca Raton, FL, 2007. (b) Perepichka, I.F.; Perepichka, D. F. *Handbook of Thiophene-Based Materials*; John Wiley & Sons: Hoboken, 2009.
22. Belo, D.; Alves, H.; Rabaca, S.; Pereira, L. C.; Duarte, M. T.; Gama, V.; Henriques, R. T.; Almeida, M.; Ribera, E.; Rovira, C.; Veciana, J. *Eur. J. Inorg. Chem*. **2001**, 3127−3133.

23. Dalgliesh, S; Labram, J. C.; Wang, J.; McNeill, C. R.; Anthopolous, T. D.; Greenham, N. C.; Robertson, N. *J. Mater. Chem.*, **2011**, *21*, 15422-15430.

24. Katritzky, A. R.; Pozharskii, A. F. *Handbook of Heterocyclic Chemistry*, 2nd ed.; Pergamon: Oxford, 2000; pp 101.

25. Kibbel, H.; Jeroschewski, P.; Rudolf, G. *Z. Chem.* **1988**, *28*, 446-447.

26. Filatre-Furcate, A.; Auban-Senzier, P.; Fourmigue, M.; Roisnel, T.; Dorceta, V.; Lorcy, D. *Dalton Trans.* **2015**, *44*, 15683-15689.

27. Filatre-Furcate, A.; Roisnel, T.; Lorcy, D. *J. Organomet. Chem.* **2016,** *819*, 182-188.

28. Bredas, J.-L.; Beljonnne, D.; Coropceanu, V.; Cornil, J. *Chem. Rev*. **2004**, *104*, 2777−2812.

29. Del Zoppo, M.; Zerbi, G. *Phys. Rev. B*, **1994**, *50*, 9815-9823.

30. Uzelac, E. J.; Rasmussen, S. C. *Eur. J. Inorg. Chem.* **2017**, *33*, 3878-3883.

31. Amb, C. M.; Rasmussen, S. C. *Eur. J. Org. Chem*. **2008**, 801–804.

32. Uzelac, E. J.; Rasmussen, S.C. *J. Org. Chem.* **2017**, *82*, 5947-5951.

33. Schnürch, M.; Spina, M.; Khan, A. F.; Mihovilovic, M. D.; Stanetty, P. *Chem. Soc. Rev*. **2007**, *36*, 1046−1057.

34. Hronec, M.; Malik, L.; Stasko, A. *J. Mol. Catal.* **1985**, *30*, 251-258.

35. Sugimoto, K.; Kuroda-Sowa, T.; Maekawa, M.; Munakata, M. *Bull. Chem. Soc. Jpn.* **2000**, *73*, 391-394.

36. Grapperhaus, C. A.; Mullins, C. S.; Kozlowski, P. M.; Mashuta, M. S. *Inorg. Chem.* **2004**, *43*, 2859-2866.

37. Schrauzer, G. N.; Zhang, C.; Reddy, H.; Chadha, R. *Inorg. Chem.* **1991**, *30*, 3865-3869.

38. Bolligarla, R.; Das, S. K. *Eur. J. Inorg. Chem.* **2012**, 2933-2939.

39. Spingler, B.; Schnidrig, S.; Todorova, T.; Wild, F. *Cryst. Eng. Comm*, **2012**, *14*, 751-757.

40. Katritzky, A.; Pozharskii, A. *Handbook of Heterocyclic Chemistry*, 2nd. Ed. Pergamon, New York, NY, 2000, pp 68, 115.

41. Cardona, C. M.; Li, W.; Kaifer, A. E.; Stockdale, D.; Bazan, G. C. *Adv. Mater.* **2011**, *23*, 2367-2371.

42. Blouin, N.; Michaud, A.; Gendron, D.; Wakim, S.; Blair, E.; Neagu-Plesu R.; Belletete, M.; Durocher, G.; Tao, Y. Leclerc, M. *J. Am. Chem. Soc.* **2008**, *130*, 732-742.

43. Amb, C. M., PhD Dissertation, North Dakota State University, Fargo, ND, 2008

44. D'Alessandro, D. M.; Keene, F. R. *Chem. Soc. Rev.* **2006**, *35*, 424-440.

45. Braude, E.; *J. Chem. Soc.* **1950**, 379-384.

46. Josse, P.; Chavez, P.; Dindault, C.; Dalinot, C.; McAfee, S. M.; Dabos-Seignon, S.; Tondelier, D.; Welch, G.; Blanchard, P.; Leclerc, N.; Cabanetos, C. *Dyes and Pigments* **2017**, *137*, 576-583.

47. Bronstein, H.; Collado-Fregoso, E.; Hadipour, A.; Soon, Y. W.; Huang, Z.; Dimitrov, S. D.; Ashraf, R. S.; Rand, B. P.; Watkins, S. E.; Tuldhar, P. S.; Meager, I.; Durrant, J. R.; McCullough, I. *Adv. Funct. Mater.* **2013**, *23*, 5647-5654.

48. Shen, K.; Fu, Y.; Li, J. N.; Liu, L.; Guo, Q. *Tetrahedron* **2007**, *63*, 1568-1576.

49. Gronowitz, S.; Bjork, P.; Malm. J.; Hornfeldt, A.-B. *J. Organomet. Chem.* **1993**, *460*, 127-129

CHAPTER VI. SUMMARY AND FUTURE DIRECTIONS

6.1. Summary of Findings

The presented work comprises new families of conjugated organic materials based upon the thiazole heterocycle. Potentially the "next-generation" of fused-ring thiophene-derived materials, little data existed in the literature as to the precise effect of thiazole substitution into thiophene materials. Direct comparisons of optical and electronic properties to existing thiophene materials were sparse. Thus, comparison to the Rasmussen group's classes of fused-ring thiophene systems needed to be undertaken in order to meet the two-part goal of this disseration's research: probing the structure-function relationships that occur with incorporation of thiazole into conjugated materials, and providing families of materials potentially more optimized for electronics applications.

The path to thiazole materials began with an examination of the brominated thiazole family, necessary building blocks for the thiazole analogues. The bromothiazole study provided the field with optimized procedures for each member, and allowed the synthesis of every molecule to be performed without elemental bromine. Full characterization of all seven bromothiazoles was provided as well, filling in data that was previously missing from the literature. Two important conclusions were drawn: exploitation of the halogen dance was necessary to selectively produce certain members of the bromoithiazole family, and the conventional thought that thiazole's 2-position is the most reactive to lithiation was not found to be experimentally encompassing. Our reaction trials showed that slight changes in reaction conditions and alpha-position functionalities resulted in large effects on reactivity between the 2- and 5-positions. For the Rasmussen group specifically, these principles were applied toward

thiazole analogues for two classes of fused-ring thiophene materials: dithieno[3,2-*b*:2',3'-*d*]pyrrole (DTP) and nickel thiophenedithiolenes.

The thiazole analogue of DTP, the pyrrolo[2,3-*d*:5,4-*d'*]bisthiazole (PBTz) unit, was already reported in the literature, but with limited characterization data. Our studies expanded the number of known PBTz units, featuring aromatic N-functionalization for the first time and the first reported crystal structure of the deprotected PBTz monomer. The optical and electronic properties of the fused-ring unit itself were characterized for the first time, and with all of these new data, the DTP and PBTz unit can be intimately compared for the first time. It was found that the PBTz HOMO was stabilized to a greater degree than both alkyl and acyl DTP units, while the $\pi \rightarrow \pi^*$ transition's λ_{max} was slightly redshifted. However, the $\pi \rightarrow \pi^*$ molar absorptivites were severely reduced compared to that of DTP. Interestingly, the narrowing of the HOMO-LUMO gap can be attributed to slight charge-transfer character from the pyrrole to the thiazole rings, which the reduced molar absorptivites reflect. Although the PBTz was the most electrochemically stable of the new family, the reduced ability to absorb light could limit PBTz's application in organic devices such as OPVs.

To quantify the effect of extended conjugation on the PBTz unit, a series of aryl-extended PBTz oligomers were synthesized. It was found that the harsher reaction conditions needed to synthesize the PBTz monomers needed to be applied to the oligomer synthesis, too. The absorption bands of the PBTz oligomers were generally redshifted from the DTP analogues. As a welcome development, the molar absorptivites of the PBTz oligomer family more closely matched those of the DTP analogues, showing that lessening thiazole content could be correlated to increased ε. Stabilization of the PBTz HOMO in the oligomers was found to be greater than

both first- and second-generation DTP molecules, matching the trend seen in the PBTz monomers.

Thiazole analogues to the nickel thiophenedithiolenes showed similar trends in their optoelectronic properties. Three new π-extended metal thiazoledithiolenes and a methyl-capped "parent" complex were synthesized and characterized using cyclic voltammetry and UV-vis-NIR spectroscopy. It was found that the metal thiazoledithiolenes all showed similar absorption properties to their thiophene analogues, with little change in the intervalence charge transfer (IVCT) band λ_{max} and a slight redshift of the $\pi \rightarrow \pi^*$ band. However, the molar absorptivites for each transition were reduced, with the parent complex exhibiting the largest reduction. The HOMO levels of the metal thiazoledithiolenes were stabilized beyond that of the thiophene analogues in a similar manner to the PBTz species, with the π-extended metal thiazoledithiolenes showing a lesser relative stabilization of the SOMO than the parent complex.

There are two clearly-defined trends that emerge from the collected data. Foremost, incorporation of the thiazole heterocycle provides a consistent stabilization of the frontier orbital levels compared to thiophene. *Every* new thiazole material exhibited a deeper HOMO/SOMO level than its thiophene counterpart. Additionally, this effect is more pronounced with greater thiazole proportion of the molecule. Both the parent metal thiazoledithiolene and the PBTz monomers exhibited greater extents of frontier orbital stabilization than the π-extended metal thiazoledithiolenes and the PBTz oligomers.

The changes in optical properties of a thiophene material upon incorporation of thiazole provide another trend that was consistent through the new thiazole materials presented in this work; across *all* of the new thiazole materials, the molar absorptivity values decreased in relation to the thiophene counterparts. Once again, an increase in thiazole proportion led to a systematic

decrease in molar absorptivity. Thiazole incorporation also slightly redshifted and broadened the $\pi \rightarrow \pi^*$ absorption band, with an onset change of approximately 20-30 nm for all of the new molecules. It can be inferred then, that thaizole has a slight impact on the LUMO energy level in addition to the HOMO.

Finally, furyl extension was developed for both classes of thiazole materials. The new molecules synthesized during this study are the first fused-ring thiazole materials reported that feature a carbon-carbon bond between thiazole and furan. Across both the PBTz and metal thiazoledithiolene families, furyl functionalization led to a decrease in HOMO stabilization compared to thienyl analogues, but an increase in molar absorptivity of the resulting optical transitions. Every furyl-functionalized thiazole material exhibited an increased molar absorptivity compared to its thiophene and phenyl counterpart.

Overall, this work advanced the field of thiazole and thiophene-based materials by providing qualitative and quantitative evidence in support of the aforementioned trends. A significant number of fused-ring thiazole materials containing varying conjugation lengths and functionalities were synthesized to provide adequate data, and the properties between thiophene materials and their thiazole analogues were directly compared, filling a gap in the scientific literature. New synthetic methods were developed to not only access the entire brominated thiazole family, but functionalize thiazole materials with a variety of aryl and alkyl groups to tune optoelectronic properties. In addition to these new data, this work also advances the field by providing a framework for researchers to anticipate effects of thiazole modifications to their materials.

6.2. Future Directions

The PBTz studies herein showed how the optical and electronic properties of the core unit can be tuned through aryl extension and sidechain functionality. Considering that attempts to synthesize an acyl PBTz unit were not successful, further stabilization of the frontier orbitals could result in a unit that can act as an electron-transport material by way of a redox-stable LUMO. This stabilization could be realized through π-extension with electron-withdrawing dicyanomethylene or tricyanovinyl units.[1] Synthesis of these molecules should be facile, and the frontier orbitals may be stabilized by up to 300 mV.

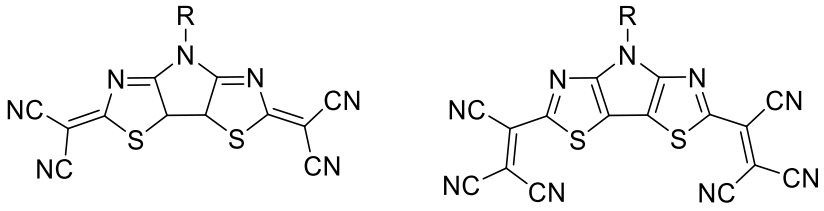

Figure 6.1. Planned PBTz units with cyano functionalization

For the metal thiazoledithiolenes, multiple new directions can be taken. As outlined in Chapter V, one of the unique aspects of the metal thiazoledithiolenes is the potential ability to form additional metal-coordinating units via π-extension with pyridine or thiazole. Priority should lie with synthesizing the pyridyl-extended metal thiazoledithiolene and forming coordination compounds with additiona metal centers. Additionally, synthesis of the analogous tetrathiafulvalenes (TTFs), which are all-organic cousins to the metal dithiolene family, should be attempted. These TTFs should still show low-energy NIR charge-transfer bands, but as a neutral species, the solubility in organic solvents for the π-extended analogues may be a limitation. The thioacetate-protected metal thiazoledithiolene precursors should react with tetrachloroethylene upon deprotonation, producing a TTF analogue to the metal

thiazoledithiolenes. The thiazole TTF could be directly compared to the metal thiazoledithiolenes and its optoelectronic properties evaluated, although solubility of the TTF may be an issue.

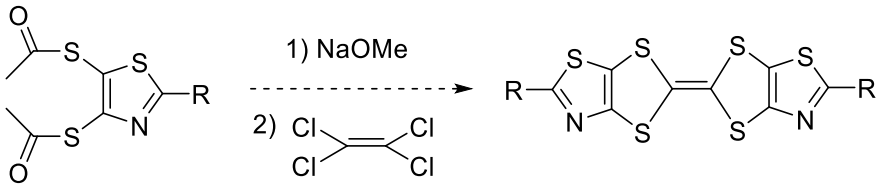

Scheme 6.1. Proposed synthesis of thiazole-based tetrathiafulvalene

Another research goal was explored during the thiazole studies: the synthesis of a furan analogue to DTP. Furan can be derived from biomass on an industrial scale and thus can be considered a "green" material.[2] Despite this incentive, furan has received less attention as an alternative to thiophene due to prevailing thought that its electron-rich nature would result in unstable materials.[3] This thought calls to mind the observed decomposition of the furyl-extended PBTz oligomers detailed in Chapter IV. However, Bendikov and coworkers have synthesized a series of linear oligofurans, which displayed good environmental stability. Additionally, their solid-state packing and planarity were enhanced compared to analogous oligothiophenes.[4]

Attempts to synthesize difuro[3,2-*b*:2',3'-*d*]pyrrole system began with copper-mediated oxidative coupling of 3-bromofuran to produce 3,3'-dibromo-2,2'-bifuran **6.1** according to the Rasmussen group's procedures. A crystal structure of **6.1** was able to be obtained, confirming that the correct isomer was being formed. The next synthetic step was an analogous Buchwald-Hartwig amination in the manner used for the DTP and PBTz synthesis, but unfortunately no success was had. Variances in the sidechain, catalyst, and reaction temperature did not produce **6.2.**

However, a luminescent solid was obtained upon switching to a tri-*tert*-butyl-phosphine catalyst. which produced a promising NMR spectrum. The spectrum was unclean, though, and the product quickly decomposed. It was thought that **6.2** was produced but oxidized quickly. If the HOMO level is indeed as destabilized as expected, this decomposition would need to be mitigated with a protecting group. Although the bulk of this work took place in 2015-2016, the authors have been made aware of a recent paper by Rupar and coworkers,[5] in which the authors reported compound **6.1** and protected it with trimethylsilyl groups, allowing bridging and completion of the fused-ring species. Although the authors bridged **6.1** with elements such as phosphorus, germanium, and silicon, the nitrogen analogue was not reported, and thus the difuro[3,2-*b*:2',3'-*d*]pyrrole **6.2** is yet unreported.

6.3. References

1. Pappenfus, T. M.; Burand, M. W.; Janzen, D. E.; Mann, K. R.; *Org. Lett.* **2003**, *5*, 1535-1539.
2. Okada, K.; Tachikawa, K. A, *J. Appl. Polym. Sci*. **1999**, *74*, 3342-3350.
3. Distefano, G.; Jones, D.; Guerra, M.; Favaretto, L.; Modellli, A.; Mengoli, G. *J. Phys. Chem.* **1991**, *95*, 9746-9753.
4. Gidron, O.; Bendikov, M. *Angew. Chem. Int. Ed.* **2014**, *53*, 2546-2555.
5. Cao, H.; Brettell-Addams, I.; Qu, F.; Rupar, P. *Organometallics*, **2017**, *36*, 2565–2572.